Control of direct current connections (HVDC) for the damping of inter-area oscillations

Yankai Xing

THÈSE DE DOCTORAT DE

L'ÉCOLE CENTRALE DE NANTES

ÉCOLE DOCTORALE N° 601
Mathématiques et Sciences et Technologies de l'Information et de la Communication
Spécialité : *Automatique, productique et robotique*

Par
Yankai XING

Commande des liaisons à courant continu (HVDC) pour l'amortissement des oscillations inter-zones

Thèse présentée et soutenue à Nantes, le 29 Janvier, 2021
Unité de recherche : UMR 6004, Laboratoire des Sciences du Numérique de Nantes (LS2N)

Rapporteur :

Oriol GOMIS-BELLMUNT, Professeur, UPC Barcelona (Espagne)

Composition du Jury :

Président :	Horst SCHULTE	Professeur, Université of Applied Sciences Berlin (Allemagne)
Examinateurs :	Antoneta BRATCU,	Maître de conférences, Grenoble INP
	Elkhatib IBRAHIM	Maître de conférences HDR, École Centrale de Nantes
Dir. de thèse :	Bogdan MARINESCU	Professeur des universités, École Centrale de Nantes
Invité :	Florent XAVIER	Ingénieur, R&D RTE , Paris la Defense

REMERCIEMENTS

J'adresse toute ma reconnaissance aux personnes mentionnées ci-dessous qui m'ont soutenu pour finir la thèse.

Je souhaite remercier en premier lieu mon directeur de thèse, Prof. Bogdan Marinescu, Professeur des universités à l'école Centrale de Nantes, un grand merci également à mon co-directeur M. Elkhatib Kamal, et M. Mohamed Belhocine, M. Mohammad Pourmahmood Aghababa, M. Florent Xavier.

J'ai apprécié beaucoup de nos discussions et j'en ai été très encouragé. Ils ont joué différents rôles dans ma thèse: Bogdan a généré des progrès et de la direction générale de la thèse, Belhocine et Pourmahmood Aghababa m'ont aidé beaucoup sur la partie théorique de la thèse (ex: la modélisation et la théorie du contrôle basique). Elkhatib m'a communiqué plus fréquemment afin de travailler dans tous les détails. Florent m'a fourni de nombreux avis utiles sur mon travail et les articles publiés.

Puisque au début, à cause de manque de la connaissance de la théorique automatique, ce dernier m'a rendu rendu à difficile d'obtenir rapidement la direction des travaux de recherche. Je n'aurais pas pu parvenir au bout de mon travail de thèse sans l'aide d'une multitude de personnes. Je tiens à vous exprimer ma gratitude pour la confiance et l'inspiration que vous m'avez accordés.

Ensuite, je voudrais exprimer ma gratitude à mon affiliation (école Centrale de Nantes) et à l'organisation CSC (China Scholarship Council) qui m'a donné cette opportunité de faire ma thèse en France.

Dans le même temps, je suis également témoin de l'approfondissement de la coopération entre la France et la Chine dans le domaine de l'éducation et la recherche, en espérant sincèrement que l'amitié entre les deux pays s'approfondira.

Et je tiens à exprimer mes sincères remerciements à RTE (Réseau de Transport d'Electricité) pour avoir fourni les données et le modèle de ce sujet et de leur soutien à la recherche.

Je désire en outre remercier les membres du jury (rapporteurs et examinateurs), pour vos aide et vos patience, vos commentaires m'ont aidé à améliorer mon travail.

Enfin, je remercie ma famille pour ses encouragements et son soutien lorsque j'ai rencontré des difficultés de recherche, ils sont ma grande motivation pour progresser la thèse.

Table of Contents

List of Figures

List of Tables

List of Acronyms

POD Power Oscillation Damping . . . 13
HVDC High Voltage Direct Current . . . 13
PSS Power System Stabilizer . . . 18
FACTS Flexible Alternating Current Transmission Systems . . . 18
AC Alternating Current . . . 13
VSC-HVDC Voltage Source Converter High Voltage Direct Current . . . 18
LCC-HVDC Line Commutated Converter High Voltage Direct Current . . . 31
WAMS Wide Area Measurement System . . . 25
PMUs Phasor Measurement Units . . . 25
ZPETC Zero Phase Error Tracking Control . . . 26
MZPEC Modified Zero Phase Error Compensator . . . 27
FLC Fuzzy Logic Control . . . 25
SMA Selective Modal Analysis . . . 22
AESOPS Analysis of Essentially Spontaneous Oscillations in Power Systems . . . 22
LQG Linear Quadratic Gaussian . . . 23
MPC Model Predictive Control . . . 24
HSV Hankel Singular Values . . . 26
LMI Linear Matrix Inequality . . . 23
SVC Static Var Compensator . . . 21
TCSC Thyristor Controlled Series Capacitor . . . 21
SSSC Static Synchronous Series Compensator . . . 21
STATCOM Static Synchronous Compensator . . . 21
RSOFC Robust H_∞ Static Output-error Feedback Controller . . . 28
DDOFC Dynamic Decoupling Output-feedback Controller . . . 28
IEEE Institute of Electrical and Electronic Engineers . . . 13
IGBTs Insulated Gate Bipolar Transistors . . . 31
EMT Electromagnetic Transient . . . 32
AVR Automatic Voltage Regulator . . . 33
SIMO Single Input Multi-Output . . . 95

CONTEXT AND ORGANIZATION OF THE THESIS

Motivation

With the increasing scale of power grids, the problem of electromechanical oscillations has become an important aspect of power system stability. The damping of the power system has become increasingly weak with the extension of the European power system. As a result, there is a growing risk of low-frequency oscillations that place severe constraints on inter-area energy exchange and the stability of the power system. Damping control is an effective way to solve the problem of low-frequency oscillations. Also, High Voltage Direct Current (HVDC) transmission systems have been progressively integrated into power grids. They can be exploited to damp such oscillations.

In the past, the inter-area modes analyzed and controlled were those of low frequencies, around 0.2Hz in Europe. These are the most widespread modes of the transmission network, i.e. those involving the largest number of generators. For an HVDC inserted in a meshed Alternating Current (AC) network, as it is the case for recent interconnection reinforcements in Europe (such as the France-Spain and France-Italy links), the inter-area modes controllable with HVDC converters may be at higher frequencies, around 1Hz (i.e., may involve a limited number of generators in the area adjacent to the HVDC). Within this frequency range, there are also other network dynamics. The inter-area modes are therefore close to other modes of different natures (see (Arioua and Marinescu 2016; Leyla Arioua and Bogdan Marinescu 2015)) that can be disturbed by the HVDC Power Oscillation Damping (POD) controller. The use of a classical Institute of Electrical and Electronic Engineers (IEEE) POD controller structure and tuning methodologies (see, for example, (« IEEE recommended practice for excitation system models for power system stability studies (ieee std 421.5-2005) » 2005)) can lead to inefficient damping for inter-area modes and can destabilize others.

In another aspect, it is well known that unstable zeros can degrade the performance of control systems. However, there is little work on the origin of unstable zeros in HVDC links inserted in a meshed AC network. Therefore, it is important to both in research and in practice to perform analyses on the parameters of networks with HVDC links to highlight their effects on unstable zeros.

Moreover, in many applications, modeling errors and system uncertainties in plant models are unavoidable. For accuracy, a design technique must account for these errors and uncertainties to be practically feasible. Thus, a robust control must be adopted to deal with the uncertainties produced by the change of operating point in the power system and the modeling errors caused by modeling

and reduction for the realistic power system.

To summarize the aforementioned problems:

1. The supplementary damping control provides the opportunity to maintain system stability by the means of well designed supplementary POD controllers for both active and/or reactive power modulations.
2. One difficulty is that the different dynamics should be taken into account more directly than in classic IEEE POD controller structure and tuning methodologies.
3. The appearance of unstable zeros and modeling errors bring more difficulties to control.
4. To develop a controller to ensure robustness of the controls in the grid context and different situations is also a motivation.

Motivated by these facts, this thesis discusses these problems and provide a solution of them.

Thesis overview

The detailed organization of this thesis is given in the sequel.

— **Chapter 1** In this chapter, the test system is proposed. The method of analysis and reduction are described in a detailed way. The several main problems are formulated in this chapter.
— **Chapter 2** This chapter introduces the problem of unstable zeros in the test system, the existing situation of these unstable zeros, and a compensator to solve this problem.
— **Chapter 3** The advanced controllers are compared with the classic method POD controller and the application results are shown in this chapter.
— **Chapter 4** More robust tests such as changing operation point cases are implemented with each controller to compare the robustness.
— **Chapter 5** The single input single output POD controller is extended into a single input multi-output controller to modulate both the active and reactive power in a coordinated way.

Publications

International journals

[1] Xing Y, E Kamal, Marinescu B, and F. Xavier. Model-matching Robust Control Strategies to Improve Power Oscillation Damped and Transient Stability in VSC-HVDC Transmission Systems. (Submitted to IMA JOURNAL OF MATHEMATICAL CONTROL AND INFORMATION)

[2] Xing Y, E Kamal, Marinescu B, and F. Xavier. LMI Optimization Approaches to Robust H_∞

Static and Dynamic Output-feedback Control of Power Oscillation Damped via VSC-HVDC Transmission Systems. (Being submitted to IEEE Transaction on power system)

International conferences

[1] Xing Y, Marinescu B, Belhocine M, and F. Xavier. Power oscillations damping controller for HVDC inserted in meshed AC grids[C], 2018 IEEE PES Innovative Smart Grid Technologies Conference Europe (ISGT-Europe). IEEE, 2018: 1-6.

[2] Xing Y, Marinescu B, Xavier F. Robust research of power oscillations damping controller for HVDC inserted in meshed AC grids[C], 2019 IEEE Milan PowerTech. IEEE, 2019: 1-6.

[3] Xing Y, Aghababa M P, Marinescu B, and F. Xavier. Analysis and Control of Non-Minimum Phase Behavior in Nonlinear AC Grids Equipped with HVDC Links[C], 2019 IEEE PES Innovative Smart Grid Technologies Europe (ISGT-Europe). IEEE, 2019: 1-5.

[4] Xing Y, E Kamal, Marinescu B, and F. Xavier. Robust H_∞ Dynamic Output-feedback Control of Power Oscillation Damped via VSC-HVDC Transmission Systems[C], 2020 IEEE Canada Power and Energy Conference, Edmonton, AB, Canada.

Chapter 1

Introduction

Contents

1.1 Power system stability

1.1.1 Overview

Power system stability is the ability of the power system, under given operating conditions, to revert to an equilibrium state of operation after being disturbed (Prabha Kundur, Balu, and Lauby 1994). An essential indicator of the regular operation of a power system is that all synchronous motors (mainly generators) in the system are in synchronous operation. Synchronous operation means that all synchronous motors operating in parallel have the same angular velocity. In this case, the parameters that characterize the operating state have close to constant values.

The electromechanical oscillations problem is one of the important aspects of power system stability. This is a problem of power system oscillatory stability, as shown, for example, in Europe in December 2016 when low damping oscillations related to the most spread inter-area mode (at 0.15Hz) have been experienced (« Analysis of inter-area oscillations of 1st december 2016. ENTSO-E SG SPD Report » n.d.). The damping of the power system has become weaker with the extension of the synchronous zones and increase of the shore renewable generation. Today, Power System Stabilizer (PSS), HVDC, and Flexible Alternating Current Transmission Systems (FACTS) auxiliary damping controller are widely used to damp low-frequency oscillation.

The main objectives of HVDC are to increase the transmission capacity of the system and the ability to control the power flow. In addition, they can improve the transient and small-signal stability of the system. With supplementary damping control, HVDC has a good damping effect on the power oscillations of the AC system. Especially, Voltage Source Converter High Voltage Direct Current (VSC-HVDC) transmission systems have the advantage of independent and fast control of active/reactive power. This plays an important role to maintain the system stability and achieve better damping of inter-area oscillation modes by the means of well designed supplementary POD controller in control loops (Hector F Latorre, Ghandhari, and Söder 2008).

1.1.2 Stability issues

Power system stability issues can be classified as the following (Prabha Kundur, Balu, and Lauby 1994):

— **Rotor angle stability** is the ability of a synchronous generator to maintain synchronous operation after it has been disturbed. Rotor angle instability can be caused by insufficient synchronizing torque or damping torque, where insufficient synchronizing torque causes non-oscillatory instability and insufficient damping torque causes oscillatory instability.

— **Voltage stability** is the ability of a power system at a given operating point to maintain the voltage of all the buses at an acceptable value after undergoing a disturbance. It depends on the ability of the system to maintain or restore the balance between load demand and load supply. Based on the magnitude of the disturbance, IEEE/CIGRE classifies voltage stability into small disturbance voltage stability and large disturbance voltage stability.

— **Mid and long-term stability** refers to the slow system dynamics following severe system disturbances and significant frequency deviations. Study periods typically range from minutes to tens of minutes and incorporate the thermal properties of boilers and generating equipment in addition to electromechanical components.

According to the magnitude of the disturbance and the dominant factors that lead to rotor angle stability, this type of stability is classified into small-signal (disturbance) stability and transient stability:

1. **Small-signal** (or small-disturbance) stability refers to the ability of the system to maintain

stable operation for a long process without periodic oscillations after a small disturbance. It is caused by insufficient damping torque and is mainly used to analyze the damping characteristics of the system under normal operation and post-incident operation mode.

2. **Transient stability** refers to the ability of each generator to maintain synchronous operation and to transit to a new stable operation point or to return to the original stable operating point after a major disturbance of the system. It usually refers to the first and second swing.

This thesis focuses on small-signal stability problems which caused growing problem frequency oscillations in the power system.

1.2 Oscillatory instability

In today's practical power systems, small-signal stability is largely a problem of insufficient damping of oscillations. The following types of oscillations are classic (Prabha Kundur, Balu, and Lauby 1994):

— **Local modes** (or machine-system modes) are related to the swing of the unit of a power station relative to other parts of the power system.

— **Inter-area modes** is associated with many machines within an area of the power system oscillating against machines in other areas of the network. They occur when tightly coupled groups of generators exist within a large power system. They are traditionally harder to damp than local modes due to the number, dispersion, and varying levels of participation of the machines involved. If any of these oscillatory modes present within a power system become unstable then they will lead to growing oscillations and eventually the disconnection of equipment, possibly leading to further cascading failures.

— **Torsional modes** are associated with the turbine-generator shaft system rotational components. Instability of torsional modes may be caused by interaction with excitation controls, speed governors, HVDC controls, and series-capacitor-compensated lines.

— **Control modes** are associated with generating units and other controls. Poorly tuned exciters, speed governors, HVDC converters, and static Var compensators are the usual causes of instability of these modes.

With the expansion of the interconnection scale and the operation of the grid closer to the stability limit due to economic and environmental factors, inter-area oscillations have been observed in many grids around the world. They are of the electromechanical type, i.e., rotors of distant generators are coupled in an oscillation. However, other oscillatory coupling modes have been recently put into evidence. In (Arioua and Marinescu 2016), it has been shown that oscillation between D-axes of distant generators may exist. Also, in (Munteanu, Bogdan Marinescu, and Florent Xavier 2020), oscillation between distant power converters have been studied. All these oscillations, called *electrical coupling modes*, are similar to the inter-area modes in the sense if distant coupling of dynamic

devices and may lead to similar oscillatory stability problems.

1.3 Particular case of inter-area oscillation modes

In the past, the inter-area oscillation modes which were analyzed and controlled were the ones at low frequencies, around 0.2Hz in Europe. These are the most spread modes of the transmission grid, i.e., the ones which involve the largest number of generators. For an HVDC inserted in a meshed AC grid as it is the case for the recent interconnection reinforcements in Europe (like, e.g., France-Spain and France-Italy links), inter-area modes which are controllable with the HVDC converters may be at a higher frequency, around 1Hz (i.e., may concern a limited number of generators in the neighbor zone of the HVDC). In this range of frequency, other types of modes exist: local modes, electric coupling modes or general electric modes linked to other electric phenomena. All these types of modes can be put into evidence by systematic modal analysis of the AC grid. However, for the control, specific cautions must be taken as detailed in next chapter.

1.3.1 The effect of inter-area oscillation on stability and damping solutions

Inter-area oscillation seriously affects the small-signal stability of the system, which greatly restricts the transmission capacities of the power system through critical corridors. For example, in December 2016, East-West inter-area oscillation were damped by damping the power transient of the France-Spain HVDC interconnection.

If they are not properly damped, such oscillations may lead to system disassembly, thus affecting the safe operation of the entire power system (Rogers 2012; Padiyar 2012; Ustinov, J. Milanović, and Maslennikov 2002; Anderson and Fouad 2008).

From the dynamic control point of view, oscillation can be damped by installing additional damping controller on existing generators, HVDC converters or FACTs devices. This method only needs to perform auxiliary design on the basis of the original voltage controller, which is convenient for project realization and relatively low cost. Therefore, damping control is one of the effective means to solve the problem of inter-area and local oscillation in the power system. Thus, studying the design methods and control strategies of additional damping controllers for PSS, FACTS, and HVDC links is of great significance for improving system stability. These solutions are detailed in the following section.

1.4 Research status on inter-area oscillation damping control

There are mainly two types of damping controller: one is in the excitation system using an additional signal and the design of the additional damping controller like PSS, the other are installed on the HVDC and FACTS equipment as the additional damping loops.

1.4.1 Devices-based control strategies

1. **Generator-based control** The traditional PSS, with its fixed structure and parameters, is the most widely used controller in the power industry today. The control input of the PSS can be the rotor speed deviation $\Delta\omega$, the accelerating power deviation ΔP, the frequency deviation Δf of the system, or a combination of one or more of these signals. The main parameter design methods are phase compensation method and eigenvalue configuration method (« IEEE recommended practice for excitation system models for power system stability studies (ieee std 421.5-2005) » 2005). The phase compensation method first calculates the open-loop phase of the residue of the mode to be damped and compensate it to 180°. Next the gain of the PSS is computed to provide the desired damping of the oscillatory mode. For the eigenvalue configuration method, the position of the eigenvalue in the complex plane is determined by the desired damping ratio, usually, several parameters are fixed first, and then other parameters are obtained by relying on the eigenvalue equation and the desired eigenvalue.

2. **FACTS-based control**
   FACTS equipment mainly includes Static Var Compensator (SVC), Thyristor Controlled Series Capacitor (TCSC), Static Synchronous Series Compensator (SSSC), Static Synchronous Compensator (STATCOM), etc,. Each type of FACTS damping controller is constituted by attaching a damping controller to the main control of each device. Although the main control structure of various FACTS devices is different, the structure and principle of their damping controllers are generally the same, and similar to that of PSS. With more and more FACTS devices applied to the power system, FACTS damping controller design and coordination between FACTS damping controller and PSS has become a current research hot spot.

   FACTS damping controller control method and PSS design method is basically the same, mainly the use of phase compensation method design of the conventional fixed structure of additional damping controller (S. Lee and C.-C. Liu 1994), combined with specific approaches for the tuning of parameters, like, for example robust control theory (X. Yu, Khammash, and Vittal 2001; Simões et al. 2009) or on artificial intelligence (Al-Alawi and Ellithy 2000; J. Lu, Nehrir, and Pierre 2004).

3. **HVDC-based damping control**
   The Western Pacific HVDC system installed in the United States in the middle of last century, adopted power modulation function to reduce the oscillations of the system. In particular, the increasingly widely used VSC-HVDC can effectively improve the system's ability to resist small disturbances due to their independent decoupling control of active and reactive power (Pipelzadeh, Chaudhuri, and Green 2012; H. Latorre, Ghandhari, and Soder 2006; Robin Preece and Jovica V Milanović 2013).

1.4.2 Oscillation modes identification techniques

Studying inter-area oscillations and taking appropriate measures to suppress them all rely on effective analytical tools. Normally, the first stage in designing a wide-area damping controller is to identify the oscillation modes which can be damped by the control. This is a very important issue as failures at this stage would result in inaccurate damping actions of the controller or even amplification of the oscillations.

The modal analysis is the most used method to determine the nature of the different types of oscillation modes (including coupling modes aforementioned) for wide-area systems. It separates different types of modes that are mixed with each other in time-domain simulation. Moreover, it allows using linear control techniques. The oscillations analysis method is the eigenvalue analysis method, and it is also the most widely used method in the small disturbance stability analysis. The basic steps are to linearize the system around an equilibrium point to obtain the system state equation matrix, and then the eigenvalues can be obtained to analyze modes of oscillations along with damping ratios, participation factors, and sensitivities against various system's parameters. The critical step of this method is the eigenvalues computation. Currently, there are basic methods for finding eigenvalues: one is to find the solution of all eigenvalues (the representative method is the QR method). This method can find all modes of the system at once, but it cannot be used for large systems with more than 200 state variables. If the number of variables is too high, the problem of "dimensionality disaster" will occur. For large systems, some well-chosen eigenvalues can be computed to deal with this problem. The representative method is Selective Modal Analysis (SMA) (Rouco and Perez-Arriaga 1993). Other methods of this type also are Analysis of Essentially Spontaneous Oscillations in Power Systems (AESOPS) (Byerly, Bennon, and Sherman 1982; Kundur et al. 1990; Sauer, Rajagopalan, and Pai 1991), S matrix method (Uchida and Nagao 1988), improved Arnoldi method (Wang and Semlyen 1990; B. Lee et al. 2003), dominant pole iteration method (Martins and Quintão 2003) and JACOBI-DAVIDSON method (Du, W. Liu, and Fang 2006). The eigenvalue analysis method should also provide information for the controllers to synthesis like, e.g., the compensation phase of the PSS from the frequency of the transfer function between the excitation system input and the speed of the synchronous generator.

There are also other signal-based analysis methods, like Prony analysis (C. Lu et al. 2012): this is an extension of the Fourier analysis method. It can directly estimate frequency, but measurement or communication noise severely affects the performance of this method; Hilbert-Huang Transform (Laila et al. 2009): the problem of this method is the computation burden; and a numerical algorithm for subspace state-space system identification called Stochastic subspace identification (Eriksson and Lennart Soder 2011).

In this research, SMA was selected as the method to compute the modes in the test system.

1.4.3 Reduction of the open-loop model of the power system for controller design

Normally, a realistic power system nowadays has more than 1000 state variables and the studied benchmark system in this thesis has also high orders (724) if full modeling is done. Thus, a large-scale representation of the grid should be considered and it is desirable to reduce the order of the system to design the controller. Reduction model strategies were studied in the literature as the following:

— **1.** Balanced Schur reduction method (Rimorov, Innocent Kamwa, and Joós 2015)
— **2.** Balanced realization state truncation (Chaudhuri and B. C. Pal 2004)
— **3.** Curve fitting method (Peres, Júnior, and Passos Filho 2018)
— **4.** Nonlinear model reduction (Qi et al. 2016)

In this research case, the above standard approaches cannot be used because of the size of the system. Curve fitting method in (Leyla Arioua and Bogdan Marinescu 2015) captures the grid dynamics into a reduced-order control model in the whole frequency range around the frequencies of the inter-area modes to be damped is suitable for this case.

1.4.4 Different control strategies

— **Phase compensation**
This is a classic way to tune the parameters of standard IEEE PSS structure like PSS2A and PSS4B to damp multiple different frequencies modes (Rimorov, Innocent Kamwa, and Joós 2015) (Peres, Júnior, and Passos Filho 2018). This method has limitation for multiple modes, if they are not well separated in the frequency band. This is the case in the case of an HVDC link inserted in a meshed AC system studied here.

— **Robust control techniques for damping control:**

1. Linear Quadratic Gaussian (LQG)
   The LQG control problem is one of the most fundamental optimal control problems. It concerns linear systems driven by additive white Gaussian noise. The problem is to determine an output-feedback law that is optimal in the sense of minimizing the expected value of a quadratic cost criterion. Output measurements are assumed to be corrupted by Gaussian noise and the initial state, likewise, is assumed to be a Gaussian random vector (Rimorov, Innocent Kamwa, and Joós 2015) (Preece et al. 2011).

2. (H_2/H_∞) control based on Linear Matrix Inequality (LMI) techniques
   The most important and traditional robust control technique is H_2/H_∞ control. H_∞ control maintains system robustness. H_2 control can handle stochastic aspects such as

measurement noise, random disturbance. So there are researches on mixed H_2/H_∞ techniques (Bensenouci and Ghany 2007; Chilali and Gahinet 1996; Mondal, Sengupta, and Chakrabarti 2012; Ke and Chung 2012). This method minimizes the sensitivity of a system over its frequency spectrum, and this guarantees that the system will not greatly deviate from expected trajectories when disturbances enter the system (Zhou, Doyle, Glover, et al. 1996).

The LMI methodologies, which are computationally simple and numerically reliable for solving convex optimisation problems (Boyd et al. 1994; Dullerud and Paganini 2013; Pascal et al. 1995; Iwasaki and Skelton 1994; Scherer, Gahinet, and Chilali 1997), are effective tools for robust controller design of linear uncertain systems. H_∞ controllers can be synthesized using LMI (Chilali and Gahinet 1996), (Scherer, Gahinet, and Chilali 1997) which results in imposing poles to belong to specified regions of the complex plane. This provides the possibility to directly specify and take into account in the controller synthesis the desired damping of the inter-area modes to be damped. This is the main performance specification for the HVDC POD control. The LMI framework was already used for damping specification in TCSC control (Mondal, Sengupta, and Chakrabarti 2012). This control technique can handle multiple modes, and through adding constraints, the reasonable desired damping ratio can be achieved.

Recently, some attempts have been made to design robust dynamic output-feedback controllers (Kanev et al. 2004; Kose and Jabbari 1999; Mahmoud and Xie 2000; Suplin and Shaked 2005; VanAntwerp and Braatz 2000; Xie, Fu, Souza, et al. 1992), either for norm-bounded uncertainty or polytopic uncertainty based on LMI methodologies. The model-matching is a method which force the closed-loop to provide a desired dynamics. This is achieved by minimizing the gap (H_∞ norm) between a reference model and the one of the closed loop system. Model-matching controller schemes via static and dynamic output-feedback are proposed in this thesis to reduce the conservatism of the classic ones, that is, Robust Static Output-error Feedback Controller (RSOFC) and Dynamic Decoupling Output-feedback Controller (DDOFC) based on reference model. Sufficient conditions are derived for robust stabilization in the sense of Lyapunov asymptotic stability and in the format of LMIs to obtain H_∞ RSOFC and DDOFC gains based on a well designed reference model.

3. **Model Predictive Control (MPC)**
   MPC (see e.g., (Papangelis et al. 2017)) is an advanced method of process control that can be used in the balancing model. MPC allows real-time optimization against hard constraints. However, it typically solves the optimization problem in smaller time windows

than the whole horizon and hence obtains a suboptimal solution.

4. **Non-linear control techniques**
   In wide-area damping control applications, these methods show promising results especially in the case of large perturbations. One of them is slide mode control (Liao et al. 2016). However, the complexity and size of the power systems limit applications of this method (Padhy, Srivastava, and Verma 2011).

5. **Fuzzy Logic Control (FLC) method**
   FLC method (Padhy, Srivastava, and Verma 2011) (Mokhtari et al. 2012) (Bakhshi, Holakooie, and Rabiee 2017) has strong robustness against variations of input signals and system operating conditions. There are several papers combining FL with LMI like (Soliman and El Metwally 2017) or comparing FL and H_∞ like (Tayal and Lather 2015). In (Bakhshi, Holakooie, and Rabiee 2017), a fuzzy logic POD has been proposed for a power system. The research (Liao et al. 2016) has derived a nonlinear control methodology for canceling out the effects of the oscillations in the electricity network with HVDC.

6. **Artificial intelligence**
   There are also some other researches based on artificial intelligence methods such as Neural Network (Ray and Venayagamoorthy 2008), genetic algorithm (Do Bomfim, Taranto, and Falcao 2000), and Bacteria Foraging algorithm (Tripathy and Mishra 2015).

Although these advanced controllers have shown good performances, they may be affected by unstable zeros in the open-loop system. These kind of zeros have been systematically put into evidence for application in this thesis as discussed in the next chapter.

1.4.5 The other research aspects

— 1. Input and output signals selection
   Wide Area Measurement System (WAMS) are systems which can collect data from various points within a large interconnected network to provide greater observability of any inter-area oscillations. These measurement systems use Phasor Measurement Units (PMUs) to collect time-stamped data which can be used to significantly improve the damping of inter-area oscillations (Aboul-Ela et al. 1996; Innocent Kamwa, Robert Grondin, and Hébert 2001; Sanchez-Gasca et al. 1989).
   Thanks to the developing of these measurement systems, the class of input and output signals used for the POD controller can be enlarged and this directly affect the effectiveness of damping control can be selected as the following methods.

There are some techniques to select input and output signals:

— a. Transfer function residue method (Belhocine, Marinescu, and Xavier 2017).

— b. Geometric method

This approach depends on geometric measures of controllability and observability (Heniche and Innocent Kamwa 2008).

— c. Hankel Singular Values (HSV)

This can be done by transferring the linearized system to a balanced realization. The choice of the input-output combination depends on HSV value: larger HSV value shows higher controllability and observability properties.

— 2. Coordinate HVDC POD control loop with other loops (Li et al. 2012)

The impact of this control loop on the other loops (i.e. PSS of neighbor generators, the other FACT devices) should be considered.

1.5 Control difficulties in the considered formulation

1.5.1 Unstable zeros

A non-minimal phase system is a system that has zeros in the right half of the complex plane. These zeros are called unstable zeros in control theory. It is well known that unstable zeros can degrade the performance of the control systems. Especially, they bring some delays to the system making the closed-loop system to be unstable in large gains (Hoagg and Bernstein 2007), (Zhou and Doyle 1998). The appearance of unstable zeros in HVDC links has been reported in the literature (Zhang, Harnefors, and Nee 2011). However, there is little work about why and how the unstable zeros appear in the HVDC links inserted into a AC grid. As a consequence, it is important in both research and practice to do an analysis of the parameters of the grids with HVDC links to highlight their effects on the unstable zeros. In this thesis, the first research objective is to detect the existence of unstable zeros in HVDC links embedded into AC grids and to develop a method to cancel out their effects.

Subsequently, in Chapter 3, the sensitivity analysis of unstable zeros is done on two realistic zones of the European electricity network with different types of HVDC links. This investigation shows that this power system exhibits non-minimum phase behavior. To investigate the existence of unstable zeros furthermore, a simple benchmark system equipped with an HVDC link and 5 AC lines which can reproduce all the AC grid situations, is built. In this system, the most important parameters that determine the existence or non-existence of unstable zeros are found as the length of the AC transmission lines. This means that unstable zeros depend on the topology of the network.

Since the traditional Zero Phase Error Tracking Control (ZPETC) (Tomizuka 1987) aims to track the command signal, they put the characteristic equation of the system followed by the mirror of system unstable zeros in the numerator of their transfer functions. Thus, a non-proper

transfer function generally results in the structure of the standard ZPETC. However, it is well known that non-proper transfer functions are very sensitive to noises and external disturbances. Furthermore, such improper expressions should be implemented by a series of derivative blocks which is quite hard to be achieved in practice. To overcome this problem, a Modified Zero Phase Error Compensator (MZPEC) as a supplementary feed-forward controller to the POD controller is proposed in Chapter 3 to decrease the non-minimum phase behavior of the system responses. In order to verify the effectiveness of the MZPEC, a classic POD (i.e., vector control (« IEEE recommended practice for excitation system models for power system stability studies (ieee std 421.5-2005) » 2005)) is selected as an example to show the effectiveness.

1.5.2 Robustness issues

Besides unstable zeros, the problem becomes more complex when plant parameters are uncertain. The parameter uncertainties may come with the change of environment on grid (line/generators trips or load changes) or on HVDC side (temperature change, pressure change, etc.). They make the values of the parameters of the control model deviate from the nominal values and may worsen system performance or even cause instability of the system. The mentioned parameter uncertainties may be considered to be measurable or unmeasurable depending on the implementation of sensors. For instance, the temperature change can be measured by thermal sensors. Some other parameter changes such as the resistance change of a power converter, aging of components, and measurement errors are difficult to measure and are treated as unmeasurable parameter uncertainties. Moreover, the parameter uncertainties will become unmeasurable if sensors cannot be used due to some physical constraints or cost considerations. In addition, in many applications, modeling errors in plant models are inevitable. For preciseness, a design technique must accommodate these errors and uncertainties to be practically feasible. Thus, robust control must be adopted to deal with the uncertainties produced by operation point changing in the power system and modeling errors caused by modeling and reduction for the realistic power system.

1.6 Global approach of this thesis and main contributions

1.6.1 Global approach

Motivated by facts aforementioned, a large-scale nonlinear benchmark model that has unstable zeros behavior has been developed as a test system. To develop the advanced robust supplementary POD controllers for the test system, the *nonlinear full model* of this system is linearized around an equilibrium point with Eurostag software (Meyer and Stubbe 1992) to obtain the *linearized full model* of the same order. Advanced controls (robust H_∞, H_2, LQG or LMI pole placement) have already been proposed to improve performances and robustness of grid-connected power electronics as, for example, in the research studies (Vance, A. Pal, and Thorp 2012; Zolotas et al. 2007; Robin

Preece, Milanovic, et al. 2013; Chaudhuri and B. C. Pal 2004; Kotb et al. 2017). This kind of control usually needs a state representation of the system (Skogestad and Postlethwaite 2007). Since the target is higher frequency inter-area modes which are closed to other different nature modes, the standard reduction methods discussed in the last section are no longer suitable for this research case. The large-scale state representation becomes difficult due to the fact that all interested dynamics must be integrated.

In literature (Bogdan Marinescu and Petesch 2014), a methodology to capture the grid dynamics into a reduced-order control model in the whole frequency range around the frequencies of the inter-area modes to be damped is proposed. The same methodology is adopted in this work but for the context of oscillations damping by VSC-HVDC power modulation. This is a way to simultaneously detect and consider the modes to be damped (as a target of the POD controller) and the other modes of the grid which may be affected by the POD controller. Based on this model which carefully integrates the dynamics of interest, several robust controllers for the HVDC link are designed to damp inter-area oscillations and enhance the robustness. The whole process of this research is shown in Fig. 1.1.

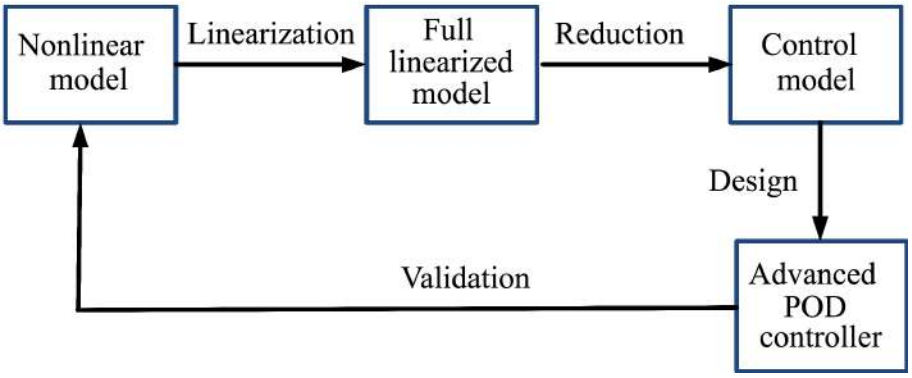

Figure 1.1 – The process of this research.

To be more precise, based on the control model, first, a controller based on the LQG robust control framework is designed as a basis of comparison. Another comparative controller design has been carried out based on the H_∞ mixed-sensitivity formulation in an LMI framework with pole-placement constraints.

Finally, a model-matching Robust H_∞ Static Output-error Feedback Controller (RSOFC) and model-matching Dynamic Decoupling Output-feedback Controller (DDOFC) are proposed. Sufficient conditions are derived for robust stabilization in the sense of Lyapunov asymptotic stability and are formulated in the format of LMIs to obtain H_∞ RSOFC and DDOFC gains based on a reference model. Investigations with the nonlinear model of the system were done to settle and validate the approach. The efficiency and robustness of the proposed controller are tested and compared with each other.

Comparative studies are carried out on a realistic test grid as investigations between different approaches in the application chapter. Also, the advantages of each controller are put into evidence in the analysis.

1.6.2 Main contributions of this research

The work within this thesis contributes to a number of areas of power systems research, specifically surrounding the effects of HVDC systems on the small-disturbance stability of transmission networks. The main outcome of this research is the comprehensive systematic assessment of the improvement to power system small-disturbance stability that can be achieved through the use of supplementary damping control applied to HVDC systems. Assessment of the robustness of these controllers has in turn guided the controller synthesis procedure, resulting in improved system performance in the presence of operational uncertainties.

The contributions of this thesis can be summarised as follows:

— According to the realistic test system, an effective and economic way to build a suitable and low-order control model is proposed.

— This research analyses the relationship between system topology and unstable zeros. Based on these results, the unstable zeros are proven to naturally and systematically exist in certain conditions of the HVDC line inserted in AC grid system.

— A model-matching robust H_∞ static output-error feedback controller and a model-matching robust H_∞ dynamic decoupling output-feedback controller is proposed to improve the damping and maintain robustness to face the different operation points along with the influence of the unstable zeros. The different control frameworks like LQG, mixed sensitivity H_∞ are designed for the benchmark to compare with the proposed controllers.

Chapter 2

Power system modeling and problems formulation

Contents

2.1 Introduction

The stability problems are formulated in a benchmark embedded HVDC system, and the benchmark model is introduced in this chapter. The original nonlinear system is linearized around an equilibrium point to obtain a linear system to do the eigenvalue analysis. The HVDC model and the method to select the input signals of the POD controller are introduced in Sections 2.2 and 2.4.

2.2 HVDC models

Fig. 2.1 depicts the considered VSC-HVDC which uses Insulated Gate Bipolar Transistors (IGBTs). It has seen rapid development in recent years and overcomes many of the shortcomings of Line Commutated Converter High Voltage Direct Current (LCC-HVDC). There are some advantages (Arrillaga, Y. H. Liu, and Watson 2007; Reed, Pape, and Takeda 2003; Ming et al. 2004):

— VSC-HVDC is presently competitive in terms of converter station losses and costs. Until recently this was not the case and VSC-based systems was rarely selected for HVDC projects due to high costs.

— The VSCs display very low harmonic content, in some cases removing the need for filters entirely.

— VSC-HVDC systems are capable of providing reactive power support at each converter station—whereas LCC-HVDC demands reactive power support.
— VSC-HVDC lines can be connected to weak or even passive AC networks, supporting black start situations.
— Point-to-point VSC-HVDC lines can be easily extended into multi-terminal HVDC grids due to the constant voltage polarity during bidirectional power flow.
— The development of VSC-HVDC systems into modular designs has also meant that converter stations can be delivered fully assembled to the site allowing fast installation and testing (ABB 2008).
— VSC-HVDC systems however cannot operate at the same power levels as the more mature LCC-HVDC and are currently limited to 500 kV and 1500 MW (Arrillaga and Arrillaga 1998).
— The smaller footprint of VSC-HVDC converter stations, as well as the ability to provide reactive power support, enables their offshore placement.

The high-frequency switching operation of the power electronics is neglected, and each converter is modeled as an injector (current or power). Two degrees of detail are considered here: first one, called *HVDC model I*, in the sequel, consists of the harmonized Electromagnetic Transient (EMT) and transient model of injections (Meyer and Stubbe 1992). The second one called *HVDC model II* in what follows, is a simplification of the first one in order to capture only lower frequency behavior for transient dynamics. Then, the voltage source whose magnitude U_{ac} and phase angle θ can be controlled. P_1, P_2 and Q_1, Q_2 are active and reactive powers exchanged with the power system respectively.

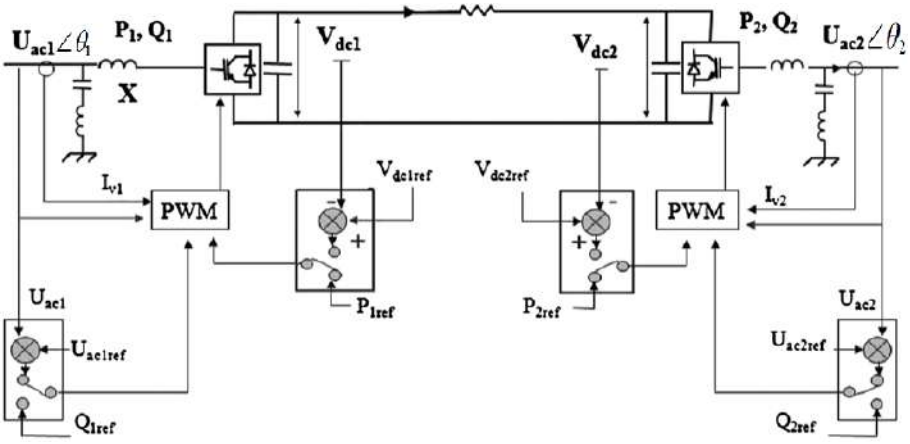

Figure 2.1 – HVDC model.

2.3 Test system

Consider an HVDC transmission line inserted into an AC grid as shown in Fig. 2.2. The situation becomes particular when the AC grid is highly meshed. As aforementioned in Section 1.3, when such high-frequency inter-area modes should be damped, specific cautions should be taken for the regulator to not disturb the other above mentioned modes in close frequency. Mainly, the *control model* (to take into account not only the modes to be damped but also the other modes) and *robustness* against neglected dynamics (which are at higher frequencies) should be improved. Such control model consists of HVDC dynamics and main dynamics of the grid (the ones related to the modes of interest). It consists in transfer matrix $H(s)$ of Fig. 2.4 and 2.5. It is much more difficult to be defined/extracted from the combined HVDC and AC grid model which is a large-scale model.

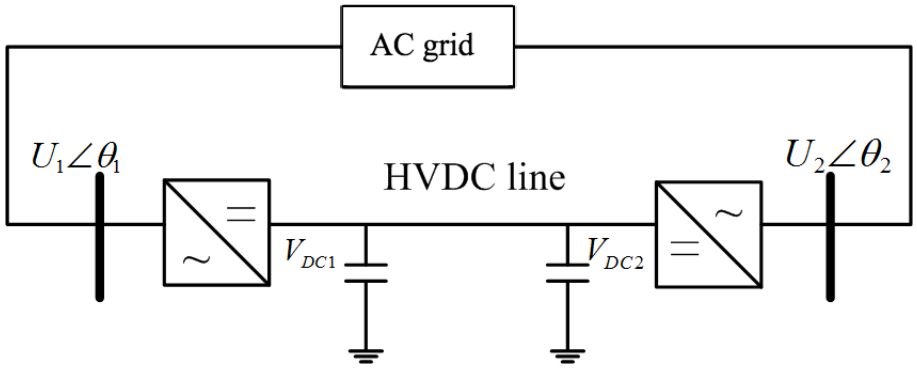

Figure 2.2 – HVDC inserted in an AC grid.

The benchmark proposed in this work is a model that sums-up these problems. It is composed of an HVDC line (HVDC model I) inserted in an AC grid composed of 19 generators (Fig. 2.3 shows the part of them). All generators are equipped with Automatic Voltage Regulator (AVR) and PSS. The full nonlinear model of this system, which is of order 724, is linearized around an equilibrium point with Eurostag software (Meyer and Stubbe 1992) to obtain the called *full linear model* of the same order. This is a benchmark with formerly mentioned particularities.

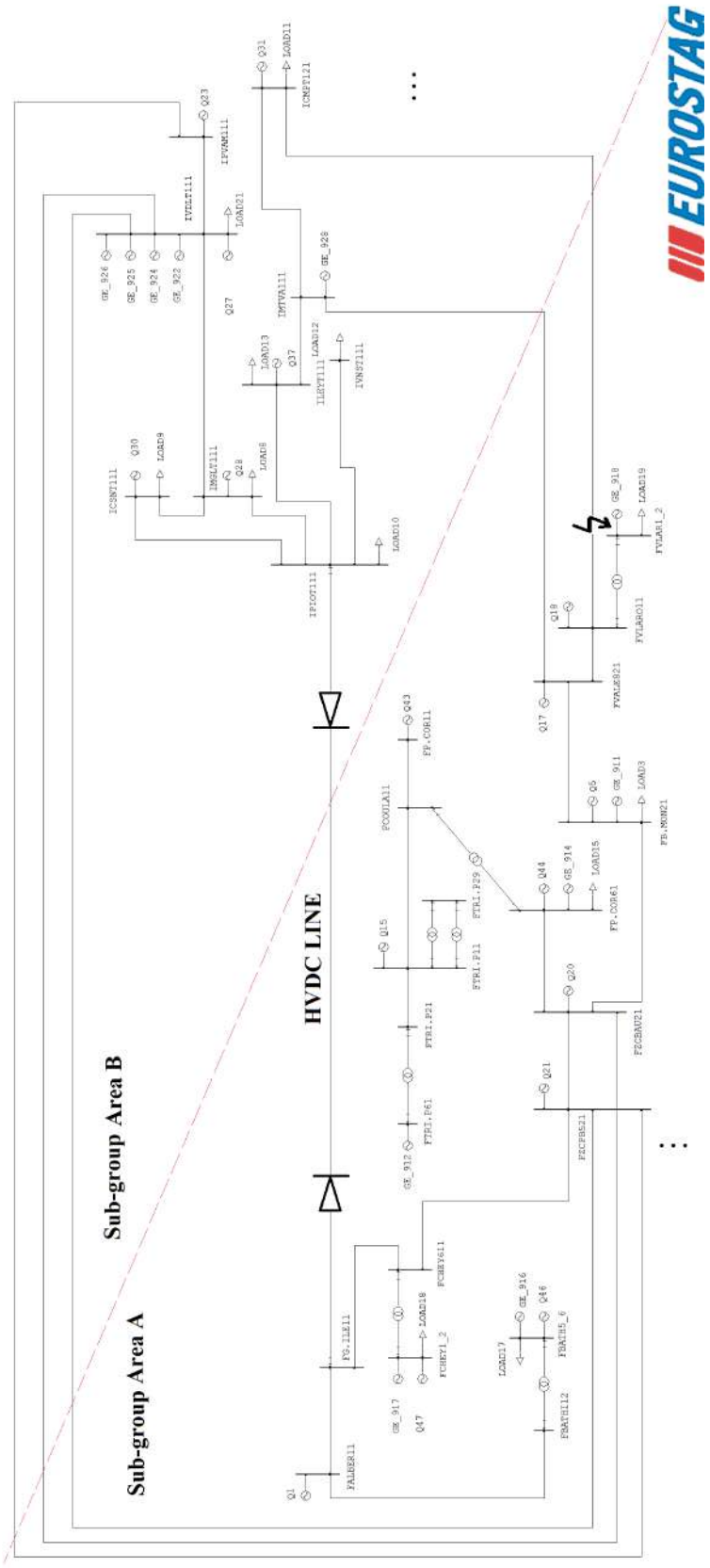

Figure 2.3 – Sub-diagram of the network benchmark model.

Generally, it is desirable to have high controllability and high observability degrees of an oscillation mode to achieve high damping. Such that, the modes which can be damped via HVDC control are the ones highly *observable* and *controllable*, i.e., which have high *residues* (see Appendix B for more details) in the open-loop transfer $H(s)$ in Fig. 2.4 and 2.5. In other words, only the modes of the grid which have high residues in the transfers of the HVDC line can be damped by power modulation of the latter link. Table 2.1 provides the highest residues modes found in the full linear model. For each mode (characterized by its damping and frequency), most participating machines are reported in the table and categorized into two sets ('+' and '-') of generators oscillating against each other. For example, the most participating generator to mode 2 is GE_911 and the second one is GE_917. These two machines are swinging against each other. This is concluded from the difference of the phase of right eigenvector components of the mode which corresponds to the machine angles, which is close to 180°. This mode is an *inter-area mode* as it involves two coherent groups of generators swinging against each other at a low-frequency. The magnitudes of participation factors evaluates the contribution of each generator to the modes. For instance, 100% in the list means this generator is the most participating machine of this mode. The injectors of HVDC are involved in each of these modes in this table. But, as their participation factors are not the highest one, thus, they are not shown in this table.

Table 2.1 – The linearized model

No.	Mode	Damping ξ (%)	Freq. (Hz)	Mode shape (participation mag (%))		Residue	
				+	−	ABS MAG	Phase
1	-1.62+j8.19	19.5	1.30	GE_914 (100)	GE_913 (32.4)	0.0157	35.0
2	**-0.24+j5.53**	**4.5**	**0.88**	**GE_911 (100)**	**GE_917 (68.8)**	**0.0181**	**83.4**
3	-0.53+j5.29	10.1	0.84	GE_917 (100)	GE_918 (55.1)	0.0129	-56.2
4	-0.40+j4.79	8.3	0.76	GE_918 (44.3)	GE_912 (100)	0.0038	-33.3
5	-0.33+j3.29	10.1	0.52	GE_915 (100)	GE_918 (17.7)	0.0121	104.5
6	-18.83+j7.21	93.3	1.14	GE_921/922 (100)	GE_923/924 (74.1)	0.0034	14.5
7	-1.54+j6.55	22.9	1.04	GE_914 (100)	GE_911 (68.3)	0.0125	151.5
8	-19.32+j6.47	94.8	1.03	GE_921 (100)	GE_922 (37.6)	0.0117	118.9
9	-20.33+j4.86	97.2	0.77	GE_921/922 (84.5)	GE_927 (100)	0.0026	-168.1
10	-18.72+j3.35	98.4	0.53	GE_913 (33.4)	GE_912 (100)	0.0072	136.1

From Table 2.1, it can be seen that mode 2 has poor damping (4.5%) and the operation of the system in the presence of a lightly damped inter-area mode is a serious issue and has to be considered in the control design phase. Besides, notice that this inter-area mode is at 0.88 Hz and several modes (highly damped (6 to 10) or poorly damped (1 to 5)) are at frequencies close to this one.

It should be highlighted that mode 8 is not an inter-area mode since related generators (GE_921, GE_922) swinging against each other are in the same area and connected to the same bus. It is a so-called *local mode*.

The pattern of oscillation of mode 2, the less damped one, corresponds to area A and B indicated in Fig. 2.3.

2.4 Control scheme and input signal selection

According to (Henry et al. 2013), the embedded HVDC system can perform not only the basic function of bulk power transmission but also, importantly, some additional control functions within the AC network such as power flow control, voltage control, system stability improvement.

The basic regulation loops called *first-level control* are to control the HVDC converter to fulfill local objectives (like control the voltage, current and power transmission) (see details in Appendix A). The POD studied in this thesis is a supplementary control called *second-level* controller which is devoted to power modulation to damp inter-area modes (see Fig. 2.4).

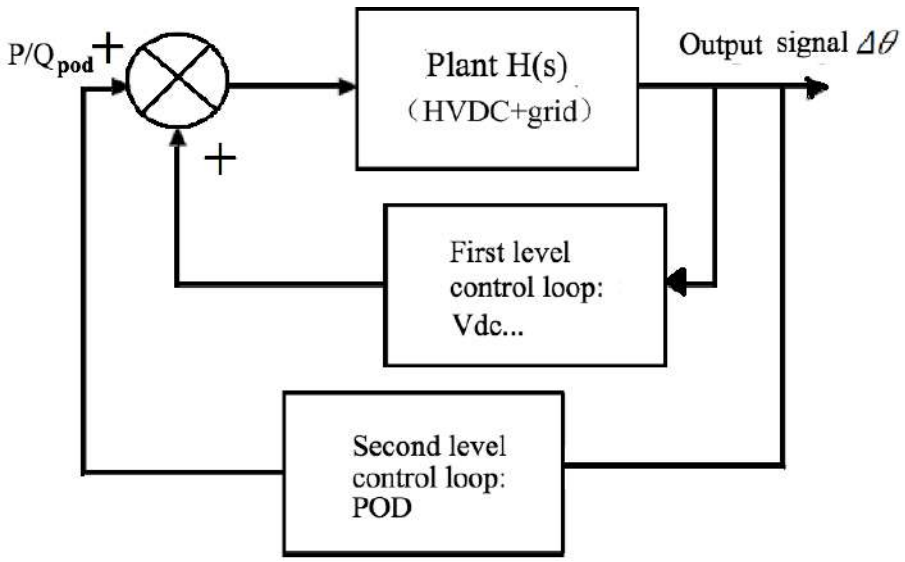

Figure 2.4 – Control loops for HVDC link.

The input signal selection is important to the effectiveness of the POD controller. According to (Belhocine, Marinescu, and Xavier 2017), the suitable input signals are the ones which provide high residues of the modes to be damped in transfer $H(s)$. The definition of residue and details are given in Appendix C.

In this benchmark, the terminal angle difference, $\Delta\theta = \theta_1 - \theta_2$ has the highest residue value, and, as a consequence it is selected as the input signal of POD controller to provide power (active power P and/or reactive power Q) modulation. In Chapter 1, the reactive power Q modulation POD controller is considered to smoothly compare the effectiveness between different control synthesis. After that, in Chapter 6, a coordinated P/Q modulation controller will be designed and tested.

2.5 Classic POD and its limitations

The classic POD implemented here is the current controller typically employed. First, the principle and structure of classic POD are recalled.

The classic IEEE HVDC POD controller (« IEEE recommended practice for excitation system models for power system stability studies (ieee std 421.5-2005) » 2005) has the same structure as the PSS for generators, which contains a gain K, a wash-out filter, and n phase lead-lag blocks (Fig. 2.5). It is defined by the following transfer function

$$H_{POD}(s) = K\left(\frac{T_w s}{1+T_w s}\right)\left(\frac{1+T_1 s}{1+T_2 s}\right)^n \tag{2.1}$$

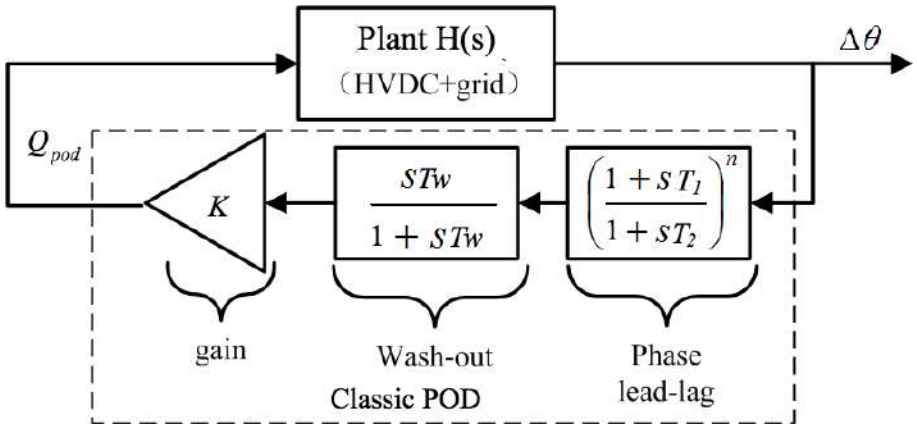

Figure 2.5 – Structure of classic POD.

The washout filter is usually used in practice as an interface between the measured signal and the used one in the control loop to wash out (reject) the steady-state component of the measures while passing transient ones (Hassouneh, H.-C. Lee, and Abed 2004). The classic tuning of the parameters K, T_1, and T_2 consists of two steps (see, e.g., (Rouco 2001)) :

— *i)* Compute T_1 and T_2 in order to compensate the phase of the residue of the mode to 180°.

— *ii)* Adjust the gain K to obtain the desired damping.

This methodology can be precisely implemented for one mode and it can be approximately extended to multiple modes (multi-band POD) (Kamwa, Grondin, and Trudel 2005). However, only the residue of the mode to be damped in the plant is used as information from the grid. And in a situation like the one presented above, interactions with the modes having close frequencies may lead to poor results. In this approach, the higher desired damping means higher gains in the control loop, and this may give the opposite results. Table 2.2 and Fig 2.6 shows that the relationship of the desired damping with obtained damping in the closed-loop. From 6 % of desired damping, the obtained damping increases from around 6% to around 7% and after decreases.

According to Table 2.2 and Fig 2.6, indeed, this is put into evidence on this test system when

Table 2.2 – The relationship between desired damping and actual damping in the full linearized system (classic POD)

Desired damping (%)	6	7	8	9	10	11	12	13	14	15
Actual lowest damping (%) in full model closed-loop	6.1	6.3	6.5	6.6	6.9	5.9	5.8	5.7	5.55	5.45

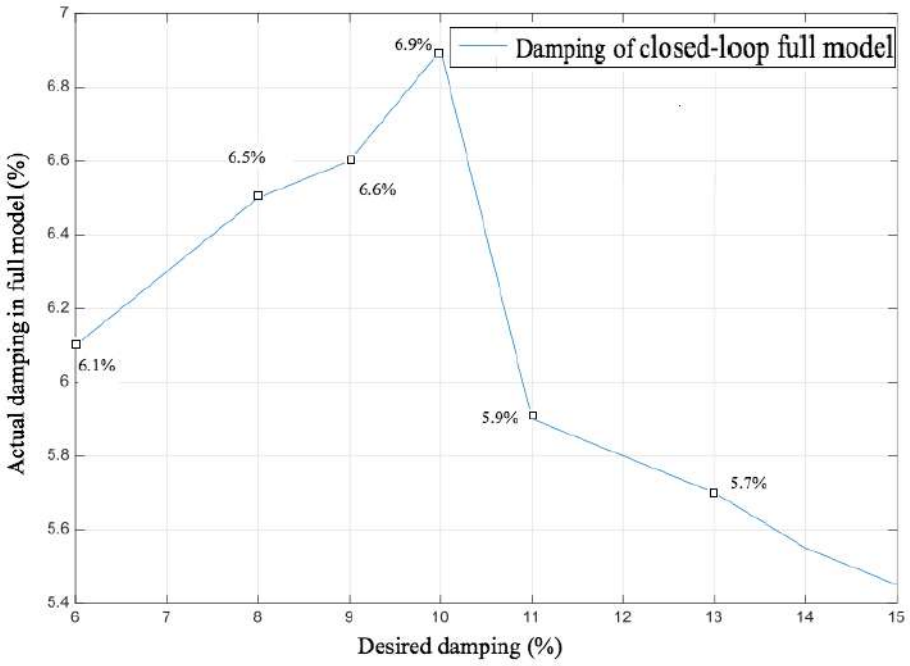

Figure 2.6 – Relationship of actual damping with desired damping (classic POD).

a target damping of 10% was fixed for mode 2. The tuned parameters according to this desired value of classic POD are shown in Appendix D. However, using this tuning approach, the obtained damping of this mode is only about 6% as reported in Table 2.3 which is much below the tuning target of 10%. It should be noted that the damping of mode 1 is improved, even this is not the target of the designed POD controller. This is due to the fact that the phase compensator of the POD compensates the residue phase of mode 1 close to 180°. Despite the fact that this can be considered as an advantage, it may act also in the opposite way as the case of mode 4.

The classic IEEE damping controller design synthesis (« IEEE recommended practice for excitation system models for power system stability studies (ieee std 421.5-2005) » 2005) is simple but tends to lack of robustness even after careful tuning. To overcome these difficulties, a state-space method that takes into account all involved dynamics (interacting modes at a specific range of frequencies) is used as explained in the next chapter to design the advanced controllers. Also, the robustness against changes of the grid of the pole placement can be improved by the formalism

Table 2.3 – Comparison of damping of modes

No.mode	Damping without POD (%)	Damping of modes with classic POD (%)
1	19.5	30.5
2	4.5	6.1
3	10.1	12.0
4	8.3	8.1
5	10.1	12.4

below which has also the advantage to directly consider the damping target specification in the control synthesis.

2.6 Robustness

Robustness is the capability of a closed-loop to deal with mainly two classes of uncertainties of the model for which the control law is synthesized: variation of some of its parameters - called *parametric robustness* - and variation of the model structure itself - called *unstructured robustness*. In the case of power systems, in the first class, it can be included line trips, load or generation level evolution, or other changes that preserve the system dimension but vary the operation point of the grid. For the HVDC case, change of the (amount and direction of) transferred active power is in this class. A control model is a reduced representation that focuses on the dynamics of interest for the control. To be efficient and to lead to a small-size controller and easy to synthesize, the latter should be of small-size. All neglected at this stage dynamics of the system enter in the class of unstructured robustness. The regulator should be such that the closed-loop provides high *attenuation* of such dynamics. In this research case they may be due to more rapid (than inter-area modes) dynamics like the voltage/electric ones (voltage), speed/frequency disturbance (coming from load/production imbalance, oscillatory phenomena of other nature than inter-area modes, like, e.g., sub-synchronous oscillations, higher-order harmonics, etc,.), noises (as disturbance signals generated by high-frequency exogenous signals) or effect of transmission delays in the regulation chain. Indeed, in the transfer formalism, a delay modeled by $e^{-\tau s}$ can be viewed as neglected high-frequency dynamics if exponentials are approximated by rational transfer functions (i.e., Padé approximation).

Moreover, in the particular context considered here, as the modes to be damped are at higher frequencies and thus closer to the band of the un-modeled dynamics mentioned above, their attenuation is more difficult in the process of regulator synthesis.

2.7 Summary-problems formulation

VSC-HVDC was addressed in the particular context where the link is inserted in a meshed AC grid. The introduction of the benchmark model and the basic of the VSC-HVDC line, along with the oscillation modes are given. The reactive power modulation is chosen as first step to design the controllers as an investigation. The residue analysis is done to chose the supplementary power oscillation damping control input signal. The difference of two-terminal of HVDC lines angle is selected as the input signal for classic POD and the other advanced POD controllers in the following chapters. Some limitations of the simple lead-lag structure of the classic POD are put into evidence in the complicated operation situation of the meshed power grids. In the benchmark model, the trade-off between the robustness and performance of the classic POD is analyzed to tune the parameters.

In this research, there are main problems for the POD controllers listed below. Another problem of unstable zeros will be clarified in the next Chapter.

— *Control model synthesis*: As mentioned before, it should be stressed that in a highly meshed AC grid, the inter-area modes tend to be at a higher frequency range. In this range of frequency, other types of modes exist. Due to these facts, *robustness* against neglected dynamics and more accuracy reduced model *control model*, which takes into account all these dynamics should be improved.

— *Enhance robustness*: Uncertainty modeling error and uncertainties of a system like a load changing, etc,. in plant models are inevitable. Thus, for preciseness, a design technique must accommodate these errors and uncertainties to be practically feasible.

Chapter 3

Problem of unstable zeros

Contents

3.1 Introduction

In the control of non-minimal phase systems, it is necessary to suppress the negative tuning caused by the unstable zeros and reduce the adjustment time of the system. In particular, as the loop gain is increased, poles move toward zeros, and thus destabilization inevitably occurs in closed-loop when the open-loop transfer function has unstable zeros. Hence, feedback control systems have limited gain margin when the open-loop transfer function has unstable zeros, and thus limited gain margin implies a limitation on the performances of the closed-loop system (Hoagg and Bernstein 2007).

In this work, the existence of unstable zeros in the HVDC lines embedded into AC grids described in Chapter 1 brings difficulties to POD controllers. Because of this phenomenon, these unstable zeros should be investigated. This chapter aims to identify the existence of unstable zeros and to develop a method to cancel out their effects. Subsequently, the processes on two realistic power grids with two different HVDC models are examined to detect the possible unstable zeros in their dynamics. Accomplishing linear and nonlinear simulations in Matlab and Eurostag, the location of unstable

zeros is determined. Then, a benchmark model is used to identify the influence of the parameters of the power system on the occurrence of the unstable zeros. Finally, to avoid the harmful effects of these unstable zeros, a modified zero phase error compensator (MZPEC) is proposed, which is noise insensitive in the control loop.

3.2 Description of two types of test power grids

In this section, examples are given to study and quantify the unstable zeros.

Case I is the same large-scale system introduced in the previous chapter. To examine more deeply the existence of unstable zeros in practical power grids, another system called case II (the France-Spain network (Fig. 3.1)) which is presented in (Arioua and Marinescu 2016) is investigated. The case II system consists of 23 machines. It is represented by a detailed nonlinear model including generators along with their regulations. Only the high-voltage network 225 kV and 400 kV are modeled. The interconnection between France and Spain, which consists of four AC lines, is reinforced by adding a VSC-HVDC link of 65-km length with a nominal active power of 1000 MW and a rated pole voltage of 320 kV.

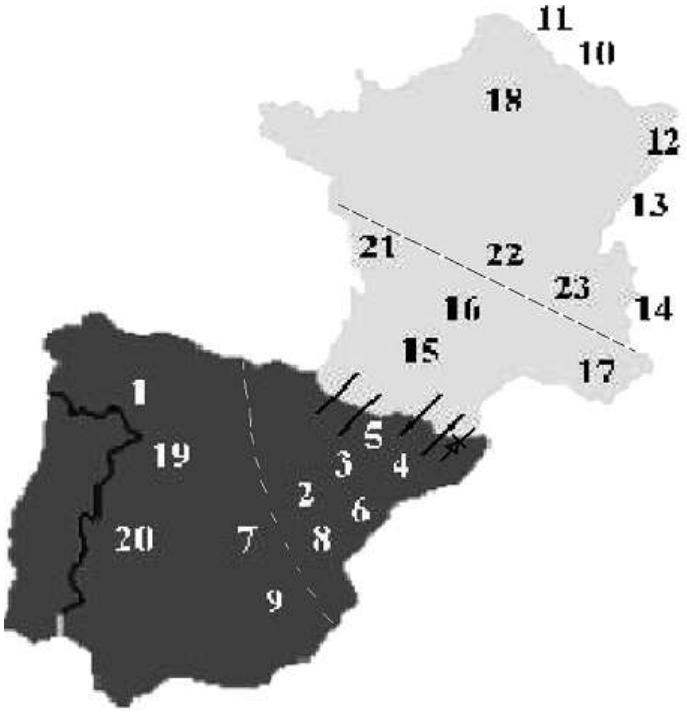

Figure 3.1 – France to Spain network.

To study the existence of unstable zeros in the grids, the cases are combined with two types of HVDC models (HVDC model I and model II in Section 2.2). The POD input signal (output

signal of plant) is chosen the same as in Chapter 2 ($\Delta\theta$) to the facilitated comparison. Two transfer functions of linearized open-loop system without any PODs, from active power P and reactive Q power modulation signal to $\Delta\theta$ are investigated. Unstable zeros are found in both of them as shown in Table 3.1.

Table 3.1 – Unstable zeros responses in the open-loop test systems

Cases	Unstable zeros/Non-minimum phase behavior (Transfer function from Q modulation to $\Delta\theta$)	Unstable zeros/Non-minimum phase behavior (Transfer function from P modulation to $\Delta\theta$)
Case I+HVDC model I	Yes/Yes	Yes/Yes
Case I+HVDC model II	Yes/Yes	No/No
Case II+HVDC model II	Yes/Yes	No/No

Cases in Table 3.1 show the combinations of different types of AC grid and different HVDC models. Non-minimum phase behavior in Table 3.1 is detected in nonlinear responses in accordance with this fact that within unstable zeros, the curve, in the beginning, goes in the opposite direction of the final value (Hoagg and Bernstein 2007). Each case in this table has this behavior. For instance, Fig. 3.2 shows the $\Delta\theta$ response to a step on the reference of Q modulation loop for Case I+HVDC model II. The curve goes in the opposite direction at $t = 2s$ compared with the final value. From Table 3.1, unstable zeros found with the linearized model are coherent with non-minimum phase behavior in nonlinear simulation responses. Another conclusion is that no-matter the model of the HVDC line, this phenomenon appears systematically for this kind of system (HVDC inserted in a meshed AC grid).

3.3 The impact of unstable zeros on POD controllers

Because of the existence of unstable zeros in the open-loop system, the effectiveness of POD controllers can be weakened even with some advanced controls.

To indicate this influence of unstable zeros, an example (classic POD) application is investigated on an example case (case I+HVDC model I). The parameters of classic POD is tuned to damp the mode 2 to the desired damping as 10 % as previously described in Chapter 1. From Fig. 3.6 (curves of $\Delta\theta$ response to steps on the reference of Q modulation loop in the linearized system), although the dampings of modes are improved a little, the desired damping is not achieved. Moreover, at $t = 2s$, curves have an overshoot which is a delay actually. With this kind of delay, the POD controller may lose effectiveness. Thus, it can be summarized that the system of HVDC link inserted in the AC grid may have unstable zeros which disturb the POD controller performance in the grid. So, a solution should be found to overcome the influence of unstable zeros.

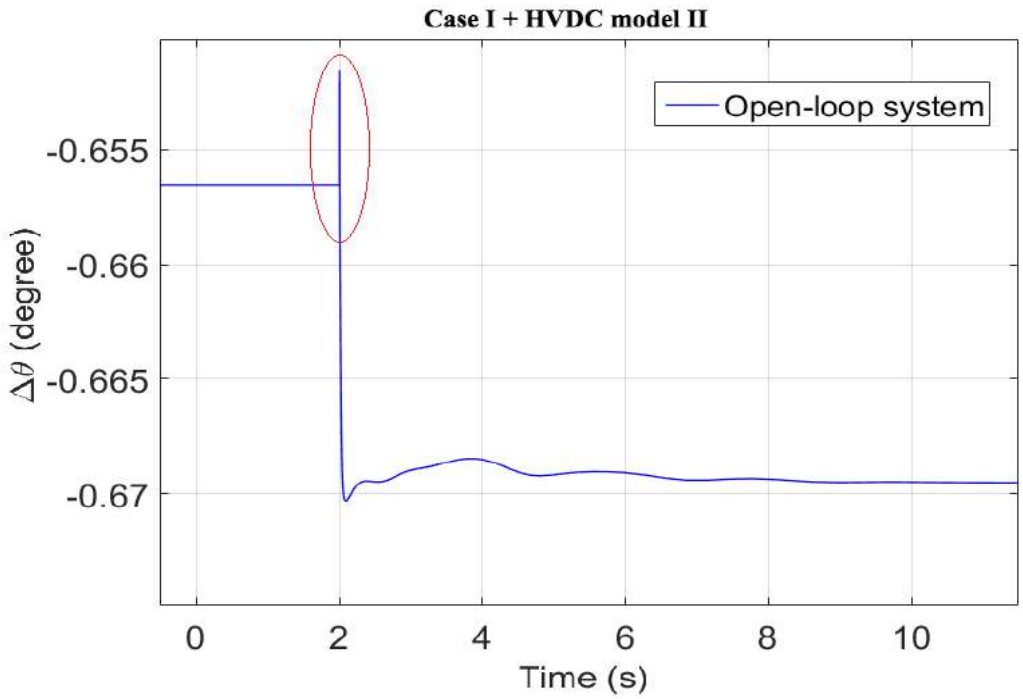

Figure 3.2 – Step response of Q for Case I+HVDC model II.

3.4 Systematic analysis with a benchmark model

To investigate the relationship between the unstable zeros and the components of the grid, the benchmark in Fig. 3.3 according to (Belhocine, Marinescu, and Xavier 2017) is used in this section. This is a benchmark that reproduces the main properties (like frequency, damping, and residue) of an inter-area mode of an HVDC line embedded in a large-scale AC power system by tuning the parameters of the benchmark. In this benchmark, there are two generators, one HVDC line, 5 AC lines, and 5 buses with one load. HVDC model here is a simple injector model. By simply changing the parameters, one structure can be switched to another. For instance, if impedances of all the transmission lines change, the position of zeros of the transfer function from Q to $\Delta\theta$ will change for each case. In Table 3.2, 6 cases are investigated by modifying the length of lines. Notice that topology in Fig. 3.3 covers all HVDC AC grid connections scenarios.

Table 3.2 lists the analysis results. Unstable zeros in this table are obtained in the transfer function from Q modulation to $\Delta\theta$. It is concluded that the most influential parameters of the model on the existence of unstable zeros are impedances of AC lines. This means that the distance from the generators is the most important factor for the location of system zeros.

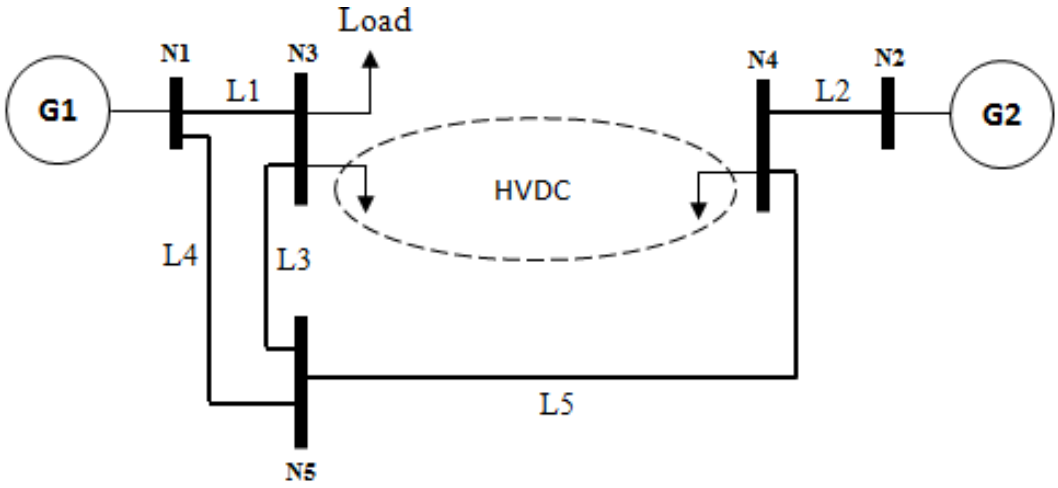

Figure 3.3 – Benchmark system to investigate the unstable zeros.

Table 3.2 – Results of analyzing the benchmark system

No. of case	length of L1	length of L2	length of L3	length of L4	length of L5	unstable zeros
case 1	25	25	300	25	25	No
case 2	100	25	300	25	25	Yes
case 3	25	40	300	25	25	Yes
case 4	25	25	100	25	25	No
case 5	25	25	300	100	25	Yes
case 6	25	25	300	25	100	Yes

3.5 Feedforward zero phase compensator

Due to the fact that the existence of unstable zeros depends on the topology of the grid, this may make them unavoidable in some situations. Besides, they impact the performances of the POD controller as discussed in Section 3.3. Thus, in this section, after reviewing the original ZPETC method, a MZPEC is proposed to enhance the performance of the standard ZPETC in dealing with unstable zeros.

3.5.1 Traditional ZEPTC

ZPETC is a controller (Tomizuka 1987) which reduces the phase error caused by the unstable zero dynamics. Let us consider a transfer function expressed in the continuous-time domain,

$$\frac{y(s)}{r(s)} = \frac{N(s)}{D(s)}, \tag{3.1}$$

where,

$$\begin{aligned} D(s) &= a_0 + a_1 s + a_2 s^2 + ... + a_n s^n \\ N(s) &= b_0 + b_1 s + b_2 s^2 + ... + b_m s^m, (n \geq m). \end{aligned} \tag{3.2}$$

For a non-minimum phase system, $N(s)$ can be split into two parts as follows,

$$N(s) = N^a(s) N^u(s), \tag{3.3}$$

where, $N^a(s)$ represents the stable zeros, $N^u(s)$ stands for unstable zeros. The original ZPETC can be designed as the following form,

$$ZPETC = \frac{D(s) N^u(-s)}{N^a(s)[N^u(0)]^2}, \tag{3.4}$$

which makes the transfer function of overall model

$$\frac{y_d}{y_d^*} = \frac{N^u(-s) N^u(s)}{[N^u(0)]^2}. \tag{3.5}$$

With this feed-forward controller, the transfer between y_d and y_d^* in Fig. 3.4 will have no phase shift for all frequencies. To demonstrate this fact, one has,

$$\begin{aligned} N^u(-s)|_{j\omega} &= Re(N^u(j\omega)) - jIm(N^u(j\omega)) \\ N^u(s)|_{j\omega} &= Re(N^u(j\omega)) + jIm(N^u(j\omega)). \end{aligned} \tag{3.6}$$

So that,

$$\begin{aligned} N^u(-s)N^u(s)|_{j\omega} &= Re^2(N^u(j\omega)) + Im^2(N^u(j\omega)) \\ &= |N^u(j\omega)|^2. \end{aligned} \tag{3.7}$$

Equation (3.7) shows that the transfer function between $y(s)$ and $y^*(s)$ does not have an imaginary part, which means no phase shift at all.

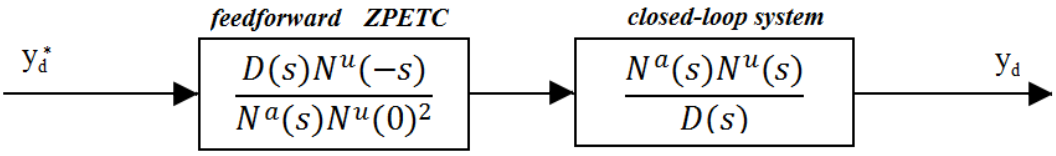

Figure 3.4 – Block diagram of the original ZPETC.

3.5.2 Modified ZEPC

According to Fig. 3.4, the original ZPETC removes the closed-loop system poles by applying $1/D(s)$. On the other hand, in both case I and case II, the systems contain a high number of states. For this reason, the original ZPETC cannot be directly applied to cancel out the effects of $D(s)$ and the original ZPETC (3.4) is revised as in Fig. 3.5. Since the aim is to compensate the unstable zeros, this controller can be designed as a low-order structure called modified zero phase error compensator (MZPEC). It is noted that the non-proper transfer functions simulate the behavior of derivatives and can thus result in a noise-sensitive system. As a consequence, some other real poles ($D^{'}(s)$) are added to obtain a proper compensator. The final degree of $D^{'}(s)$ is greater or equal to the number of unstable zeros. So, the proposed MZPEC is less complex compared to the standard ZPETC that uses $D(s)$. The locations of the poles in $D^{'}(s)$ are chosen quite far from the dominant poles of the original closed-loop system. And $D^{'}(0)^2$ is added in the numerator to cancel the gain brought by this term.

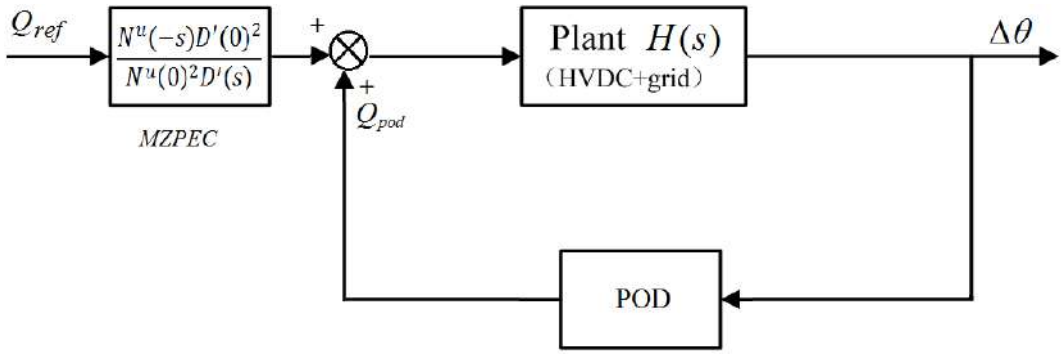

Figure 3.5 – MZPEC feed-forward controller for the closed-loop system.

3.6 Results of MZPEC application

In this section, the proposed POD-MZPEC is implemented for both linearized and nonlinear power networks of case I+HVDC model I.

3.6.1 Linear simulations

$\Delta\theta$ responses to a step on reference of the Q modulation loop are shown in Fig. 3.6. It can be seen that with MZPEC, non-minimum phase behavior is eliminated with less undershoot and the classic POD can reach the desired damping in this case. A smoother response in $\Delta\theta$ leads to smoothening responses of all variables of the HVDC and neighbor generators.

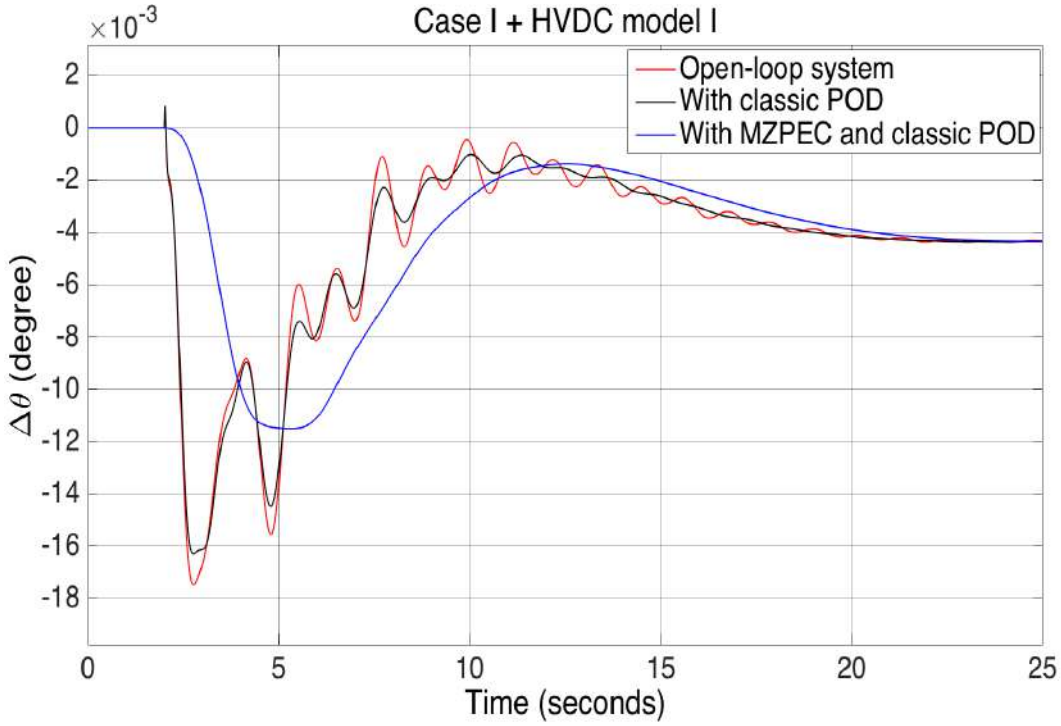

Figure 3.6 – Step responses of the linear system.

3.6.2 Nonlinear simulations

In this section, nonlinear model simulations are carried out with Eurostag software. From these results, the improvement of the POD-MZPEC controller is clearly shown in Fig. 3.7.

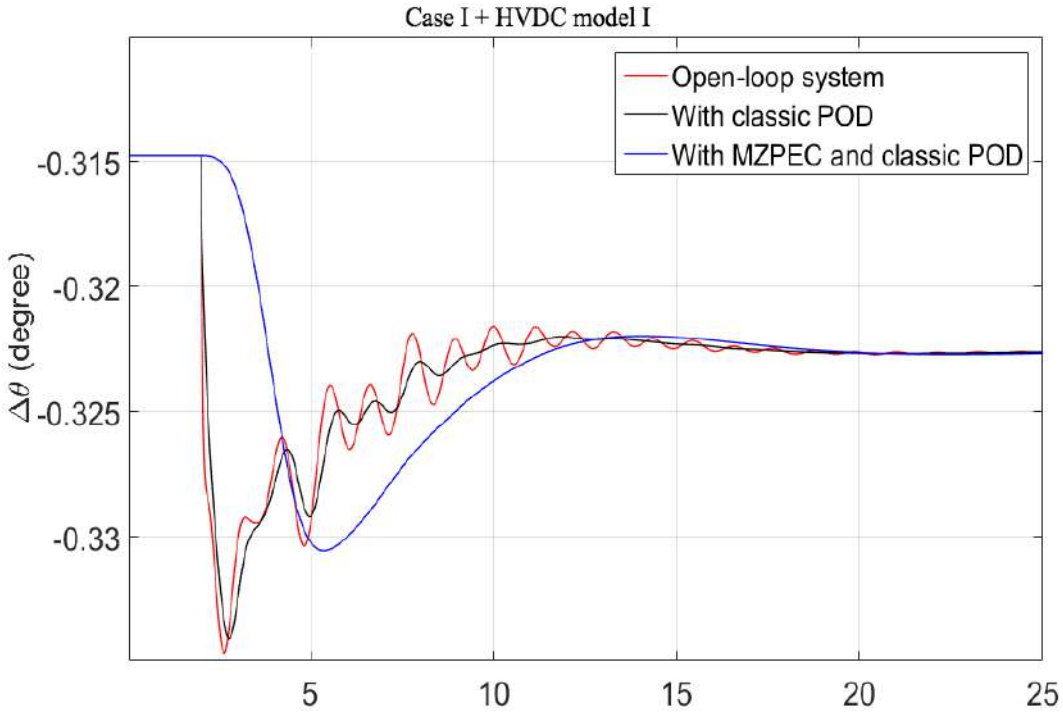

Figure 3.7 – Step responses of the nonlinear system.

3.7 Limitation of MZPEC in case of uncertainty

Simulation results reveal that the use of the provided MZPEC along with a classic POD controller can greatly improve the action of the POD and, therefore, can increase the power transfer quality of the grid. In this perfect model, the fixed unstable zeros can be canceled by the compensator. However, if the unstable zeros are not perfectly captured in the control model, cancellation can be ineffective. This is the case, for example, when the grid operation point changes. To avoid this failure, a more robust controller should be developed.

3.8 Summary

This chapter is concerned with the non-minimum phase behavior of electrical networks equipped with POD controlled HVDC links. The existence of unstable zeros of HVDC inserted in the AC grid system depends on the topology of the grid. Since these unstable zeros bring more difficulties for the stability control of the power system, much more attention should be paid to reduce these harmful characteristics. Subsequently, a modified zero phase error compensator was proposed to handle the grid unstable zeros. The simulation results on a real power grid along with the suggested co-compensator MZPEC indicate that the non-minimum phase behavior of both linearized and nonlinear network models was effectively suppressed. Also, the introduced MZPEC is free of the

controller type applied and it can be implemented on some advanced POD controllers to cancel this kind of unstable zeros delays to perfect the dynamic responses. However, this compensator also has its limitation to face evolution of the model like, e.g., different operation point cases. Thus, more robust controllers should be developed in the next chapter.

Chapter 4

Different control strategies and their results of application

Contents

4.1 Introduction

To overcome the difficulties mentioned in the above chapters, state-space based methods which take into account all involved dynamics (interacting modes at a specific range of frequencies) are used below to design the controllers. Different classic robust control strategies like LQG and mixed

sensitivity H_∞ approaches are designed for the test system to compare with the proposed two types of model-matching controllers.

4.2 Control model

The advanced controllers have the same order as the control model. Thus, the reduction of the large-scale system is necessary to ensure that the order of the controller is acceptable. Also, the reduced *control model* needs to capture the dynamic information for the AC grid. All this information exists in a *state-representation* systematically used by all the advanced control methods. In the frequency range of inter-area oscillations, the control model should have the same response as the full model. In (Bogdan Marinescu and Petesch 2014), a reduction method has been proposed by an identification approach based on this principle. The same approach will be adopted in this research to obtain a suitable control model for advanced control in the context.

In the meshed grid context mentioned above, the control model based only on sensitivities of the modes to be damped against the gain of the controller usually used in POD controller synthesis (« IEEE recommended practice for excitation system models for power system stability studies (ieee std 421.5-2005) » 2005) is no longer sufficient. In order to capture the above dynamics at frequencies close to the mode to be damped, there are two different strategies. The first one consists of starting from a full model of the power system and reducing it at a reasonable scale (about 10 state variables) for control by preserving dynamics of interest. This is very difficult for large-scale systems and led to a second approach based on *aggregation* of a transfer model around the modes of interest. If the open-loop transfer function of the full model is $H(s)$, the proposed *control model* consists in the low order transfer function $\tilde{H}(s)$ in (4.1) where the modes to be damped are $\Lambda = \{\lambda_1, ..., \lambda_l\}$ and r_k is the residue of mode λ_k.

$$\tilde{H}(s) = \frac{A(s)}{B(s)} + \frac{P(s)}{Q(s)} \tag{4.1}$$

$$\frac{A(s)}{B(s)} = \sum_{k=1}^{l} \left[\frac{r_k}{s - \lambda_k} + \frac{\bar{r}_k}{s - \bar{\lambda}_k} \right], \tag{4.2}$$

$$\begin{aligned} P(s) &= p_{n-1}s^{n-1} + ... + p_0 \\ Q(s) &= s^n + q^{n-1}s^{n-1} + ... + q_0 \end{aligned} \tag{4.3}$$

Polynomials $P(s)$ and $Q(s)$ are computed to minimize objective function (4.4) such that the

reduced-order model fits the full model system in the working frequency band.

$$J = \sum_{\omega_\Lambda^- \leq \omega_k \leq \omega_\Lambda^+} [\alpha_k (A_k - |\tilde{H}(i\omega_k)|)^2 + \beta_k (\varphi_k - \arctan(\tilde{H}(i\omega_k)))^2] \tag{4.4}$$

where (A_k, ω_k) and (φ_k, ω_k) are points of the Bode plots of the transfer of the full model $H(s)$, ω_Λ^- and ω_Λ^+ define the frequency working band (from Λ). The weights α_k, β_k are used to manage the trade-off between magnitude and phase fitting and, eventually, to give priority to the fitting at specific frequencies. It should be noted that the degree n of polynomials ($P(s)$ and $Q(s)$) is chosen by trial and error starting from low values and increasing it until a sufficient degree of precision is reached for the curves fitting.

For the case tested here, Λ is composed of the first 5 modes in Table 2.1, the detailed parameters are listed in Appendix D. Notice that degree of $Q(s)$ is 7 so that the order of $\tilde{H}(s)$ is 12. The obtained results are shown in Fig. 4.1 where the reduced model fits the full model in the specified frequency range.

Thus, in state-space format, consider the control model as a linear time-invariant continuous system is given by:

$$\begin{aligned} \dot{x} &= Ax + Bu \\ y &= Cx \end{aligned} \tag{4.5}$$

where $x \in \Re^{n\times 1}$, $y \in \Re^{g\times 1}$ and $u \in \Re^{m\times 1}$ are the state vector, output vector and the control input, respectively, $C \in \Re^{g\times n}$ is the system output matrix, $A \in \Re^{n\times n}$ and $B \in \Re^{n\times m}$, are the system and input matrices, respectively. This control model will be used in following POD controllers design procedure.

4.3 LQG controller

One of the simplest robust controllers is the Linear Quadratic Gaussian control (see, e.g., (Skogestad and Postlethwaite 2007), (Zhou and Doyle 1998)). The solution of the LQG control problem is a control law u which stabilizes the closed-loop and minimizes the quadratic performance index:

$$J_{LQG} = E\left\{ \lim_{T\to\infty} \frac{1}{T} \int_0^T [x^T Q x + u^T R u] dt \right\} \tag{4.6}$$

where $E\{\cdot\}$ is the expectation operator, Q and R are weighting matrices, which are used as design parameters, along with W and V, for the synthesis of the controller gains K_r and L:

$$K_r = R^{-1} B^T X \tag{4.7}$$

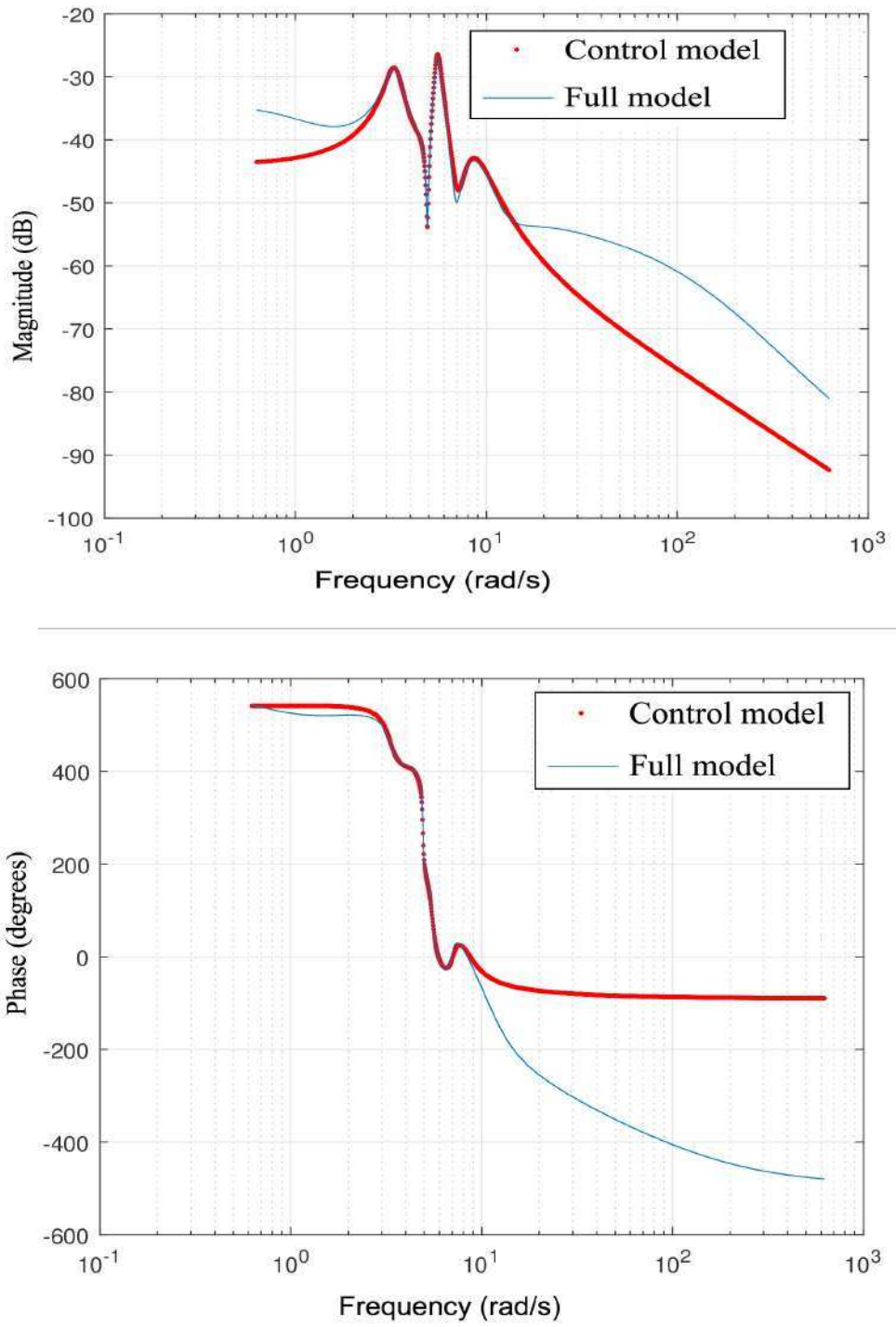

Figure 4.1 – Curve fitting of Bode plots of the full model and control model.

$$L = YC^T V^{-1}, \tag{4.8}$$

where X and Y are solutions of the following two Riccati equations:

$$\begin{aligned} XA + A^T X - XBX^{-1}B^T X + Q = 0 \\ YA^T + AY - YC^T R^{-1} CY + W = 0. \end{aligned} \tag{4.9}$$

Notice that (4.7) is the solution of the control problem (state feedback), while (4.8) gives the gain L of the Kalman filter (used for state estimation):

$$\dot{\hat{x}} = A\hat{x} + Bu + L(y - C\hat{x}). \tag{4.10}$$

Hence, the structure of the LQG controller is given by $u = -K_r\hat{x}$ where $\hat{x}$ is provided by the above Kalman filter. Fig. 4.2 illustrates a general representation of the LQG regulator.

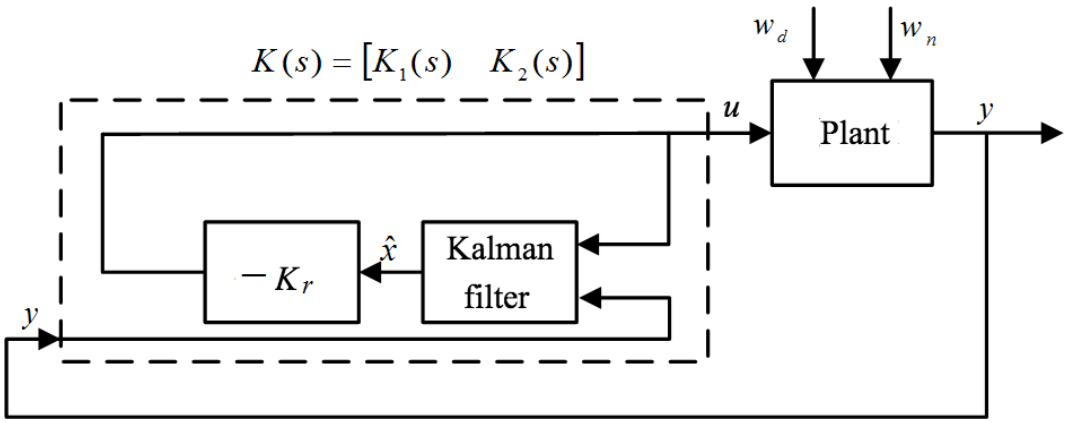

Figure 4.2 – General scheme of LQG controller.

4.3.1 Controller design

In this research case, the control model is (3.2) with $y = \Delta\theta$. $\Delta\theta$ is angle difference mentioned in Chapter 2. The same wash-out filter used in Fig. 2.5 is added to the LQG POD controller. With this in mind, considering the new output $\Delta\theta_w$, which corresponds to the output of the wash-out filter as depicted in Fig. 4.3, the LQG controller is designed based on an equivalent model $H'(s)$, which includes the reduced model ($H(s)$) in series with the wash-out filter with $T_w = 1$.

Usually, the weighting matrices Q and R are diagonal matrices and their entries are chosen according to state dynamics. A higher value in Q (or, equivalently, a low value in R) will lead to faster dynamics (more control action on that specific state), i.e., more *performances*. A higher value in R will conversely lead to a lower control level in that state direction, i.e., to more *robustness*. The same holds for the choice of V and W for the estimator synthesis. This control framework provides

thus an easy way to handle the trade-off performances/robustness. The numerical values used for case treated here are $Q = I$, $R = 10^{-4}$; $W = I$, $V = 10^{-2}$. The LQG control is implemented as in Fig. 4.3 and the transfer matrix of the regulator is:

$$Q_{pod} = -K_r\hat{x} = -K_r(sI - A + LC)^{-1}\begin{pmatrix} B & L \end{pmatrix}\begin{pmatrix} u \\ \Delta\theta_w \end{pmatrix} \tag{4.11}$$

where gains K_r and L are obtained by Matlab function lqr (see detailed values in Appendix D). The transfer function of LQG controller is presented in Appendix D.

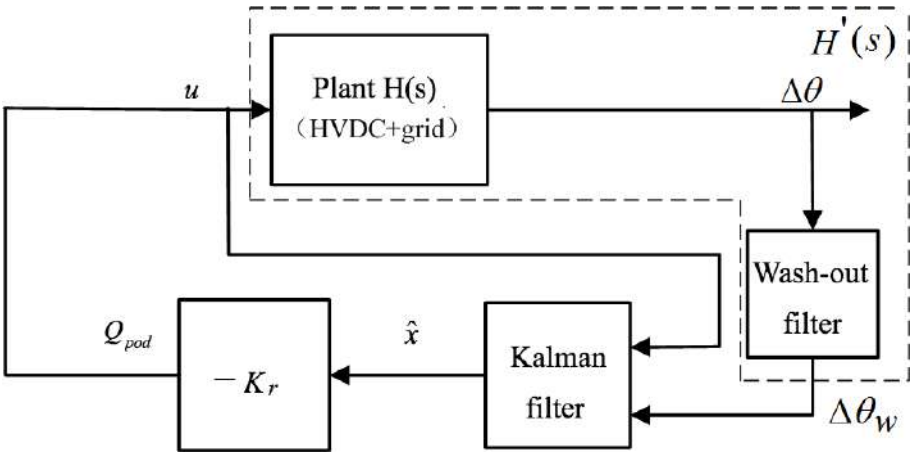

Figure 4.3 – The implemented control structure.

4.3.2 Validation on linearized system

To compare with classic POD, the developed LQG POD controller has been designed for the same damping target of 10% for all modes in question. Table 4.1 reports the obtained damping results in the following situations: i) without POD, ii) with classic POD and iii) with LQG POD.

Table 4.1 – Comparison of damping

No.mode	Damping without POD	Damping of modes with classic POD (%)	Damping of modes with LQG POD (%)
1	19.5	30.5	21.7
2	4.5	6.1	10.9
3	10.1	12.0	14.9
4	8.3	8.1	11.4
5	10.1	12.4	13.6

The proposed controller achieves the control requirements as the dampings of all modes (Λ) are

improved to values larger than the fixed target (10%). This is due to the amount of information about the modes with close frequencies contained in the model used for the controller design. This is compared with the results obtained with the classic IEEE POD controller, which uses less information and neglects the other modes. As a consequence, the target damping is not reached for all modes, even not for mode 2 for which the tuning is performed.

To highlight the effect of the proposed controller on the whole frequency band, an impulse response of the full linearized model of the power system in the above three situations is considered. Fig. 4.4 illustrates the response of the output of the plant ($\Delta\theta$) to such an impulse. It can be seen that the output response with the LQG controller has clear damped oscillations compared to the classic POD and the open-loop responses. This qualitative behavior is coherent with the modal analysis estimation in Table 4.1. Notice also that the damping of mode 1 is lower with the LQG control than with the classic one. This is not an issue since the level is much above the target of 10% and it is normal since globally (for all modes) optimal result is expected with the LQG control.

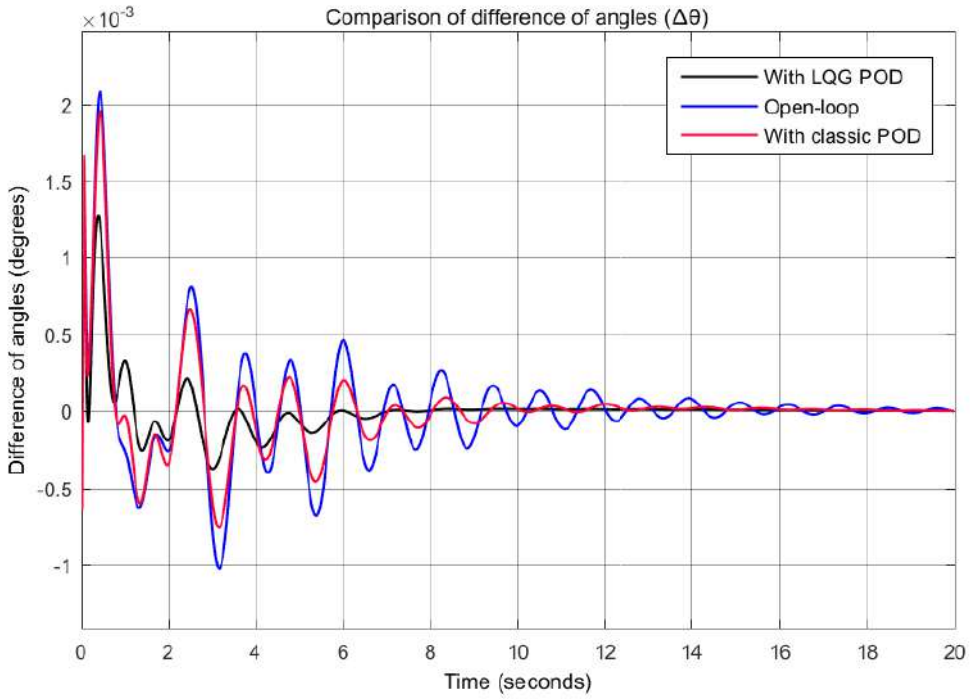

Figure 4.4 – Comparison of $\Delta\theta$ between open-loop system, system with classic POD controller and system with LQG POD controller in full linear model response to an impulse on the input.

4.3.3 Validation on the nonlinear system

In this subsection, the nonlinear model of the power system with the VSC-HVDC link in the same three situations studied in the previous subsection is considered. Simulations were performed

in Eurostag and plotted in Matlab.

Due to nonlinearities, the analysis is here more difficult. Each response curve captures the contribution of several modes mixed with nonlinear dynamics. It is thus difficult to put into evidence each mode individually. The disturbance scenarios should be well chosen. Also, the observability of the modes depends on the choice of the output signal (generator and variable to be displayed).

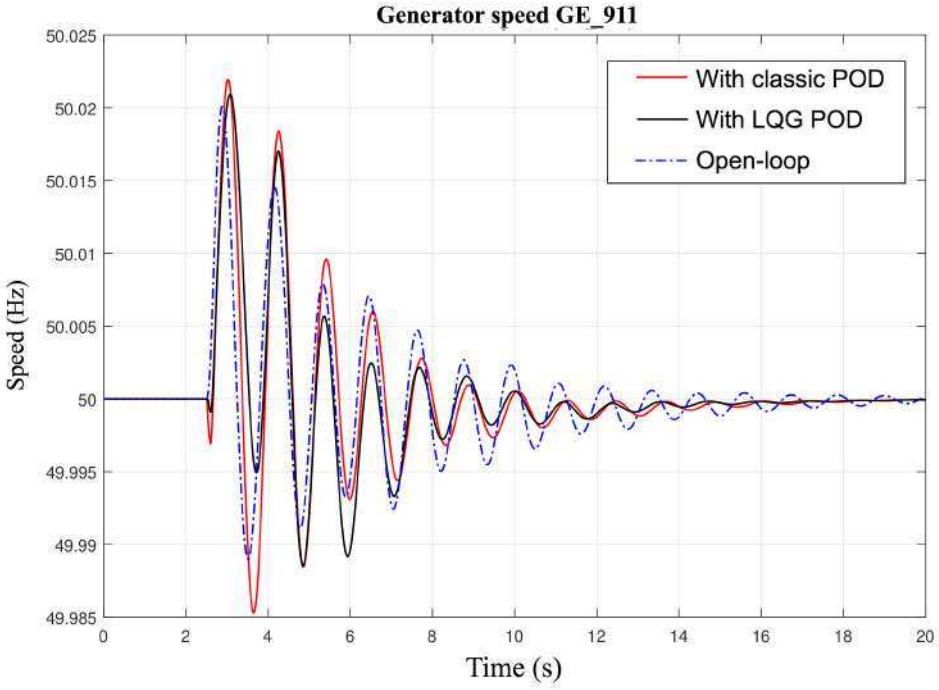

Figure 4.5 – Comparison of generator GE_911 speed responses of open-loop system and system with LQG POD controller.

To excite the lowest damped inter-area mode (mode 2), a short-circuit at the terminal bus of generator GE_918 (FVLAR1-2 in Fig. 2.3) is considered. Fig. 4.5 illustrates the speed response of generator GE_911 in open-loop, with classic POD and with LQG POD controller. One can notice that mode 2 is observable from the 7^{th} swing in the open-loop curve and its frequency can be measured from two peaks. High oscillations (close to 4.5% damping) can be observed for the open-loop response. However, these oscillations are clearly damped by the LQG POD controller. Besides, the damping is lower with the classic POD controller.

Consider now a short-circuit at the terminal bus of generator GE_911. Mode 4 is observable in the responses of GE_912 in Fig. 4.6 after 3^{th} swing as this generator is the most participating one in mode 4. It is damped with the LQG controller, but close to the open-loop value with the classic POD. Mode 1 is observable in the first two swings of Fig. 4.7 which gives the responses of GE_914 to the same short-circuit. Notice that the damping in this case is again above the one provided

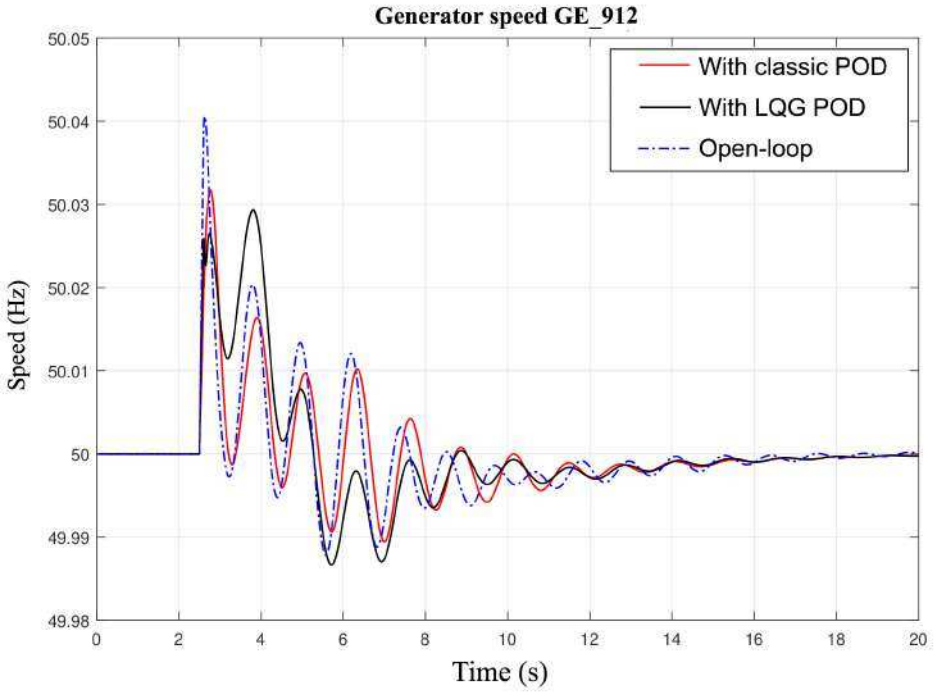

Figure 4.6 – Comparison of generator GE_912 speed responses of open-loop system and system with LQG POD controller.

by the classic controller. The LQG POD controller guarantees thus sufficient damping in a wide frequency band which contains several modes and of different natures.

4.4 Mixed sensitivity H_∞ with LMI controller

The robustness of the pole placement (done by LQG control) in the improved control framework reported in the previous section can be further improved by the formalism below which has also the advantage to directly consider the damping target specification in the control synthesis which is called mixed sensitivity H_∞ with LMI controller (e.g., (Skogestad and Postlethwaite 2007),(Zhou and Doyle 1998)).

4.4.1 Basics of mixed sensitivity H_∞ control method

H_∞ is one of the classic control formalism in which robustness specifications above can be met. It provides a multi-variable frequency loop-shaping using the H_∞ norm as a quantitative measure of the attenuation. More precisely, the regulator is computed to minimize the input-output transfer of the modified plant in Fig. 4.8. The input/output of the POD are the same as the ones considered in Section 4.3.

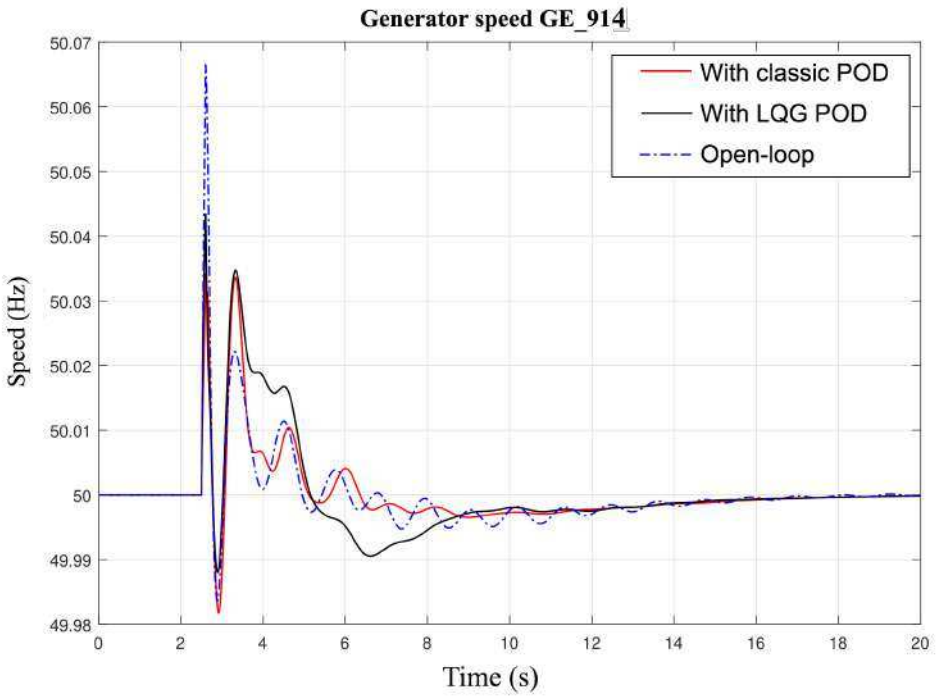

Figure 4.7 – Comparison of generator GE_914 speed responses of open-loop system and system with LQG POD controller.

The H_∞ problem input is disturbance d which stands for noise or the other dynamics mentioned above. The output z consists in the plant output y together with the control u in order to ensure minimum level control. The transfer function from d to y is the well-known *sensitivity function* $S(s) = (I + H(s)K(s)) - 1$. In order to minimize also the level of control, one has to consider

$$\left\| \begin{bmatrix} W_1(s)S(s) \\ W_2(s)KS(s) \end{bmatrix} \right\|_\infty < \gamma, \tag{4.12}$$

where $W_1(s)$ and $W_2(s)$ are frequency weights used to manage the trade-off between robustness/performance. They are low-pass and respectively high-pass filters and their tuning is given in the next subsection. γ is the bound on H_∞ norm which guarantees the H_∞ performance.

According to (4.5) and Fig. 4.8, the augmented plant $P(s)$ is,

$$\begin{cases} \dot{x}_p = Ax_p + B_{p1}d + B_{p2}u \\ z = C_1x_p + D_{p11}d \\ y = C_2x_p + D_{p21}d \end{cases} \tag{4.13}$$

where x_p is state of the augmented plant $H'(s)$.

According to (4.5), the controller $K(s)$ can be realized in the following output-feedback state-

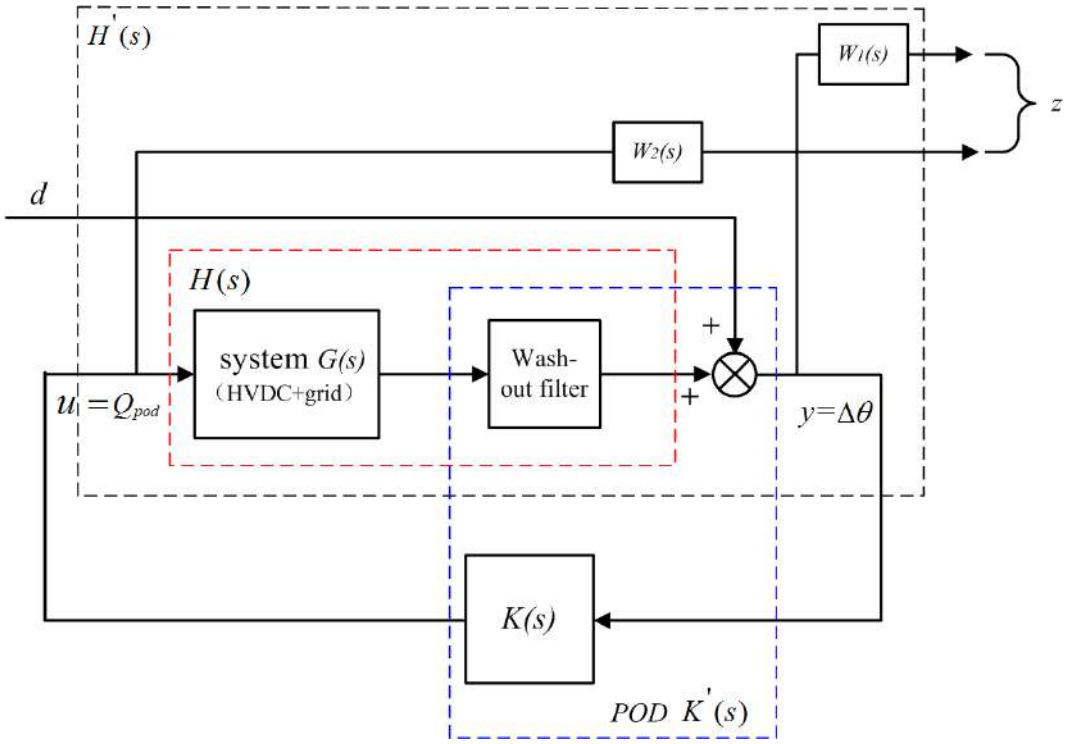

Figure 4.8 – Controller structure of mixed sensitivity H_∞ POD.

space form

$$\dot{\hat{x}} = A_k\hat{x} + B_k\mathrm{y}$$
$$u = C_k\hat{x} + D_k\mathrm{y}$$

Let

$$\dot{\chi} = A_{cl}\chi + B_{cl}d$$
$$z = C_{cl}\chi + D_{cl}d \tag{4.14}$$

be a closed-loop state-space representation. The problem (4.12) can be converted into LMI sub-optimization problem if and only if there exist a solution $X_{cl} = X_{cl}^T > 0$, such that the Bounded real lemma (Duan and H.-H. Yu 2013; Boyd et al. 1994) given by (4.15) is satisfied (Chilali and Gahinet 1996; Scherer, Gahinet, and Chilali 1997). The latter can be solved by LMI approach explained in Section 4.4.3.

$$\begin{bmatrix} A_{cl}^T X_{cl} + X_{cl}A_{cl}^T & B_{cl} & X_{cl}C_{cl}^T \\ B_{cl}^T & -I & D_{cl}^T \\ C_{cl}X_{cl} & D_{cl} & -\gamma^2 I \end{bmatrix} < 0 \tag{4.15}$$

4.4.2 Performance and robustness analysis

It is well known that there is a trade-off between the performance and robustness of a controller. Therefore, in order to achieve the required damping and satisfy robustness, this trade-off should be investigated. Due to the advantage of free desired damping specification of mixed sensitivity H_∞ strategy (described in the next section), it is discussed in this section the relationship between performance and robustness. Table 4.2 presents dampings estimated with the control model against the ones really obtained with the full model. All the modes of damping higher than 6% (value which corresponds to the lowest damping obtained with classic POD) are presented. In this table and Fig. 4.9, it can be seen that the control model closed-loop lowest damping increases with the desired damping, but the damping of closed-loop for full model is limited a top value due to the modeling error. This put into evidence that the suitable damping requirements should be set to enhance the robustness to compensate modeling errors and system uncertainties.

Table 4.2 – The relationship between desired damping for all modes and obtained lowest damping among all modes

Desired damping(%) (Angle θ (deg) in the left plane in Fig.4.10)	Actual lowest damping (%) in closed-loop full model	Actual lowest damping (%) in closed-loop control model
6.1 (173)	8.16	8.25
6.9 (172)	8.35	8.35
7.8 (171)	8.37	8.37
8.72 (170)	9.24	9.25
9.5 (169)	10.14	10.14
10.4 (168)	10.89	10.85
11.3 (167)	**12.23**	**11.86**
12.1 (166)	13.14	10.88
13 (165)	13.96	9.97
13.92 (164)	14.72	8.97
14.78 (163)	15.52	7.59
15.64 (162)	16.29	4.51

4.4.3 Performance specification

According to the previous section, the desired damping is adopted as the top value ($\xi_{desired} = 11\%$) for all modes in Fig. 4.9 to have the desired performance and acceptable robustness. The desired level of dampings for all modes is fulfilled by means to place the closed-loop poles in a sector region as in Fig. 4.10. It is shown in (Chilali and Gahinet 1996) that the state matrix, A_{cl} of the closed loop plant, has all its poles inside the conical sector if and only if there exists $X_c = {X_c}^T > 0$

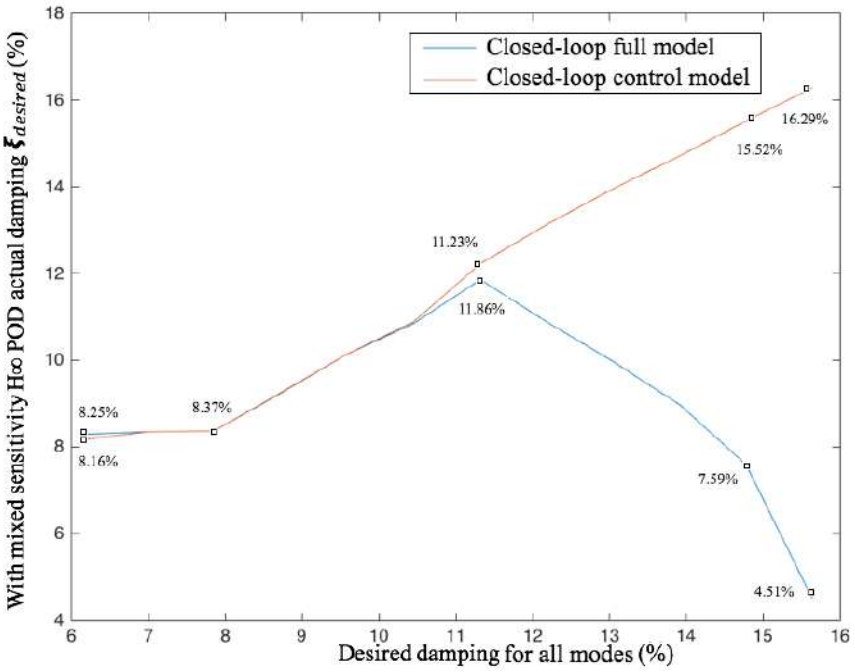

Figure 4.9 – Relationship of obtained lowest damping among all modes with the desired damping for all modes.

such that

$$\begin{bmatrix} \sin\frac{\theta}{2}\left(A_{cl}X_c + X_cA_{cl}^T\right) & \cos\frac{\theta}{2}\left(A_{cl}X_c - X_cA_{cl}^T\right) \\ \cos\frac{\theta}{2}\left(X_cA_{cl}^T - A_{cl}X_c\right) & \sin\frac{\theta}{2}\left(A_{cl}X_c + X_cA_{cl}^T\right) \end{bmatrix} < 0. \tag{4.16}$$

This also can be formulated as an LMI optimization problem in Kronecker product form given by (4.17).

$$[\eta \otimes A_{cl}X_c + \eta^T \otimes X_cA_{cl}^T] < 0, \eta = \begin{bmatrix} \sin\frac{\theta}{2} & \cos\frac{\theta}{2} \\ -\cos\frac{\theta}{2} & \sin\frac{\theta}{2} \end{bmatrix} \tag{4.17}$$

θ is directly correlated with damping ratio $\xi = \cos\frac{\theta}{2}$ in left complex plane. In the case tested here $\xi_{desired} = 11\%$ for the modes in Table 2.1, so $\theta = 167°$ in Fig. 4.10.

According to (Chilali and Gahinet 1996), the jointly convexity of inequalities (4.15), (4.17) can be achieved by searching common solution, $X_{cl} = X_c = X_d$. These two inequalities also have non-linear terms $C_{cl}X_d$ and $A_{cl}X_d$ which cannot be solved by LMI optimization directly. To make it

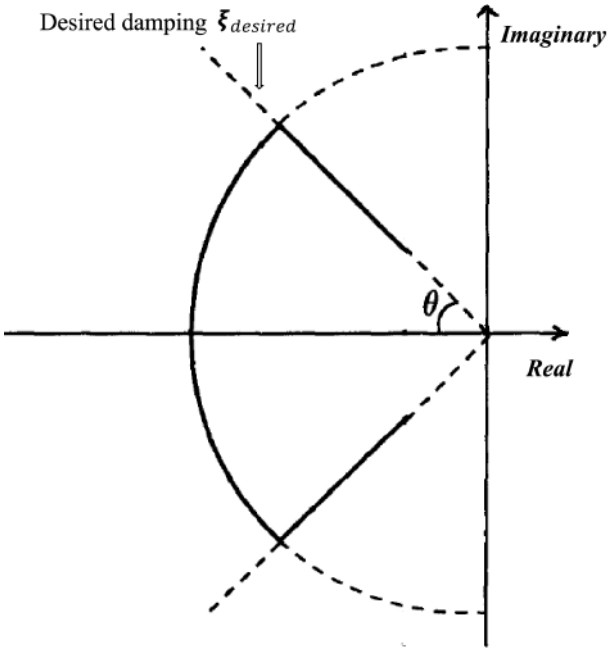

Figure 4.10 – LMI region.

linear, a change of controller variables is necessary as shown in (Chilali and Gahinet 1996).

$$\begin{bmatrix} Q & I \\ I & S \end{bmatrix} < 0 \tag{4.18}$$

$$\begin{bmatrix} \Pi_{11} & \Pi_{21}^T \\ \Pi_{21} & \Pi_{22} \end{bmatrix} < 0 \tag{4.19}$$

$$[\eta \otimes \Psi + \eta^T \otimes \Psi^T] < 0 \tag{4.20}$$

Thus, formulas (4.15) and (4.17) are transferred into (4.19) and (4.20). $\otimes$ is symbol of Kronecker product, Q and S are unknown variables to be solved in the terms of Π_{11}, Π_{21}, Π_{22} and Ψ below.

$$\Pi_{11} = \begin{bmatrix} A_p Q + Q A_p^T + B_{p2}\hat{C} + \hat{C}^T B_{p2}^T & B_{p1} + B_{p2}\hat{D}D_{p21} \\ (B_{p1} + B_{p2}\hat{D}D_{p21})^T & -\gamma I \end{bmatrix} \tag{4.21}$$

$$\Pi_{21} = \begin{bmatrix} \hat{A} + (A_p + B_{p2}\hat{D}C_{p2})^T & SB_{p1} + \hat{B}D_{p21} \\ C_{p1}Q + D_{p12}\hat{C} & D_{p11} + D_{p12}\hat{D}D_{p21} \end{bmatrix} \tag{4.22}$$

$$\Pi_{22} = \begin{bmatrix} A_p^T S + S A_p + \hat{B}C_{p2} + C_{p2}^T \hat{B}^T & (C_{p1} + D_{p12}\hat{D}C_{p2})^T \\ C_{p1} + D_{p12}\hat{D}C_{p2} & -\gamma I \end{bmatrix} \tag{4.23}$$

$$\Psi = \begin{bmatrix} A_pQ + B_{p2}\hat{C} & A_p + B_{p2}\hat{D}C_{p2} \\ \hat{A} & SA_p + \hat{B}C_{p2} \end{bmatrix} \tag{4.24}$$

These terms also contain new linear controller unknown variables $\hat{A}$, $\hat{B}$, $\hat{C}$, $\hat{D}$.

$$\hat{A} = NA_kM^T + NB_kC_{\mathrm{p2}}Q + SB_{\mathrm{p2}}C_kM^T + S\left(A_{\mathrm{p}} + B_{\mathrm{p2}}D_kC_{\mathrm{p2}}\right)Q; \tag{4.25}$$

$$\hat{B} = NB_k + SB_{\mathrm{p2}}D_k; \tag{4.26}$$

$$\hat{C} = C_kM^T + D_kC_2Q; \tag{4.27}$$

$$\hat{D} = D_k. \tag{4.28}$$

Once these unknown variables $Q, S, \hat{A}, \hat{B}, \hat{C}$ and $\hat{D}$ are found as the solution of LMIs (4.18),(4.19) and (4.20), the controller $K(s)$ can be found by computing A_k, B_k, C_k, D_k, from (4.25) to (4.28). The relationship between M and N is

$$MN^T = I - RS$$

.

4.4.4 Controller tuning

As for the classic POD synthesis, a wash-out filter is added to cancel the steady-state value of the measure and to focus the action of the controller to the frequency of the modes to be damped. So, the control model used to synthesize the controller $K(s)$ is $H(s)$, and final applied POD is $K'(s)$ in Fig. 4.8.

As mentioned in former section, $W_1(s)$ and $W_2(s)$ are weights used to shape the open-loop transfers with regulator. In this work $W_1(s)$ and $W_2(s)$ are chosen in the following classic form (Zhou and Doyle 1998).

$$W_1(s) = \left(\frac{s/\sqrt[k]{M_s} + \omega_b}{s + \omega_b\sqrt[k]{\varepsilon}}\right)^k, W_2(s) = \left(\frac{s + \omega_{bc}/\sqrt[k]{M_n}}{\sqrt[k]{\varepsilon_1}s + \omega_{bc}}\right)^k \tag{4.29}$$

where ω_b, ω_{bc} is the bandwidth. M_s, M_n is the peak sensitivity. $\varepsilon, \varepsilon_1$ is the steady-state error, and k is the order of the weighting function. For the example treated here $\varepsilon, \varepsilon_1 = 0.1$, $k = 1$, $\omega_b = 0.628$ rad/sec, $\omega_{bc} = 12.56$ rad/sec. The target damping is $\xi_{desired} = 11\%$ for the modes in Table 2.1. The closed-loop damping ratios are shown in the first entries of Table 4.3. Notice that with the classic

controller it is not possible to provide higher damping in this case for mode 2. Also, the damping of mode 4 is lower than in open-loop. With advanced control, higher damping targets can be ensured. The synthesis was carried here at this almost common level of performance in order to facilitate a comparison of robustness provided by each regulator.

Table 4.3 – Comparison damping

No.	ξ without POD (%)	ξ with classic POD (%)	ξ with LQG POD (%)	ξ with mixed sensitivity H_∞ POD (%)
1	19.5/19.8	30.5/24.43	21.7/20.66	20.29/21.36
2	4.5/5.04	6.1/5.76	10.9/7.86	11.67/9.87
3	10.1/9.65	12.0/11.91	14.9/11.53	12.33/13.89
4	8.3/8.28	8.1/8.07	11.4/9.31	12.41/10.86
5	10.1/10.85	12.4/12.30	13.6/13.57	14.97/12.51

4.4.5 Validation tests

In this subsection, performance is tested on the full nonlinear system and compared systematically for 3 designed controllers: the classic POD, the LQG, and the mixed sensitivity H_∞ ones.

Nominal case behavior

The nominal case mentioned here is the initial operation point model considered for the definition of the benchmark in Section 2.3. This definition is also suitable for the next chapter. Fig. 4.11 shows the responses of the speed of generator GE_911 to a 100ms duration short-circuit at the terminal bus of generator GE_918. Notice that due to nonlinearities, each response curve captures the contribution of several modes mixed with nonlinear dynamics. Damping is improved with mixed sensitivity H_∞ POD particularly for the first two swings in which the nonlinearities of the system are the most present.

Consider the same duration short-circuit but at the terminal bus of GE_917. Figure 4.12 shows that the oscillations are damped with mixed sensitivity H_∞ POD better than with the others. Notice that from the 6^{th} swing till the end, mode 2 (the lowest damped in Table 4.3) is the most observable in these responses.

Consider now the same duration short-circuit but at the terminal bus of GE_911. Fig. 4.13 shows again better damping with mixed sensitivity H_∞ POD. Indeed, larger differences will be put into evidence in the next subsection.

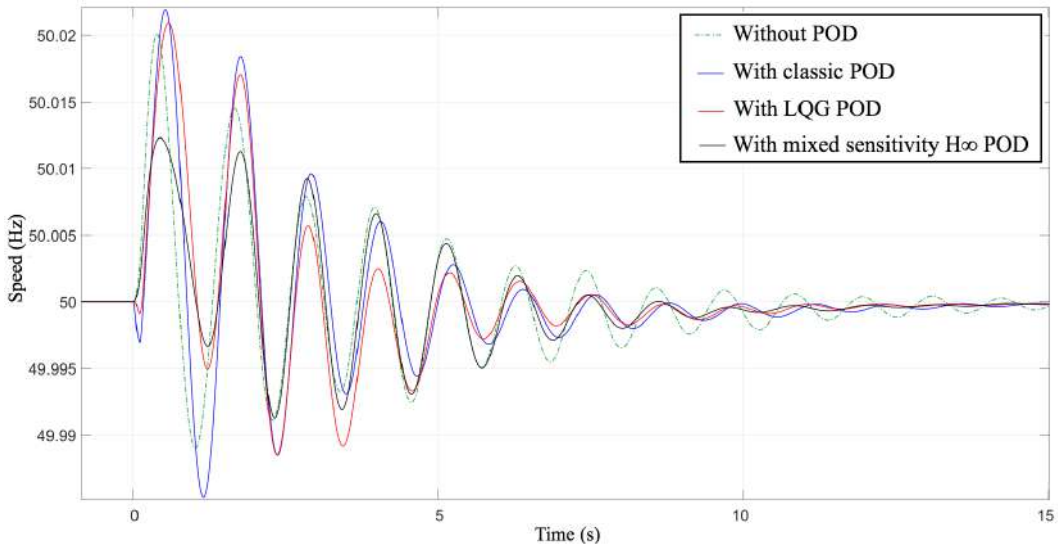

Figure 4.11 – Speed of GE911 in nominal case.

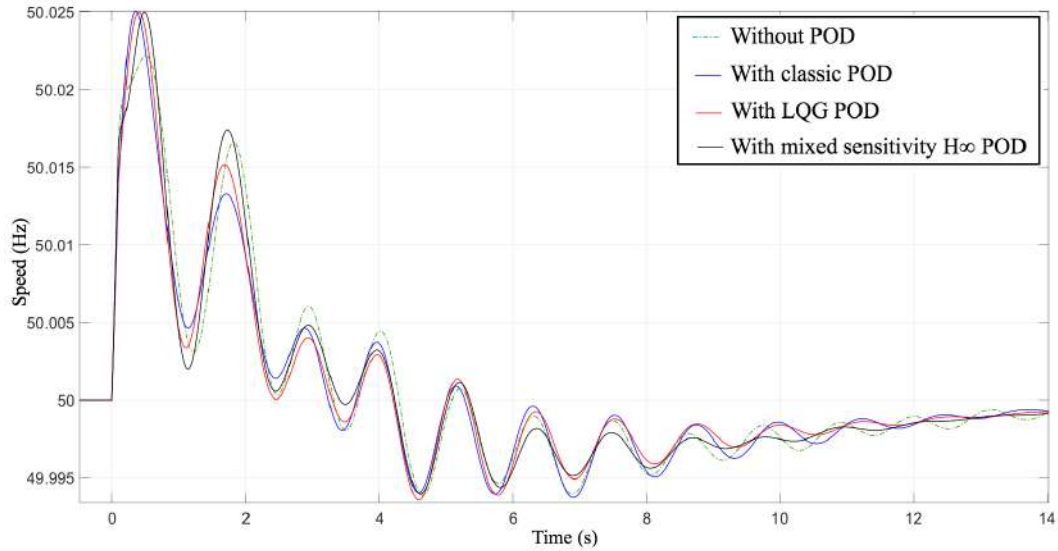

Figure 4.12 – Speed of GE912 in nominal case.

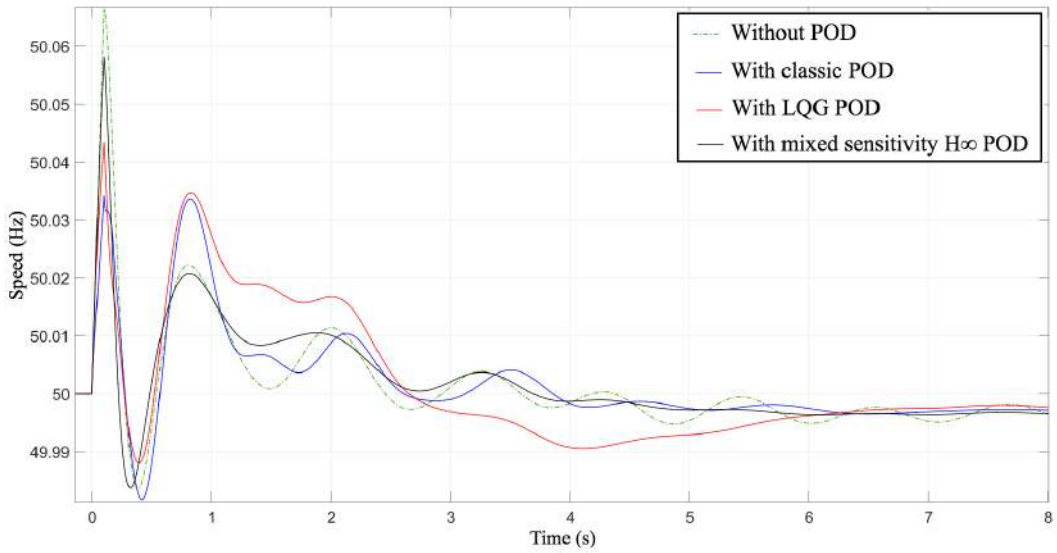

Figure 4.13 – Speed of GE914 in nominal case.

Parametric robustness

The strongest variation of the grid operating point in the case of an HVDC comes from the modification of its active power flow. The extreme case is when not only the value of this flow is changed but also its direction. Besides, more different changed operation point cases will be considered in the next chapter. Here the case where the regulators are synthesized on the nominal grid situation with active power flow $+800MW$ considered above is adopted. They are now tested on a new grid situation with a power flow $-200MW$. The new damping ratios are shown in the second entries of Table 4.3. The classic controller cannot ensure the damping objective. The most robust controller is the mixed sensitivity H_∞ one.

For nonlinear response, the same short-circuit as in the preceding section is considered. It is well known that LQ synthesis has less robustness than H_∞ approach (Zhou and Doyle 1998), (Skogestad and Postlethwaite 2007). Nonlinear responses shown in Fig. 4.14, 4.15, 4.16 confirm conclusions above.

Unstructured robustness and disturbance rejection

Consider disturbances d on the closed-loop in Fig. 4.8. From a *technological point of view*, this *output disturbance* can be due to meter dis-function (failure or bias) and/or measurement noise. From a *system point of view*, these signals may capture exogenous dynamics not taken into account in the nominal control model. This is classic for robust control (Skogestad and Postlethwaite 2007). As mentioned in Section 2.6, for the case of the interconnected power systems, d may also account for several neglected electric dynamics. As the control model is low frequency (focused on inter-area

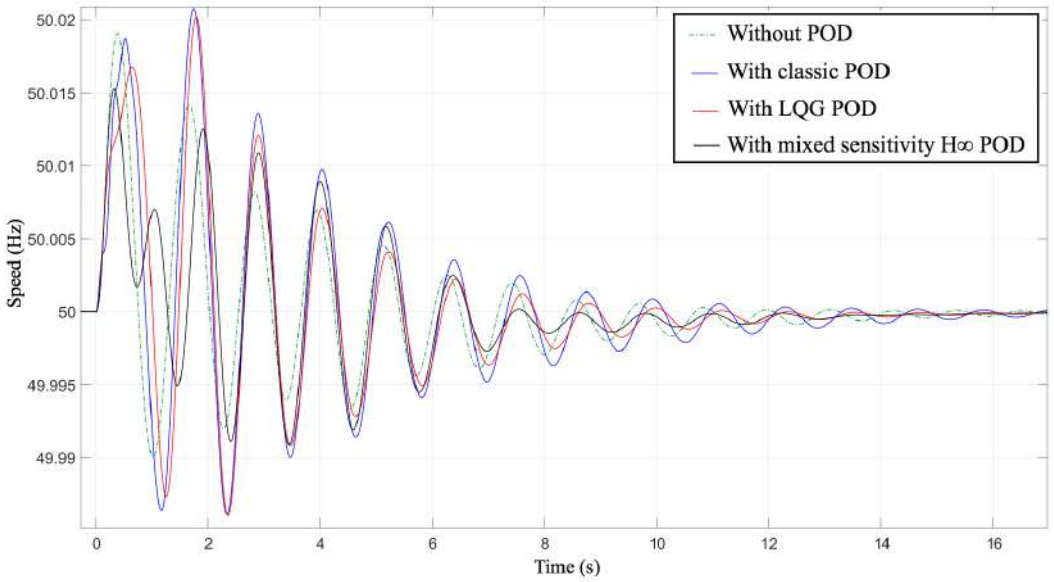

Figure 4.14 – Speed of GE_911 for reversed power flow

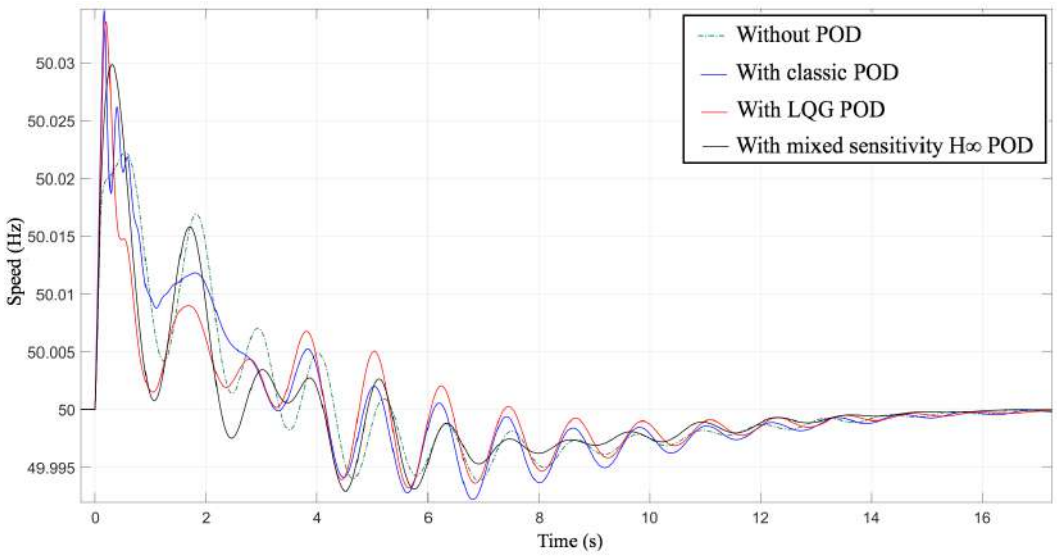

Figure 4.15 – Speed of GE_912 for reversed power flow

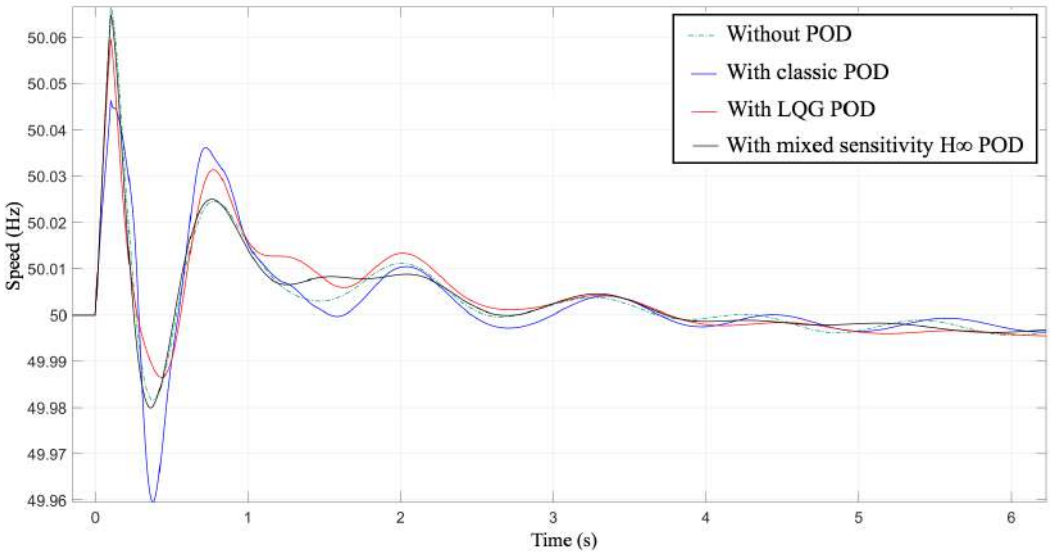

Figure 4.16 – Speed of GE_914 for reversed power flow

modes), such dynamics are of higher frequency. Here, they are considered at 10 Hz, generated as a step response of a second-order element tuned to this frequency. In other words,

$$d = \frac{\omega^2}{s^2 + 2\xi\omega s + \omega^2} u_d, \tag{4.30}$$

where $\omega = 62.8$ rad/sec, $\xi = 0.005$, u_d is a step of magnitude 0.005 pu.

The response with the full linear model is shown in Fig 4.20. The nonlinear responses are shown in Fig 4.17, 4.18, 4.19. In both cases, the loop closed with the designed mixed sensitivity H_∞ controller is the most robust one among these controllers (LQG POD and classic POD).

4.5 Model-matching robust H_∞ static output-error feedback control

To satisfy requirements formulated aforementioned, a model-matching RSOFC design method for HVDC systems based on the LMIs technique is now proposed.

4.5.1 Selection of reference model

The selection of the reference model is significant for the effectiveness of this controller. The reference model in this thesis is chosen as having the desired output, which means to horizontally shift the poles to left in the complex plane until getting the desired damping (over 10%) (in Fig. 4.21).

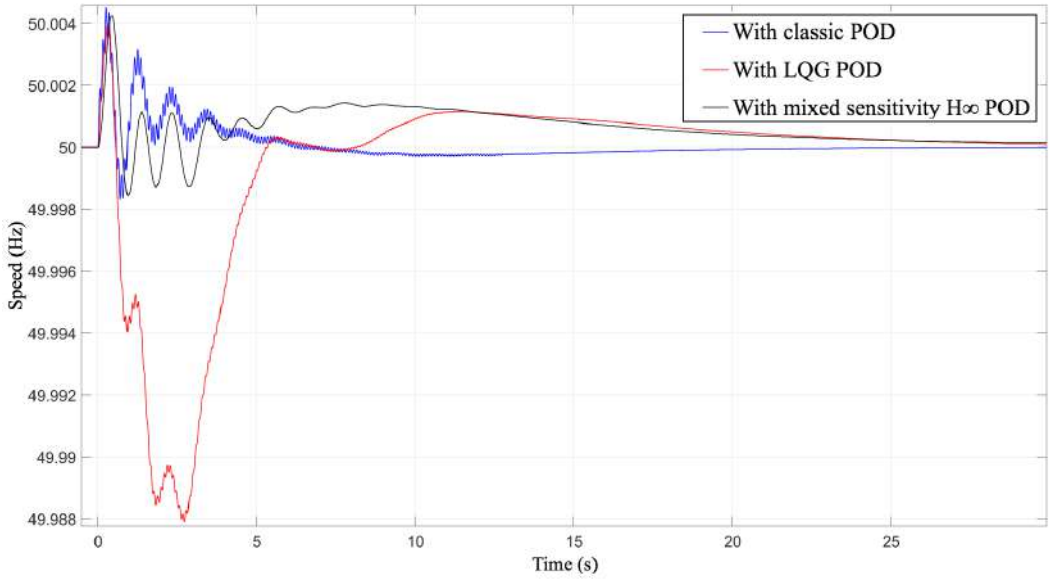

Figure 4.17 – Speed of GE911 for disturbance rejection

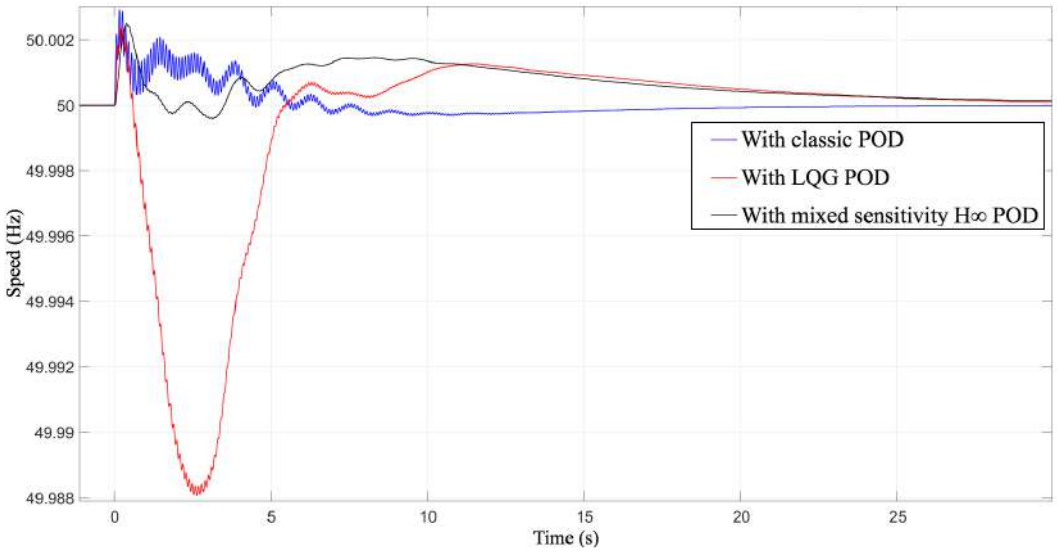

Figure 4.18 – Speed of GE912 for disturbance rejection

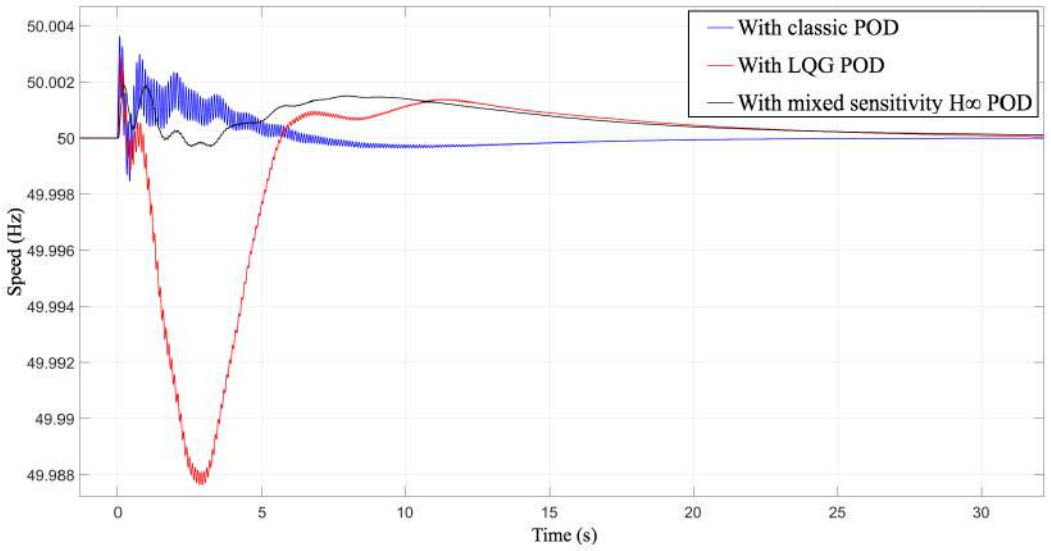

Figure 4.19 – Speed of GE914 for disturbance rejection

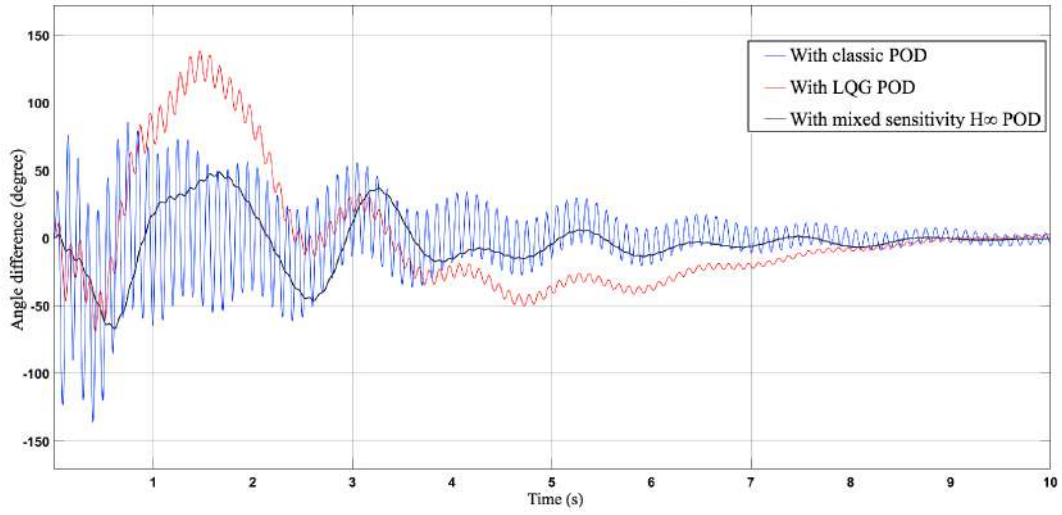

Figure 4.20 – Linear system output for disturbance rejection

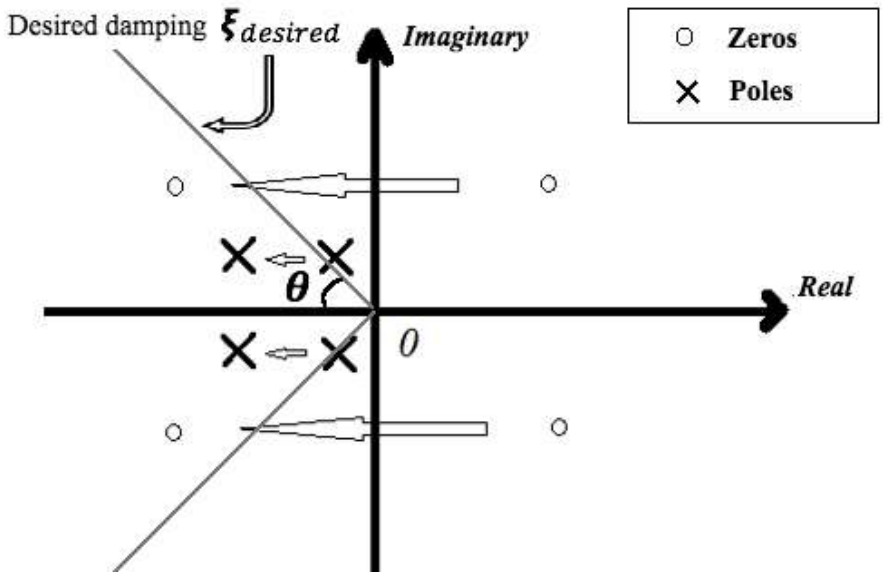

Figure 4.21 – The selection of reference model

In addition, in order to eliminate the impact of unstable zeros, unstable zeros of the control model are put in the left plane but closed to the virtual axis (to decrease the control difficulty) for the reference model. The other stable zeros are not shifted. Let

$$\begin{aligned} \dot{x}_r &= A_r x_r + B_r u_r \\ y_r &= C_r x_r \end{aligned} \tag{4.31}$$

be a state-representation of the resulting reference model.

The step response of the reference model compared with open-loop is shown in Fig. 4.22. The resulting structure of the RSOFC is given in Fig. 4.23.

Based on (4.5) and (4.31), the corresponding augmented system written in state-space in Fig. 4.23 is

$$\begin{aligned} \dot{\tilde{X}} &= \tilde{A}\tilde{X} + \tilde{B}u_c + \tilde{B}_r u_r \\ e &= C_e \tilde{X} \end{aligned} \tag{4.32}$$

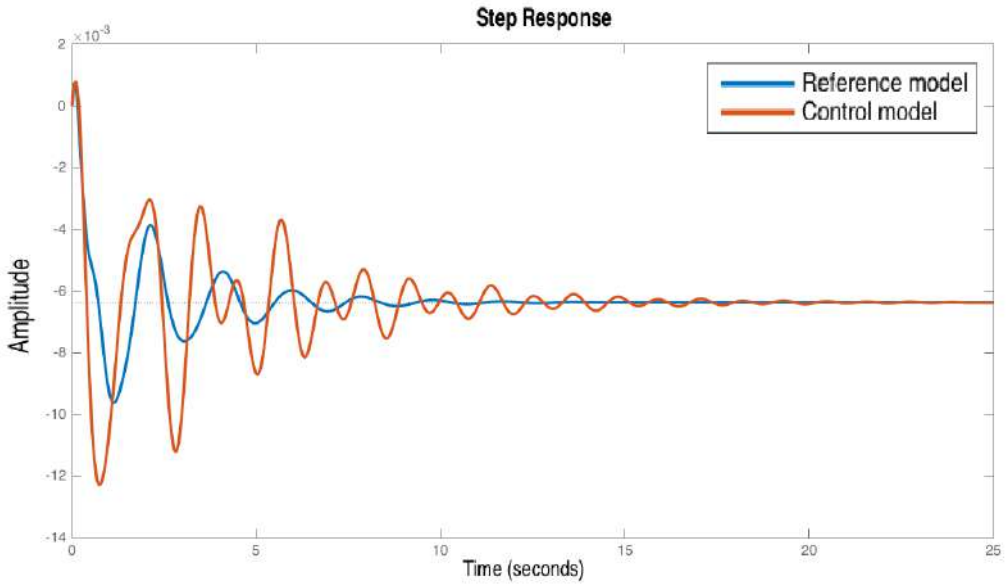

Figure 4.22 – The step response of the reference model.

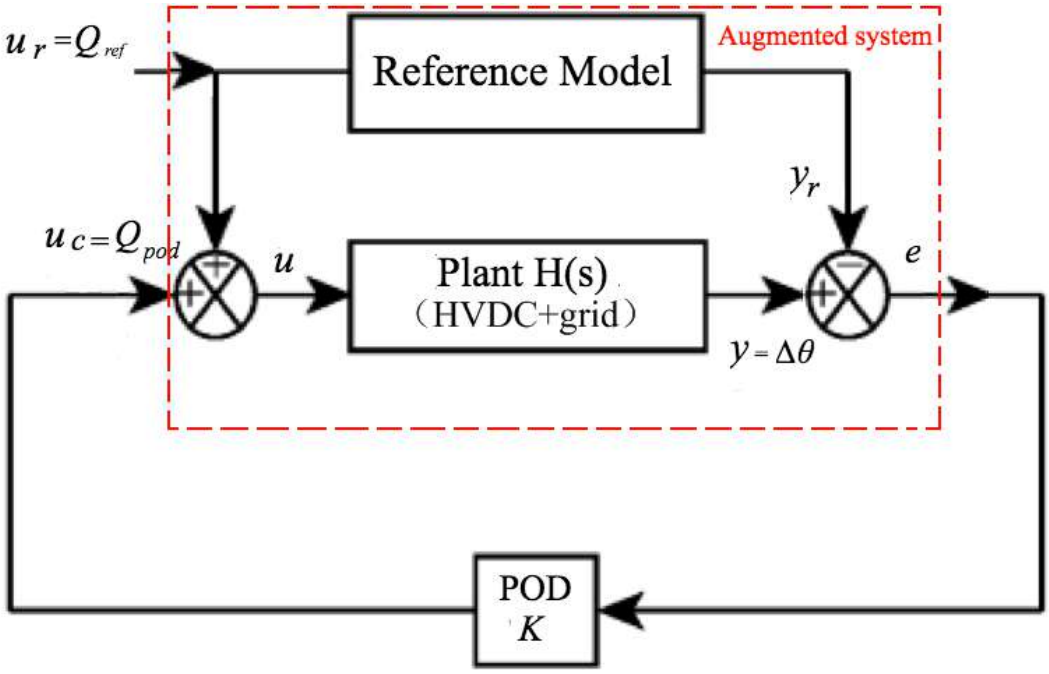

Figure 4.23 – The structure of RSOFC.

where $e = y - y_r$ is the controlled output and $\tilde{X} = \begin{bmatrix} x & x_r & e \end{bmatrix}^T$.

$$\begin{aligned} \tilde{A} &= \left[\begin{array}{cc|c} A & 0 & 0 \\ 0 & A_r & 0 \\ \hline CA & -C_r A_r & 0 \end{array}\right], \tilde{B} = \begin{bmatrix} B \\ 0 \\ CB \end{bmatrix} \\ \tilde{B}_r &= \begin{bmatrix} B \\ B_r \\ CB - C_r B_r \end{bmatrix}, C_e = \begin{bmatrix} 0 & 0 & I \end{bmatrix} \end{aligned} \tag{4.33}$$

In this section, the robust H_∞ static output-error feedback controller (RSOFC) is given by,

$$u_c = Ke, \tag{4.34}$$

where K is the RSOFC matrix controller gains.

From (4.32), (4.33) and (4.34), the closed-loop system is

$$\begin{aligned} \dot{\tilde{X}} &= \tilde{\tilde{A}}\tilde{X} + \tilde{B}_r u_r \\ e &= C_e \tilde{X} \end{aligned} \tag{4.35}$$

where $\tilde{\tilde{A}} = \tilde{A} + \tilde{B} \begin{bmatrix} 0 & 0 & K \end{bmatrix}$.

4.5.2 RSOFC gains computation for stability and robustness

The main results for the global asymptotic stability of the closed-loop system (4.35) are given in the following Theorem 1:

Theorem 1: The closed-loop system (4.35) is asymptotically stable if and only if there exists a definite symmetric positive matrix $X = X^T > 0$ and a matrix Y such that:

$$\min \gamma \tag{4.36}$$

subject to

$$\begin{aligned} &\begin{bmatrix} \tilde{A}X + X\tilde{A}^T + \tilde{B}Y + Y^T\tilde{B}^T & \tilde{B}_r & (C_e * X)^T \\ \tilde{B_r}^T & -\gamma I & 0 \\ C_e * X & 0 & -\gamma I \end{bmatrix} < 0 \\ &X > 0 \end{aligned} \tag{4.37}$$

Thus, the proposed robust H_∞ RSOFC design is given in (4.38) by solving LMIs (4.37).

$$K = XY^{-1} \tag{4.38}$$

Proof. The transfer function from the disturbance u_r to the output e is:

$$T_{u_re}(s) = C_e(sI - (\tilde{A} + \tilde{B}K)^{-1}\tilde{B}_r \tag{4.39}$$

The disturbance rejection problem is solved by minimizing the H_∞ norm of (4.39) ($||T_{u_re}||_\infty \leq \gamma$). Based on Bounded real lemma (Duan and H.-H. Yu 2013; Boyd et al. 1994), the closed-loop system is stable, if and only if there exist a symmetric positive definite matrix $P = P^T > 0$, such that:

$$\begin{bmatrix} \tilde{\tilde{A}}^T P + P\tilde{\tilde{A}} & P\tilde{B}_r & C_e^T \\ \tilde{B_r}^T P & -\gamma I & 0 \\ C_e & 0 & -\gamma I \end{bmatrix} < 0 \tag{4.40}$$

From, (4.35) and (4.40),

$$\begin{bmatrix} \phi & P\tilde{B}_r & C_e^T \\ \tilde{B_r}^T P & -\gamma I & 0 \\ C_e & 0 & -\gamma I \end{bmatrix} < 0 \tag{4.41}$$

where $\phi = [\tilde{A} + \tilde{B}\begin{bmatrix} 0 & 0 & K \end{bmatrix}]^T P + P[\tilde{A} + \tilde{B}\begin{bmatrix} 0 & 0 & K \end{bmatrix}]$. Define

$$T = \begin{bmatrix} P^{-1} & 0 & 0 \\ 0 & I & 0 \\ 0 & 0 & I \end{bmatrix} \tag{4.42}$$

where I is the identity matrix. Pre- and post-multiplying both sides of the (4.41) by T and T^T, respectively, and defining $X = KY$, $X = P^{-1}$, the LMIs (4.36) and (4.37) in Theorem 1 are obtained.

4.6 Model-matching robust H_∞ dynamic decoupling output-feedback control

Notice that to practically implement the ROSFC controller, one needs to the run reference model to produce the e signal in Fig. 4.23. Also, to avoid state reconstruction, a similar problem is solved here in an output-feedback context. Also to further improve the decoupling, a dynamic controller is proposed. Moreover, the feedback is static, i.e., only a gain K and this might limit performances. To overcome this, the structure of the control is modified as in Fig. 4.24. Indeed, for such a control, called DDOFC in the sequel, the feedback is dynamic and the reference model is decoupled from the finally implemented closed-loop (the green box in Fig. 4.24).

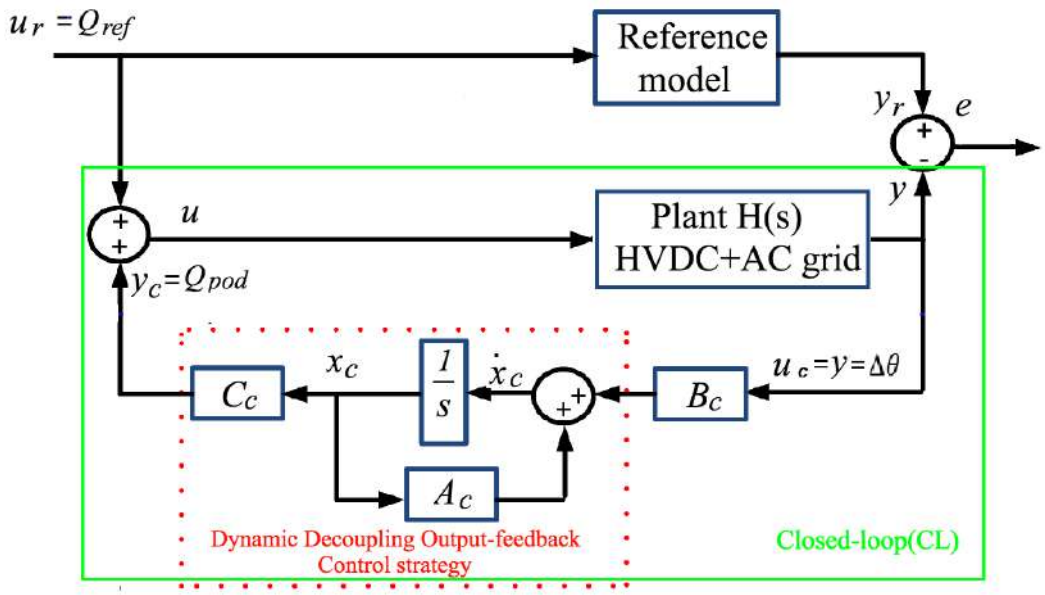

Figure 4.24 – The structure of DDOFC.

Let

$$\begin{aligned} \dot{x}_c &= A_c x_c + B_c u_c \\ y_c &= C_c x_c \end{aligned} \tag{4.43}$$

be a state-representation of the controller matrices A_c, B_c and C_c which are thus to be designed. From Fig. 4.24, it follows,

$$\begin{aligned} u &= u_r - u_c = u_r - y_c = u_r - C_c x_c \\ u_c &= y = Cx \end{aligned} \tag{4.44}$$

From (4.5), (4.31) and (4.43) , the virtual system (VS) state-space equation is

$$\begin{aligned} \dot{X} &= \bar{A}X + \bar{B}u_r \\ Y &= \bar{C}X \end{aligned} \tag{4.45}$$

where $X(t) = \begin{bmatrix} x \\ x_r \\ x_c \end{bmatrix}^T$, and

$$\bar{A} = \begin{bmatrix} A & 0 & -BC_c \\ 0 & A_r & 0 \\ B_c C & 0 & A_c \end{bmatrix}, \bar{B} = \begin{bmatrix} B \\ B_r \\ 0 \end{bmatrix}, \bar{C} = \begin{bmatrix} -C \\ C_r \\ 0 \end{bmatrix}^T .$$

4.6.1 DDOFC gains computation for stability and robustness

Theorem 2: The virtual system (VS) (4.45) is asymptotically stable if and only if there exist positive definite symmetric matrices $Q, Z \in \Re^{(n+n_r)\times(n+n_r)}$, non singular matrices $\widehat{A}, \widehat{B}, \widehat{C} \in \Re^{(n+n_r)\times(n+n_r)}$, and scalar γ, such that a solution of the problem (4.46) can be found to satisfy LMIs (4.47)-(4.48).

$$\min \gamma \tag{4.46}$$

$$\begin{bmatrix} \phi_1 + \phi_1^T & \widehat{A}^T + \begin{bmatrix} A & 0 \\ 0 & A_r \end{bmatrix} & \begin{bmatrix} B \\ B_r \end{bmatrix} & Q \begin{bmatrix} -C^T \\ C_r^T \end{bmatrix} \\ * & \phi_2 + \phi_2^T & Z \begin{bmatrix} 0 \\ B_r \end{bmatrix} + \widehat{B} & \begin{bmatrix} -C^T \\ C_r^T \end{bmatrix} \\ * & * & -\gamma I & 0 \\ * & * & 0 & -\gamma I \end{bmatrix} \leq 0 \tag{4.47}$$

$$\begin{bmatrix} Q & I \\ I & Z \end{bmatrix} \geq 0 \tag{4.48}$$

where

$$\phi_1 = \begin{bmatrix} A & 0 \\ 0 & A_r \end{bmatrix} Q + \begin{bmatrix} -B\widehat{C} \\ 0 \end{bmatrix}, \phi_2 = Z \begin{bmatrix} A & 0 \\ 0 & A_r \end{bmatrix} + \begin{bmatrix} B\widehat{B}C \\ 0 \end{bmatrix}^T,$$

Once unknown variables Q, Z, $\widehat{A}$, $\widehat{B}$, $\widehat{C}$ are computed to satisfy (4.47)-(4.48), the state matrices of the controller are

$$A_c = N^{-1}\bar{A}M^{-T}, B_c = N^{-1}\widehat{B}, C_c = \widehat{C}M^{-T} \tag{4.49}$$

where

$$\bar{A} = \widehat{A} - Z \begin{bmatrix} A & 0 \\ 0 & A_r \end{bmatrix} Q - N \begin{bmatrix} B_c C \\ 0 \end{bmatrix}^T Q - Z \begin{bmatrix} BC_c \\ 0 \end{bmatrix} M^T \tag{4.50}$$

and

$$NM = I - ZQ. \tag{4.51}$$

Proof. The disturbance rejection problem is solved by minimizing $||T_{u_r e}||_\infty \leq \gamma$ of the transfer function from u_r to output e in Fig. 4.24. As the proof of Theorem 1, based on Bounded real lemma Duan and H.-H. Yu 2013; Boyd et al. 1994, the closed-loop system is stable if and only if there

exists a symmetric matrix $W \in \Re^{2(n+n_r)\times 2(n+n_r)}$ such that,

$$\begin{bmatrix} \bar{A}^T W + W\bar{A} & W\bar{B} & \bar{C}^T \\ \bar{B}^T W & -\gamma I & 0 \\ \bar{C} & 0 & -\gamma I \end{bmatrix} \leq 0 \tag{4.52}$$

$$W \geq 0 \tag{4.53}$$

It can be seen that (4.52) is a Bilinear Matrix Inequality (BMI). To convert it to LMI, the variables substitution method based on (Scherer, Gahinet, and Chilali 1997) is used. Let the partition W and W^{-1} as

$$W = \begin{bmatrix} Z & N \\ N^T & \star \end{bmatrix}, W^{-1} = \begin{bmatrix} Q & M \\ M^T & \star \end{bmatrix} \tag{4.54}$$

where Q and Z are $(n+n_r)X(n+n_r)$ symmetry matrices, M and N are $(n+n_r)X(n+n_r)$ full matrices, $\star$ stands for unknown matrix. Set

$$\prod_1 = \begin{bmatrix} Q & I \\ M^T & 0 \end{bmatrix}, \prod_2 = \begin{bmatrix} I & Z \\ 0 & N^T \end{bmatrix} \tag{4.55}$$

From $WW^{-1} = I$, it can be inferred

$$\prod_2 = W \prod_1 \tag{4.56}$$

In this case,

$$\prod_2^T W\bar{A} = \prod_2^T \bar{A} \prod_1 \tag{4.57}$$

So that,

$$\begin{aligned} \prod_2^T \bar{A} \prod_1 &= \begin{bmatrix} I & 0 \\ Z & N \end{bmatrix} \begin{bmatrix} A & 0 & -BC_c \\ 0 & A_r & 0 \\ B_c C & 0 & A_c \end{bmatrix} \begin{bmatrix} Q & I \\ M^T & 0 \end{bmatrix} \\ &= \begin{bmatrix} \begin{bmatrix} A & 0 \\ 0 & A_r \end{bmatrix} Q + \begin{bmatrix} -BB_c \\ 0 \end{bmatrix} M^T & \begin{bmatrix} A & 0 \\ 0 & A_r \end{bmatrix} \\ Q_1 & Q_2 \end{bmatrix} \end{aligned} \tag{4.58}$$

and,

$$\prod_1^T W\bar{B} = \prod_2^T \bar{B} \prod_1 = \begin{bmatrix} I & 0 \\ Z & N \end{bmatrix} \begin{bmatrix} B \\ B_r \\ 0 \end{bmatrix} = \begin{bmatrix} B \\ B_r \\ Z \begin{bmatrix} B \\ B_r \end{bmatrix} \end{bmatrix}. \tag{4.59}$$

Then,

$$\prod_1^T \bar{C} = \left[\begin{bmatrix} -C & C_r & C \end{bmatrix} \begin{bmatrix} Q & I \\ M^T & 0 \end{bmatrix}\right]^T \begin{bmatrix} Q \begin{bmatrix} -C^T \\ C_r^T \end{bmatrix} \\ -C_r^T \\ C_r^T \end{bmatrix} \tag{4.60}$$

where,

$$\begin{aligned} &Q_1 = Z \begin{bmatrix} A & 0 \\ 0 & A_r \end{bmatrix} Q + N \begin{bmatrix} B_c & C & 0 \end{bmatrix} Q + Z \begin{bmatrix} -BC_c \\ 0 \end{bmatrix} M^T + \\ &NA_cM^T, \\ &Q_2 = Z \begin{bmatrix} A & 0 \\ 0 & A_r \end{bmatrix} + N \begin{bmatrix} B_c & C & 0 \end{bmatrix} \end{aligned} \tag{4.61}$$

Thus,

$$\begin{aligned} &\hat{A} = Z \begin{bmatrix} A & 0 \\ 0 & A_r \end{bmatrix} Q + N \begin{bmatrix} B_c & C & 0 \end{bmatrix} Q + Z \begin{bmatrix} -BC_c \\ 0 \end{bmatrix} M^T \\ &+NA_cM^T, \\ &\hat{B} = NB_c, \hat{C} = C_cM^T \end{aligned} \tag{4.62}$$

Therefore, (4.52) and (4.53) are equivalent to (4.47) and (4.48) in Theorem 2.

4.6.2 Uncertainty analysis in case of different operation points

In order to analyze and improve closed-loop behavior in case of model uncertainties, different operating points are studied in this section. They correspond to different disturbed grid situations which usually happen in realistic power systems:

1. Inverse the power flow direction and the value of the active power on HVDC lines (from $+800MW$ to $-200MW$);
2. 30% increase of the load of the terminal bus of the most participating generator GE_911 to mode 2;
3. Tripping generator GE_914 which is close to the most participating machine GE_911 in the less damped mode 2;
4. Tripping 4 lines close to the most participating generator GE_911 in the less damped mode 2 (transit 213MW, 137MW, -41MW,-118MW on these lines at the moment of the trip).

These cases correspond to the first class of the robustness issue mentioned before (i.e., the parametric case). The behavior of the regulators in all these disturbed grid situations called *robust operation cases* in the sequel will be compared with results of *nominal operation case*. The linearization for each robust operation case at an equilibrium point is done to obtain state-space matrices. *The average rate of change* σ of A, B and C state-space matrices of each robust cases against the nominal case

are shown in Fig. 4.25. Neglectable variations (less than 0.8%) have been noticed for B matrix compared to the ones of A and C matrices.

More precisely, if the nominal case state matrix is $A = [a_{ij}]$, and the robust case state matrix is $\tilde{A_{ij}} = [\tilde{a_{ij}}]$, then the rate of change Δ defined as

$$\Delta = \sum_{i=1}\sum_{j=1} \frac{|a_{ij} - \tilde{a_{ij}}|}{|a_{ij}|}. \tag{4.63}$$

The average rate of change is

$$\sigma = \frac{\Delta}{i * j}. \tag{4.64}$$

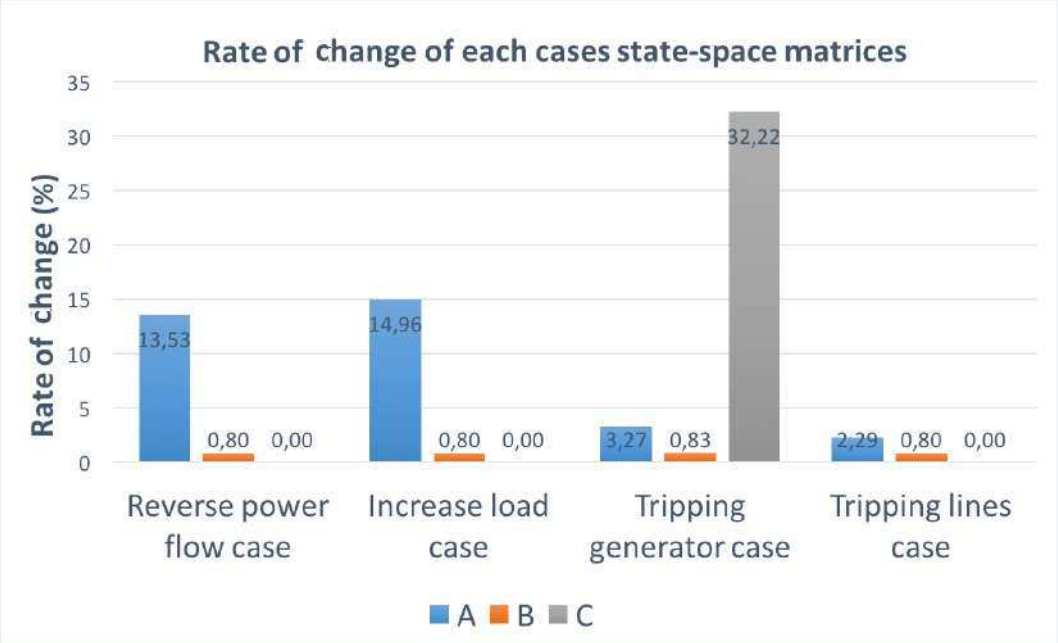

Figure 4.25 – Uncertainty analysis: average rate of change of A, B and C.

4.6.3 Synthesis of new LMI conditions for the uncertainty case

In order to enhance the robustness of the controller to face different operation points, or, roughly speaking, to ensure the effectiveness of the controller, the uncertainty terms quantified in the previous section are considered here for the control synthesis.

Then, the uncertain linear system is

$$\begin{aligned} \dot{x} &= (A + \sigma A)x + Bu \\ y &= (C + \sigma C)x. \end{aligned} \tag{4.65}$$

Theorem 2: The uncertain linear system (4.65) is asymptotically stabilized with DDOFC

controller, if and only if, for some constant $\zeta > 0$, there exist matrices P and K, and scalars ϵ_1 and ϵ_2, solutions of the following LMI condition:

$$\begin{bmatrix} -2\zeta I & \zeta A_o + P & \zeta I & \zeta M_1 & \zeta BKM_2 \\ * & -P + \delta & 0 & 0 & 0 \\ * & * & -P & 0 & 0 \\ * & * & * & -\epsilon_1 I & 0 \\ * & * & * & * & -\epsilon_2 I \end{bmatrix} \leq 0 \tag{4.66}$$

Proof. Under parametric uncertainties, the LMI condition (4.66) becomes

$$\begin{bmatrix} -2\zeta I & \zeta(A + \Delta A) + \zeta BK(C + \Delta C) + P & \zeta I \\ * & -P & 0 \\ * & * & -P \end{bmatrix} \leq 0. \tag{4.67}$$

Thresholds $\Delta A \leq 14.96\%$ and $\Delta C \leq 32.22\%$ deduce in previous section are now transformed into the LMI

$$F_1^T F_1 \leq I \tag{4.68}$$

where $\Delta A = M_1 F_1 N_1, \Delta C = M_2 F_2 N_2$.

Lemma 1 (Chen W. H. and X. 2014), (J. and S. 2015): For any matrices $D \in \Re^{r \times s}$, and $N \in \Re^{s \times r}$, and any matrix $F(t) \in \Re^{s \times s}$, satisfying $F(t)^T F(t) \leq I$, and a scalar $\epsilon \geq 0$, the following inequality holds $DF(t)N + (Df(t)N)^T \leq \epsilon^{-1} DD^T + \epsilon N^T N$. Thus, M_1, M_2, N_1, N_2, F_1 and F_2 are computed from

$$\begin{bmatrix} -2\zeta I & \zeta(A + BKC) + P & \zeta I \\ * & -P & 0 \\ * & * & -P \end{bmatrix} + \begin{bmatrix} \zeta M_1 \\ 0 \\ 0 \end{bmatrix} F_1 \begin{bmatrix} 0 & N_1 & 0 \end{bmatrix} + (*) + \begin{bmatrix} \zeta BKM_2 \\ 0 \\ 0 \end{bmatrix} F_2 \begin{bmatrix} 0 & N_2 & 0 \end{bmatrix} + (*) \leq 0. \tag{4.69}$$

By applying Lemma 1 on condition (4.69) by taking into consideration the constraints in (4.68), and by applying the well-known Schur complement Lemma, it is easy to prove that the condition (4.69) is transformed into the LMI (4.66).

The detailed validations of ROSFC and DDOFC controller compared with the other designed controllers are shown in the next chapter.

4.7 Summary

As the only information of the residues of the modes to be damped is not sufficient in our problem formulation, a dynamic control model which captures not only the modes to be damped

but also the other dynamics which might be excited by the closed-loop is proposed. A low order representation is obtained for this model even in case of large-scale grids. Advanced state-space robust control strategies based on this model were given. This provides the possibility to obtain better performances (higher dampings than with the classic controller on target modes) and to avoid undesirable interactions with modes of different nature which are at near frequencies with the target inter-area modes. Based on this so-called control model, several controllers are designed: LQG POD, mixed sensitivity H_∞ POD, and two controllers based on the reference model ROSFC, DDOFC are proposed. The model-matching controller is the one which provides the best performance for the whole laid of specifications, especially for the unstable zeros. It provides also robustness against parametric uncertainty which has been quantified to 15% for the elements of the state matrix A. It is thus the controller proposed as an outcome of this study.

Chapter 5

Validation on the benchmark system and robustness tests

Contents

5.1 Introduction

The designed controllers and proposed controllers are fully validated on the test system in this chapter. To easily compare the effectiveness between controllers, first, the controllers are applied on the linearized full model in Matlab. Second, they are tested on the nonlinear benchmark in Eurostag.

5.2 Linearized full model validation

In this section, controllers are tested in Matlab with linearized full model in the nominal operation case. Step responses of angle difference $\Delta\theta$ with different controllers are compared in this section (Fig. 5.1).

From Fig. 5.1, in the zoomed figure on the rectangle region, it can be seen that starting from the $t = 8s$, mode 2 is observable and its frequency can be measured from two peaks. The DDOFC POD and LQG POD provide more damping compared to the other POD controllers. For this mode, on the contrary, the classic POD and RSOFC strategies give comparable results and close to the open-loop. In addition, from $t = 2s$ to $t = 4s$, mode 5 can be observed: the DDFOC POD, LQG POD, and mixed sensitivity H_∞ POD, which has less undershoot than the other POD controller provide sufficient damping for this mode. It should be noticed that, from $t = 1s$ to $t = 3s$, mode 1 (with its frequency 1.3Hz) is observable (in the curve with LQG POD) (see zoomed figure in the

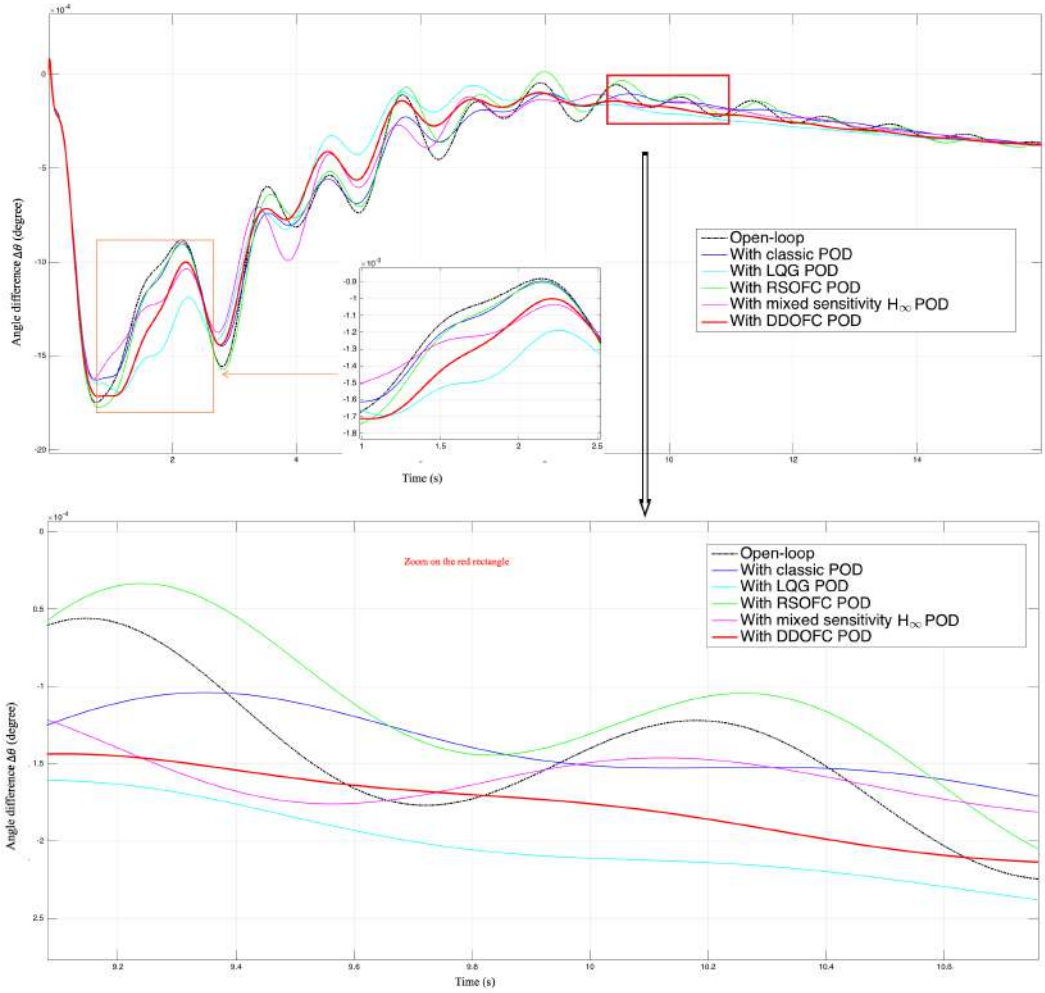

Figure 5.1 – Comparison of linearized full model.

middle of above one). This oscillation also exists in the open-loop curve. Thus, it can be concluded that the proposed DDOFC POD guarantees thus a sufficient damping in a wide frequency band. The closed-loop modes are shown in Table 5.1. It can be seen that, the classic POD improves a little the damping of mode 2, but disturbs mode 4. The DDOFC POD, LQG POD, and mixed sensitivity H_∞ POD improves the damping of each mode over 10%. To be precise, the LQG POD gives the highest value of damping on mode 3; the mixed sensitivity POD provides accepted dampings of mode 4 and 5; RSOFC POD decreases each mode damping except the one of mode 5; the DDOFC POD satisfies the target damping of modes 1 and 2 without disturbing the others. It can also be seen that the proposed DDOFC POD fulfils the damping requirement. Although calculating dampings of modes after linearizing their closed-loop systems with different controllers at an equilibrium point is an intuitive way to evaluate the effectiveness of each controller, the nonlinear dynamic features cannot be evaluated in this way and should be excited by stronger disturbances as the short-circuits studied in the next section.

Table 5.1 – Comparison of damping

No.	ξ Open-loop(%)	ξ with classic POD (%)	ξ with LQG POD (%)	ξ with Mixed sensitivity H_∞ POD (%)	ξ with RSOFC POD (%)	ξ with DDOFC POD (%)
1	19.5	30.5	21.7	20.3	18.6	23.3
2	4.5	6.1	10.9	11.6	4.2	12.6
3	10.1	12.0	14.9	12.3	9.6	10.8
4	8.3	8.1	11.4	12.4	7.9	10.6
5	10.1	12.4	13.6	14.9	14.2	14.1

5.3 Nonlinear system validation

In order to test the performances and robustness of proposed controllers, the controllers are tested on nonlinear model with Eurostag software. Both ***nominal operation case*** and ***robust operation cases*** as explained in Section 4.6.2 are considered. For all tests, the same three-phase ground short-circuit as in Section 4.3.3 at bus FVLAR1-2 which is the terminal bus of generator GE_918 (see Fig. 2.3) is considered. Because it is closed to generator GE_911 which is the most participating machine in mode 2 (see Table 2.1), this disturbance excites the modes of interest. In the nonlinear test, much more attention is paid on the generator speed, especially the most participating machine(s) in the modes of interest.

5.3.1 Nominal operation test

A comparison between controllers of the nominal operation case is shown in Fig. 5.2.

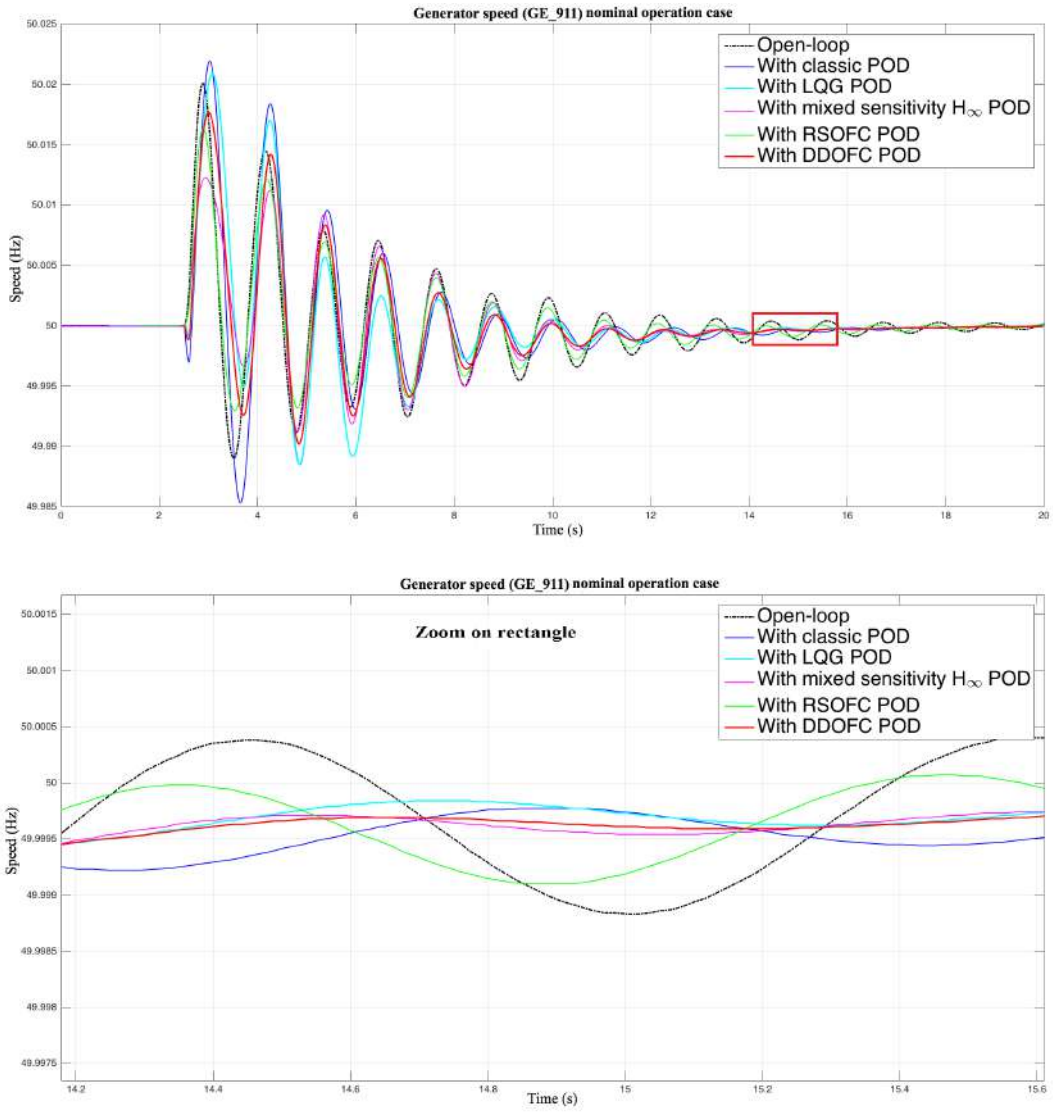

Figure 5.2 – Nonlinear nominal operation case.

From the zoomed figure in Fig. 5.2, it can be seen that for mode 2 (it is recognized by measuring the frequency between peaks in curves from the 8^{th} swing), the DDOFC POD and mixed sensitivity H_∞ provide more damping compared with the other controllers. From $t = 3s$, there are the contributions of several modes mixed with nonlinear dynamics. It can be seen that the DDOFC, mixed sensitivity H_∞, and LQG POD provide more damping than RSOFC and classic POD. However, from the 4^{th} to the 8^{th} swing (the period in which mode 1 can be observed), the damping provided by mixed sensitivity H_∞ POD is less than by DDOFC POD. These behaviours are coherent with

the modal analysis estimation in Table 5.1.

Also, the proposed controllers must have the ability to deal with different operation points of the system to settle a good trade-off between performance and robustness. This is checked by the robustness tests reported in the next section.

5.3.2 Robustness tests

In order to investigate the behaviors in the case of system uncertainties, different disturbed grid situations defined in Section 4.6.2) are now used. The same short-circuit used in the nominal operation case at the terminal bus FVLAR1-2 is considered to excite the dynamics.

Responses obtained with the same controllers considered above are now shown in Fig. 5.3, 5.4, 5.5, 5.6 for the following situations:

— **Reverse power flow case:** In Fig. 5.3, the performance of RSOFC POD and mixed sensitivity H_∞ POD are almost the same with DDOFC POD from $t = 12s$ (mode 2). It can be seen that it provides more damping than the other controllers. From the 3^{rd} swing, mode 4 is dominant. For this mode, although the RSOFC POD controller dampes more than the other controllers, its damping in the nominal operation case is insufficient. Notice that from $t = 3s$ to $t = 5s$, although the amplitude of oscillation with mixed sensitivity H_∞ POD is smaller than the one with DDOFC POD, its curve has one more tiny swing at $t = 3.5s$ (see zoomed figure in the middle). This means that the mixed sensitivity H_∞ POD may excite other nonlinear dynamics in the system. This phenomenon also appears in following increasing load case. The oscillation with classic POD, in this case, is even higher than in open-loop. Besides, the damping of the other modes is also decreased. This test shows that the proposed DDOFC POD have the ability to handle the uncertainties in reverse power flow situation without losing damping/performance for all modes.

— **Increase load case:** In Fig. 5.4, from $t = 12s$ (mode 2), the mixed sensitivity H_∞, the LQG POD and the DDOFC POD provide the same accepted damping compared with the other controllers. However, in the middle of the curves (from the 3^{rd} to the 5^{th} swing), the damping provided by mixed sensitivity H_∞ POD is not enough for mode 4. Besides, the overshoot of the curve with LQG POD in the first swing is not desirable. Although that the RSOFC POD provides less damping than the classic POD, its nonlinear dynamic in first two swings is acceptable. According to this test, in increasing load situation, the DDOFC POD is still the only controller to satisfy all requirements.

— **Tripping generator case:** In Fig. 5.5, from the zoomed picture, it can be seen that, during the first two swings, the LQG POD along with classic POD even increases the oscillations compared to open-loop. They lack of robustness to face these nonlinearities. The DDOFC, mixed sensitivity H_∞ and LQG POD, from $t = 12s$ (mode 2), have damping advantages against the other controllers. In addition, from the 3^{th} to the 6^{th} swing where mode 1 is

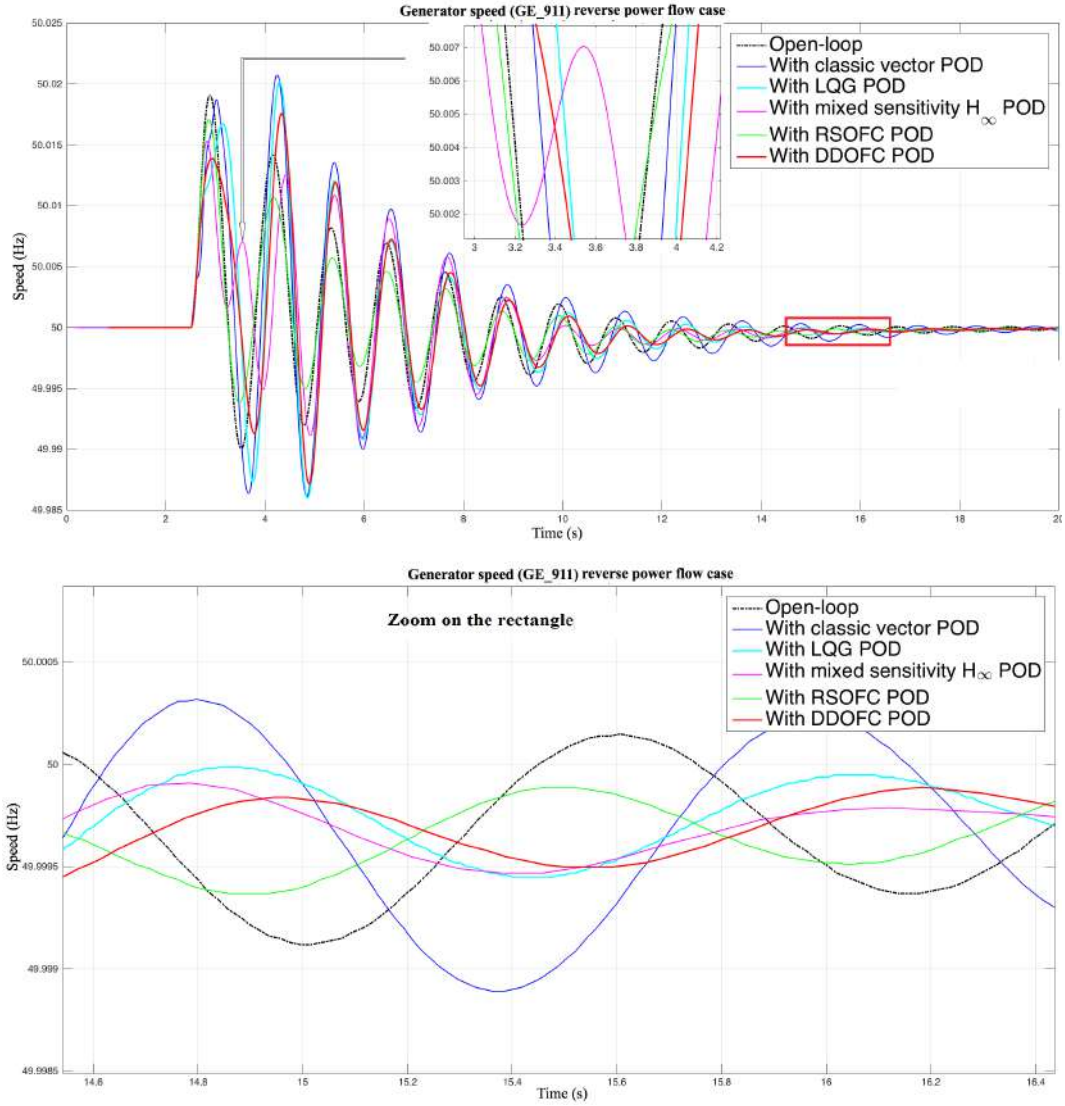

Figure 5.3 – Reverse power flow case.

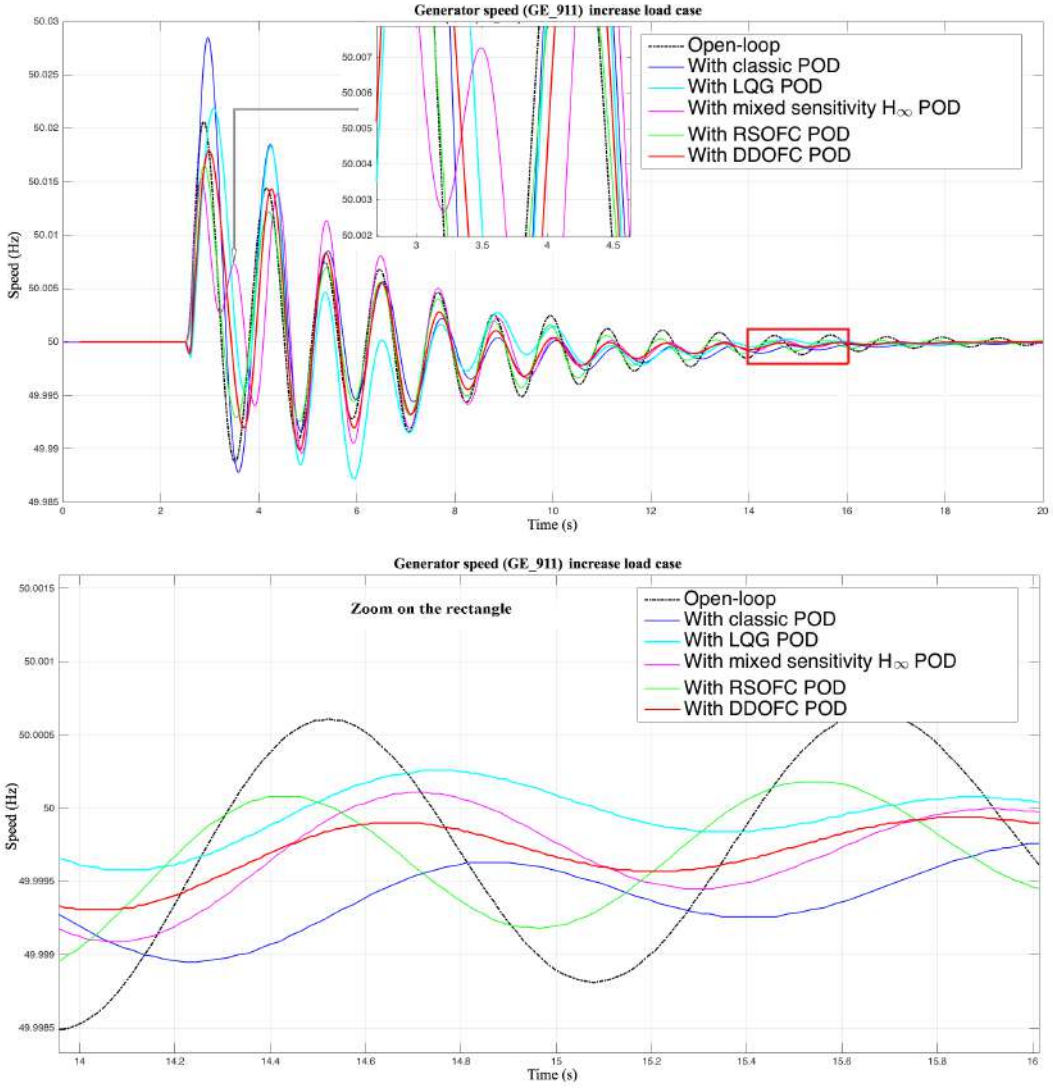

Figure 5.4 – Increase load case.

dominant, DDOFC POD provides more damping than mixed sensitivity H_∞, RSOFC POD, and LQG POD. For the tripping generator case, the best results are ensured by DDOFC POD.

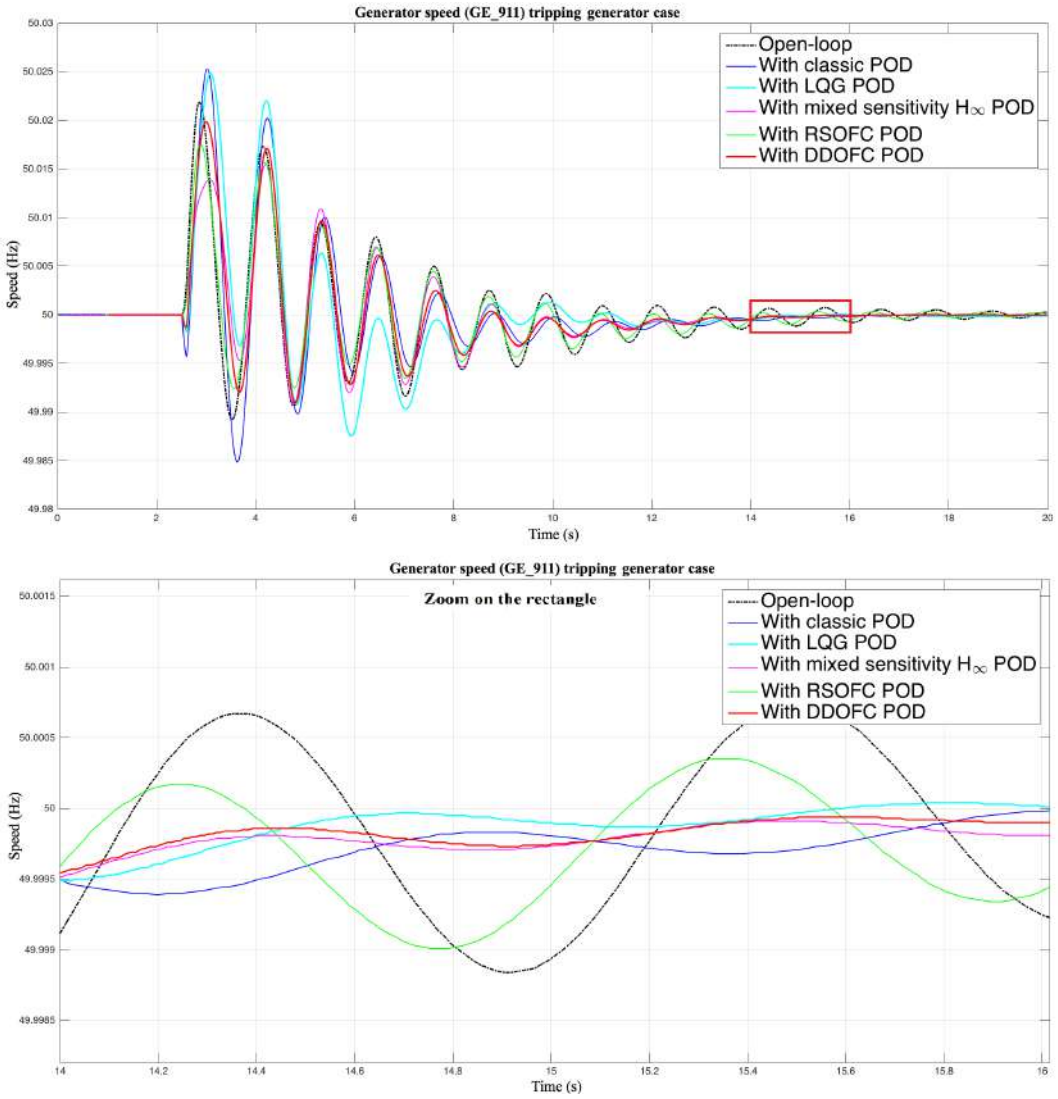

Figure 5.5 – Tripping generator case.

— **Tripping lines case:** In Fig. 5.6, in first two swings of nonlinear dynamic response, despite that the fact that the mixed sensitivity H_∞ POD response is the most damped one, the damping for mode 1 (from the 4^{th} to the 8^{th} swing) is less than the one obtained with the classic POD, the LQG POD, and the DDOFC POD. Besides, in zoomed figure, mode 2 can be observed and it is damped more with DDOFC than with mixed sensitivity H_∞ POD and RSOFC POD. Moreover, for mode 2, although LQG POD seems to provide sufficient damping, the oscillation in the first two swings is even higher than open-loop. Thus, the

DDOFC POD is again the controller which provides the best results in this case also.

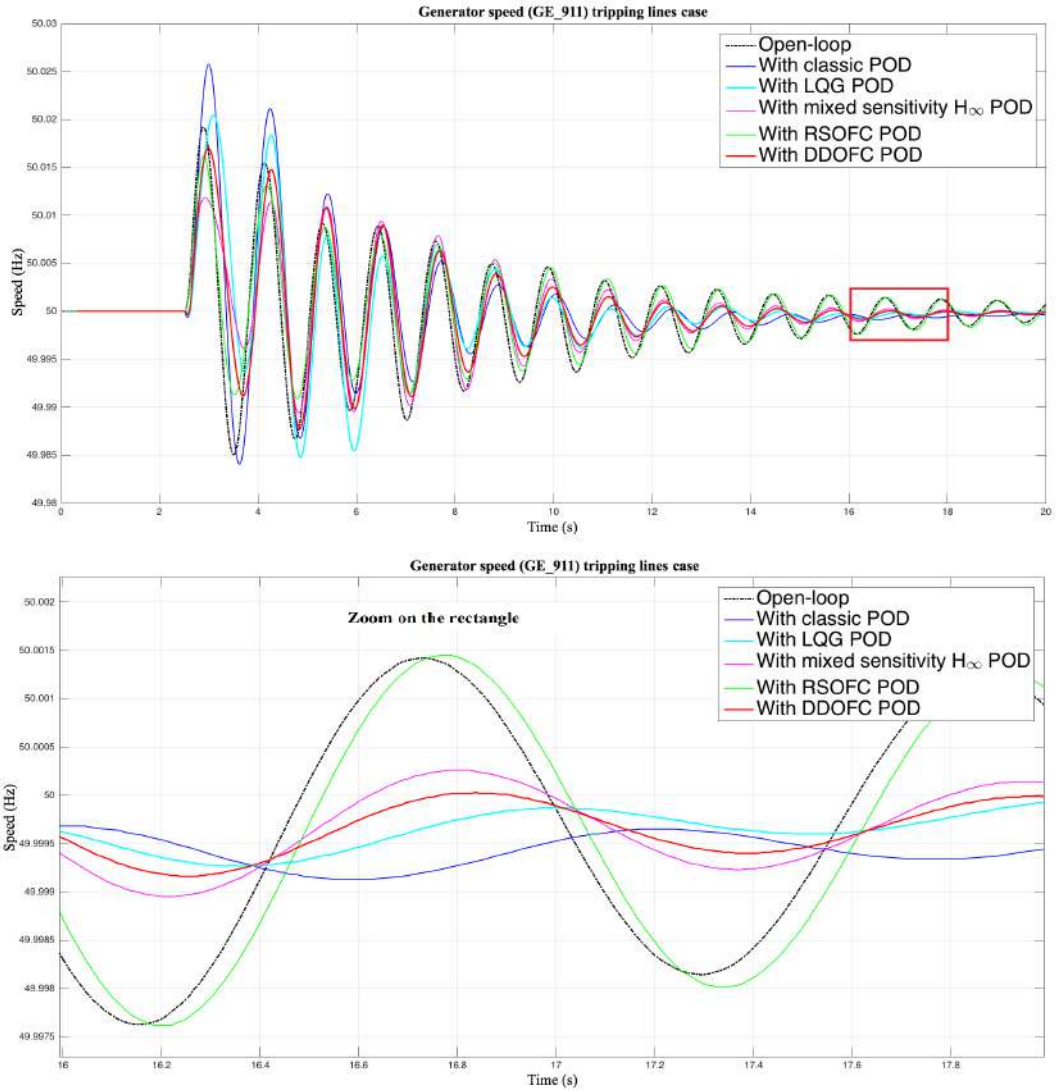

Figure 5.6 – Tripping lines case.

Thus, among all these tests, the proposed DDOFC POD controller has the robustness to deal with different operation points which also provides sufficient damping for each case. This control strategy is selected as best solution and will be next applied to coordinate active and reactive power modulation as final control solution.

5.4 Summary

The realistic situations of the power grid give the motivation to improve robustness against typical variations of the grid and un-modeled dynamics. This means to maintain the damping

properties not only in the nominal operation case but also in case of disturbances (short-circuits) and usual grid variations (line/generator trips, modification of operation point, etc). The different controllers were tested on a realistic cases in simulation with a professional grid dedicated software (Eurostag). The results prove that the proposed DDOFC POD controller has the ability to deal with the target specifications. The resulting control can be easily implemented in state-space in real-word of grid applications.

Chapter 6

Coordination of active and reactive power modulation

Contents

6.1 Introduction

As the VSC-HVDC link has the ability to independently control the transmitted active and reactive powers, in order to fully take advantage of power modulations to improve oscillations damping and robustness, the coordination of reactive Q and active P power modulation is achieved in this chapter. The same input signal as for the reactive power modulation controller is used in this coordinated controller. The proposed control approach DDOFC is applied to modulate both the active and reactive powers in this chapter. As the coordinated controller has one input and two outputs, a Single Input Multi-Output (SIMO) modulation POD controller is synthesized in what follows. The structure of the coordinated SIMO modulation controller is shown in Fig. 6.1. The classic coordinated POD controller is designed to compare its effectiveness with the proposed SIMO modulation POD. Its principle for parameters tuning is the same as the one used for Q modulation (see details in Appendix D).

6.2 Control model synthesis

The same methodology mentioned in Chapter 2 is adopted to obtain a reduced-order control model. Fig. 6.2 shows the Bode plot curve fitting results. The obtained parameters of the control

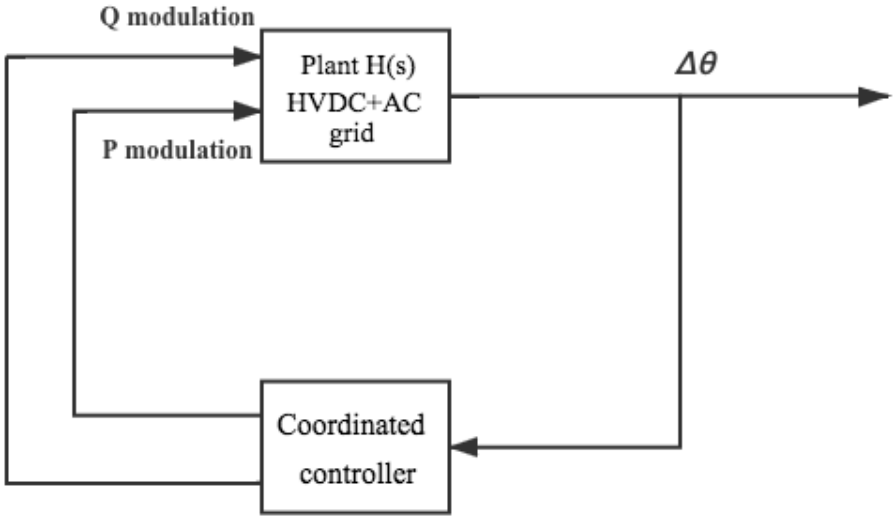

Figure 6.1 – Structure of SIMO coordinated modulation POD.

model are given in Appendix D.

6.3 Linearized model validation

The controller design process is similar to the one explained before for Q modulation. Linearized full model validation results are directly presented in this section.

The step response results in Matlab of the closed-loop system with SIMO modulation POD controllers are shown in Fig. 6.3. First, notice that classic SIMO modulation POD is more effectve than only Q POD modulation. Next, the DDOFC SIMO POD provides better damping than SIMO classic POD. Indeed, from $t = 10s$, oscillation is fully damped, which is not the case with the classic POD.

6.4 Nonlinear model validation

The proposed SIMO modulation POD controller is also validated in nonlinear simulation with Eurostag in this section. Notice that for this validation, the same short-circuit disturbance (same value and same location) used in Section 5.3.2 is considered. The tests are also divided into two parts: nominal operation case and robust operation cases.

6.4.1 Nominal operation test

Comparison between controllers in nominal operation case is shown in Fig. 6.4. The DDOFC SIMO modulation POD damp less the first 3 nonlinear swings than the classic one. However, it

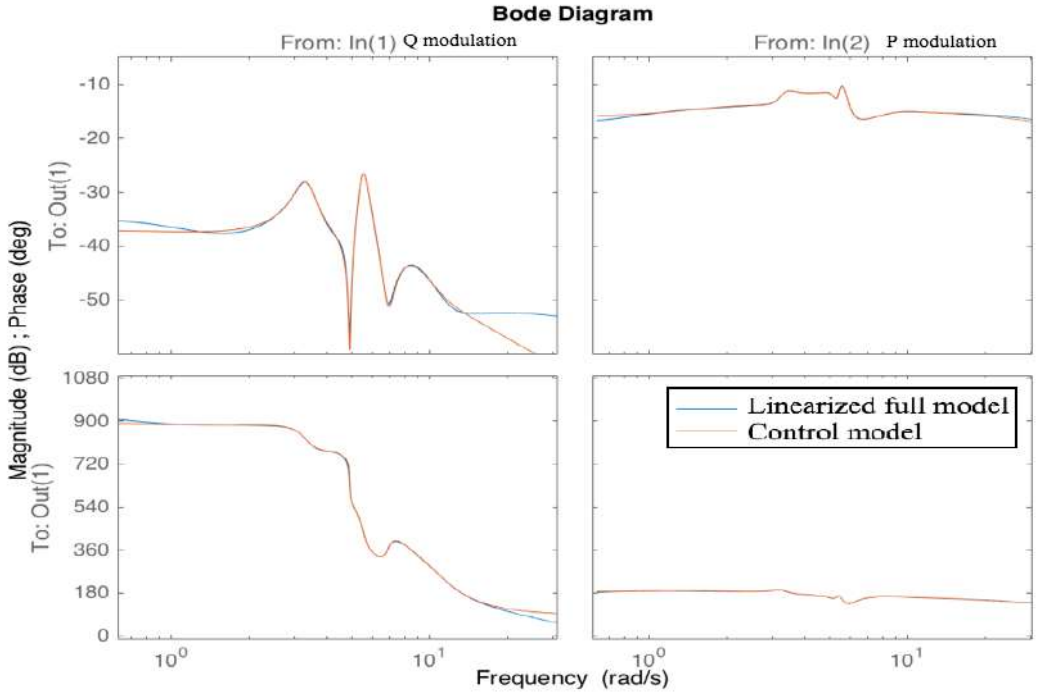

Figure 6.2 – Curve fitting for synthesis of the control model.

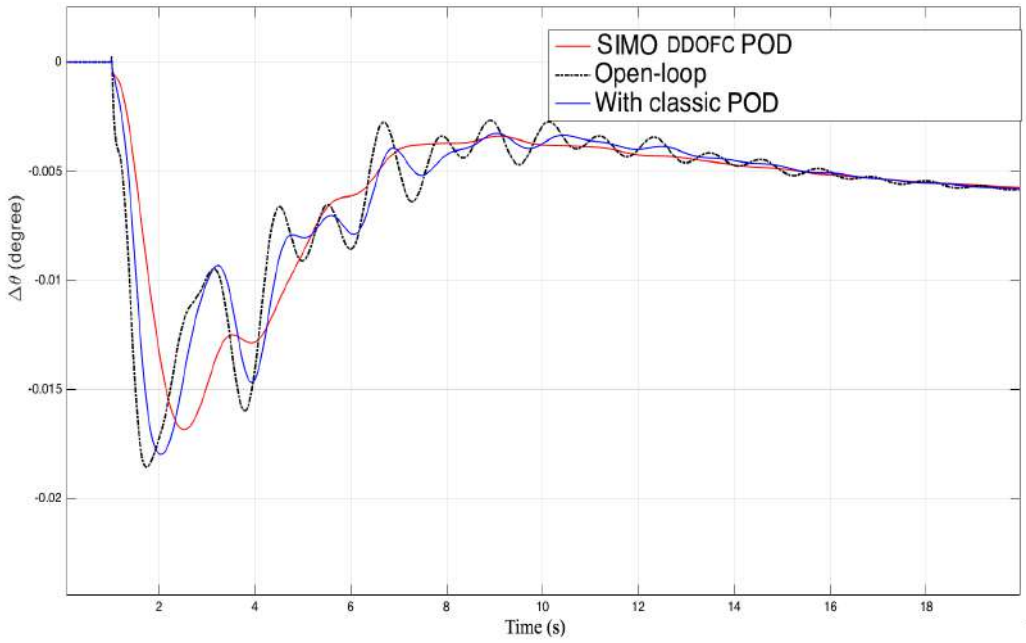

Figure 6.3 – Comparison of SIMO modulation PODs in linearized model.

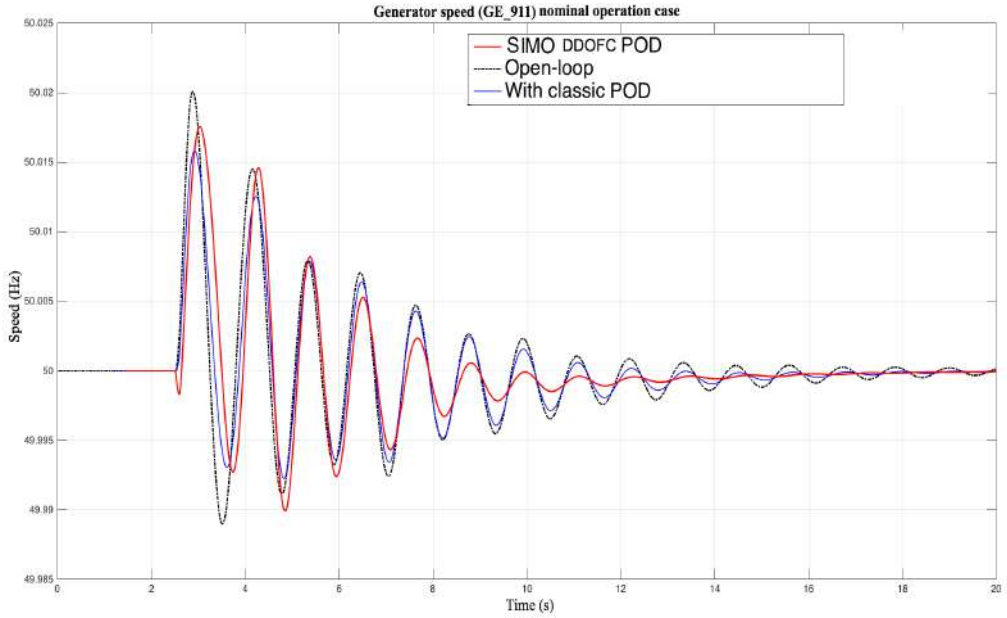

Figure 6.4 – Nominal operation case with SIMO modulation PODs.

provides better damping of the modes (can be seen from the 4^{th} swing).

6.4.2 Robust operation tests

The same scenarios of Section 5.3.2 are adopted here to test robustness. Results are shown in Fig. 6.5, 6.6, 6.7, 6.8.

— **Reverse power flow case:** The classic SIMO modulation POD amplifies the oscillations compared with the open-loop system from the 2^{nd} to the 5^{th} swing (mode 1). However, the damping of target mode 2 is improved (starting from the 7^{th} swing).

— **Increased load case:** The situation is the same as in the nominal operation case: in the first 3 nonlinear swings, the DDOFC SIMO POD provide a little less damping than the classic one for these nonlinearities, but the damping of modes (mode 2 and mode 4 can be recognized from the 4^{th} swing) is clearly better than the one provide by the classic POD.

— **Tripping generator and lines cases:** Starting from the 3^{rd} swing (for tripping generator case) and from the 4^{th} swing (for tripping lines case), the proposed controller provides much higher damping than the classic one.

From these results, it can be concluded that the proposed DDOFC SIMO modulation POD can

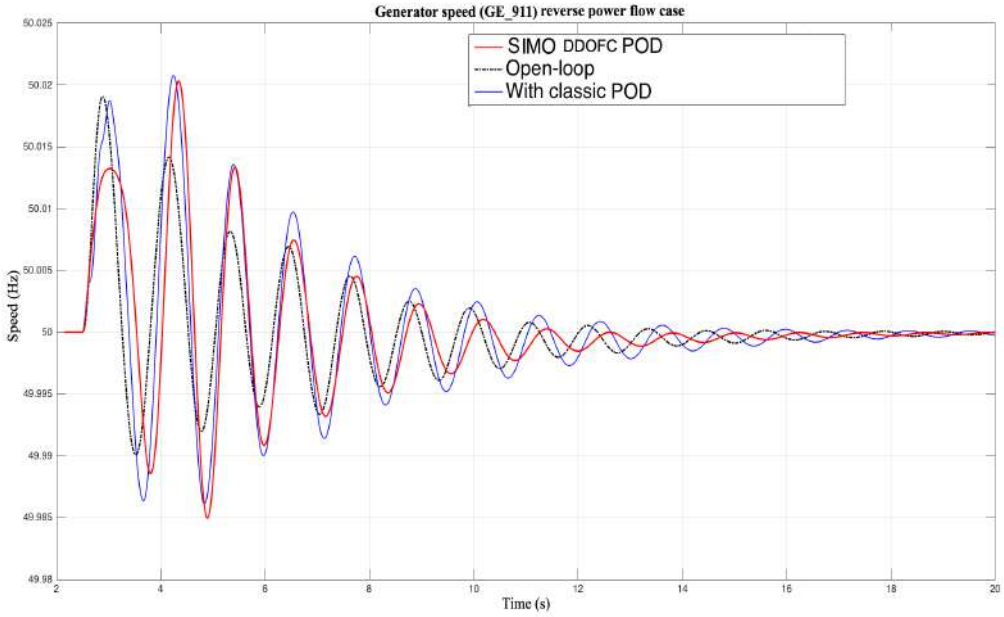

Figure 6.5 – Reverse power flow case.

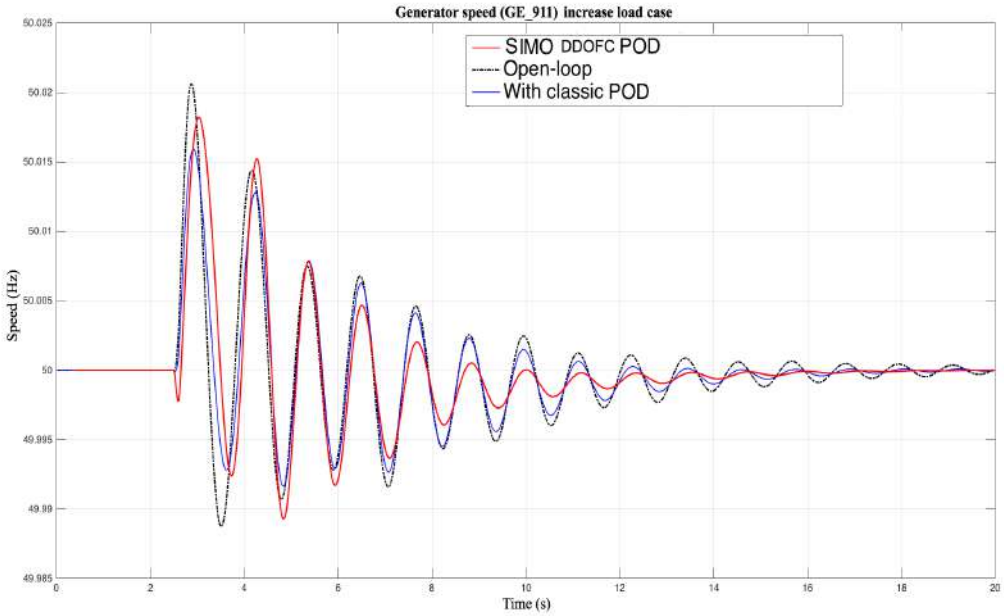

Figure 6.6 – Increase load case.

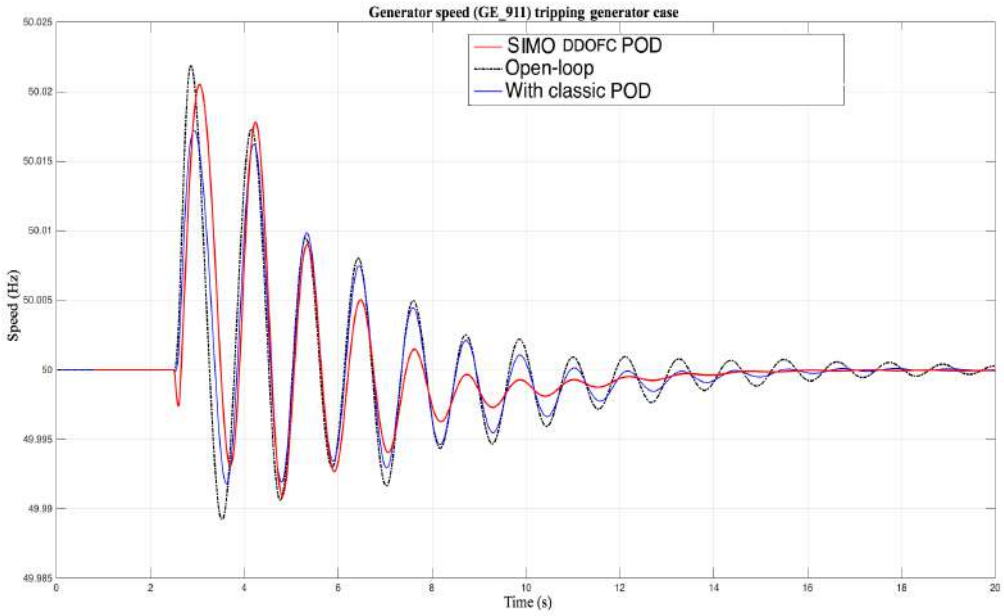

Figure 6.7 – Tripping generator case.

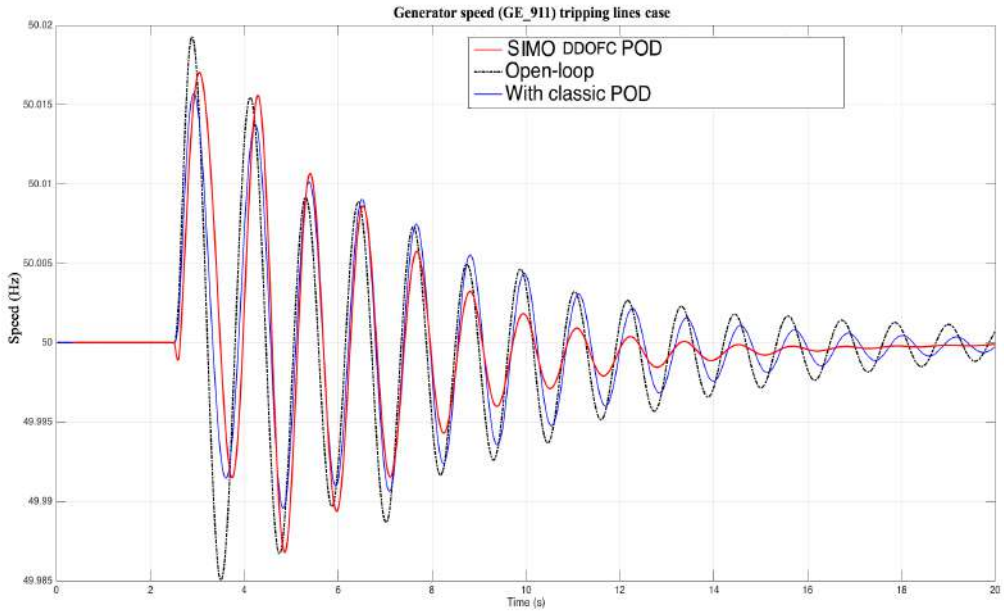

Figure 6.8 – Tripping lines case.

significantly improve the damping of target modes-especially mode 2-at more than 15% and much more than the classic POD (less than 8% for mode 2). Although the nonlinear dynamic responses in first several swings of DDOFC SIMO modulation POD controller are less damped than with only Q modulation DDOFC POD (according tests in Section 5.3.2), the damping of mode 1 in these swings is still acceptable (around 10%). Moreover, damping of modes 2 and 4 is improved compared with Q modulation and this damping level is maintained in different operation points cases.

6.5 Summary

The proposed strategy DDOFC POD is applied to the coordination of active and reactive SIMO modulation controller in this chapter. The results are compared with Q modulation of both DDOFC and classic SIMO POD. Results prove that the proposed controller has the ability to improve the damping of inter-area oscillations and maintain robustness facing changing operation points and uncertainties in models.

CONCLUSION AND FUTURE WORKS

This thesis deals with the power system small-disturbance stability issue. The problem of power oscillations damping control of a VSC-HVDC was addressed in the particular context where the HVDC link is inserted in a meshed AC grid.

Interactions with other dynamics in the frequency range around 1Hz were managed thanks to an enhanced control model which captures all these dynamics in a reasonable low order transfer function. This gives the possibility to provide better performances with advanced controllers (higher damping than with the classic controller on target modes) and to avoid undesirable interactions with modes of different nature which are at near frequencies with the target inter-area modes.

Another research aspect is concerned with the behavior of unstable zeros of electrical networks equipped with HVDC links. It was shown that, unstable zeros systematically exist in the studied system in function of the topology (length of lines) of the AC grid. Since there is barely literature researched on the unstable zeros in the model of HVDC link embedded in AC systems, this work provides an essential analysis result to further researches. Also, corrective actions have been integrated at control level to diminish the negative impact of such zeros on performances.

The realistic situation of the power grid gave the motivation to improve robustness against typical variations of the grid and un-modeled dynamics. To further improve robustness and to counteract the effect of nonlinearities and uncertainties in the large-scale system (due to load/topology variation or faults), in conjunction with the effect of unstable zeros, a model-matching approach is proposed. It forces the closed-loop to provide desired dynamics by minimizing the gap between a reference model and the one of the closed-loop.

The gap between the full nonlinear model and the control model is taken into account in the design process. The high performance requirement of the proposed controller may lead it to lose robustness. Thus, a trade-off is set to achieve the desired damping with maximum of robustness. Extensive comparison and validation tests show that the proposed DDOFC POD controller indeed provides the robustness along with desirable damping for the system. Furthermore, implementation in output-feedback state-space can be easily done in practice, including for coordinated P and Q modulation.

Work has been performed for VSC-HVDC case but the approach can be easily extended for other power electronics-based devices. For example, renewable energy sources connected to the grid by power converted can be controlled in the same way.

Appendix A

Basic control of VSC-HVDC link

A.1 Dynamic modeling of a VSC conversion station

As shown in Fig. A.1, the dynamic model of the VSC converter, consists of the models of both sides AC and DC and the equations which connect them. In a stationary reference frame $\alpha\beta$, seen from the connection the terminal bus of the AC filter, the AC dynamics are given by the dynamics of the phase reactances.

$$\frac{di_{\alpha\beta}}{dt} = v_{\alpha\beta} - u_{\alpha\beta} - Ri_{\alpha\beta} \tag{A.1.1}$$

In the reference d_q it has,

$$L\frac{di_{dq}}{dt} = v_{dq} - u_{dq} - (R + j\omega_e L)\, i_{dq} \tag{A.1.2}$$

The term $j\omega_e L i_{dq}$ of equation (A.1.2) represents the derivative with respect to time of the rotation of the reference frame d_q. Equation (A.1.2) can be written for each axis

$$L\frac{di_d}{dt} = -Ri_d + \omega_e L i_q - u_d + v_d, L\frac{di_q}{dt} = -Ri_q - \omega_e L i_d - u_q + v_q \tag{A.1.3}$$

From equation (A.1.3), the equivalent circuit of the VSC in the synchronous reference frame d_q is described in Fig. A.2. Note that the projection on d axis is zero so that the magnitude on this

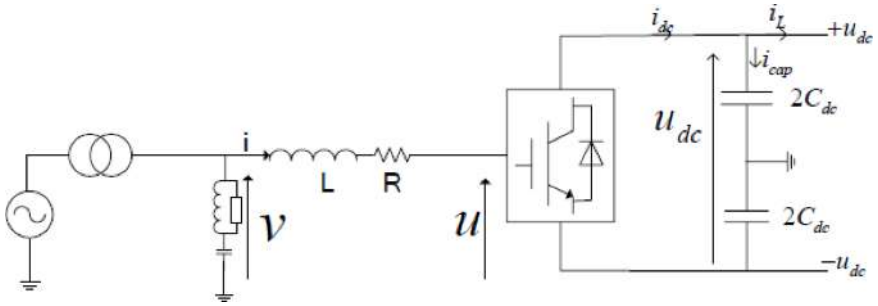

Figure A.1 – Dynamic model of a VSC converter

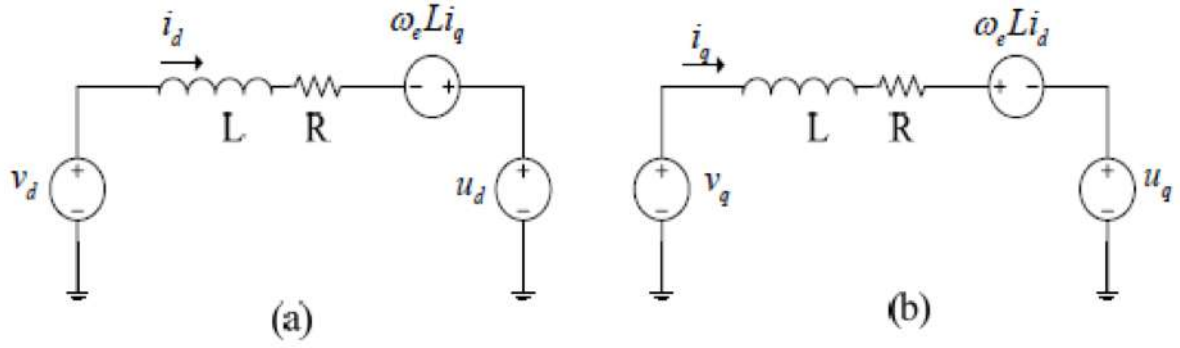

Figure A.2 – Equivalent circuit of the VSC in the d_q reference

axis is aligned with the AC voltage of the filter, i.e.,

$$v_q = 0, v_d = v. \tag{A.1.4}$$

The instantaneous active and reactive powers in per/unit (pu) are given by

$$\begin{aligned} p &= (v_d i_d + v_q i_q) = v_d i_d \\ q &= (v_q id - v_d i_q) = -v_d i_q \end{aligned} \tag{A.1.5}$$

In order to complete the dynamic model of the VSC converter, the dynamic range of the DC line is given by

$$\begin{aligned} C_{dc}\tfrac{du_{dc}}{dt} &= i_{dc} - i_L, \\ P_{dc} &= u_{dc} i_{dc} \end{aligned} \tag{A.1.6}$$

Equations (A.1.3), (A.1.5), and (A.1.6) fully describe the VSC converter in Fig. A.1.

A.2 Standard vector control for HVDC VSC links

As mentioned in Chapter 1, the standard vector control (first-level) approach of an electric machine involves the representation of the three-phase quantities of these in a rotating referential d_q.

The passage in coordinates d_q allows us to control the two components of the current, i_d and i_q in an independent way. This makes it possible to independently control the active and reactive powers.

As the standard control approach allows decoupled control of the active and reactive powers, a control structure with two cascaded loops is possible: an external loop which supplies the current set-points and an internal current loop.

Notice that the supplementary POD controller is in the outer controller block to further more

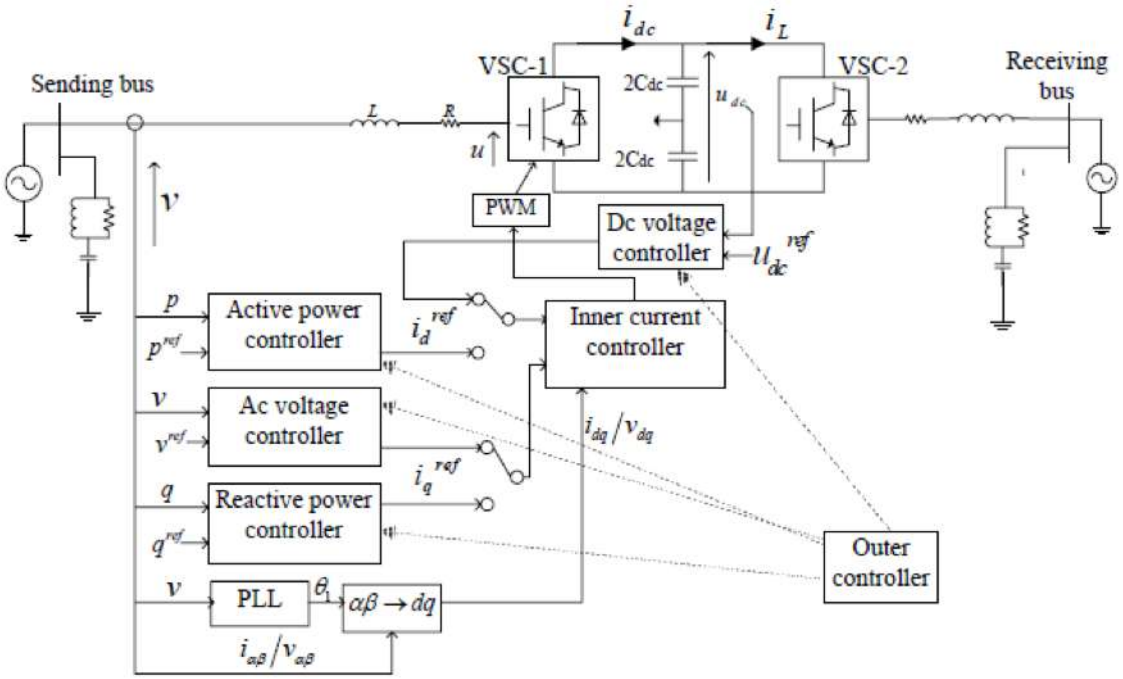

Figure A.3 – Schematic of the standard control of the HVDC VSC link

modulate active and reactive power. In this appendix, the internal control loops are presented.

The internal loop includes the basic control of active power, DC voltage and reactive power (or AC voltage depending on the application). The reference value for the active current can be provided by the active power or DC voltage loop. However, the reactive current set-point is provided by the AC voltage or reactive power loop. The active power withdrawn from the network must be equal to the active power injected into the network minus the losses of the DC system.

Fig. A.3 shows the different control loops of the HVDC VSC link. Note that the VSC-2 control system is similar to that of VSC-1.

A.3 Active and reactive power control

If v_d is assumed constant in equation (A.1.5), then the active and reactive powers will depend exclusively on the references of the active and reactive currents respectively. The simplest method

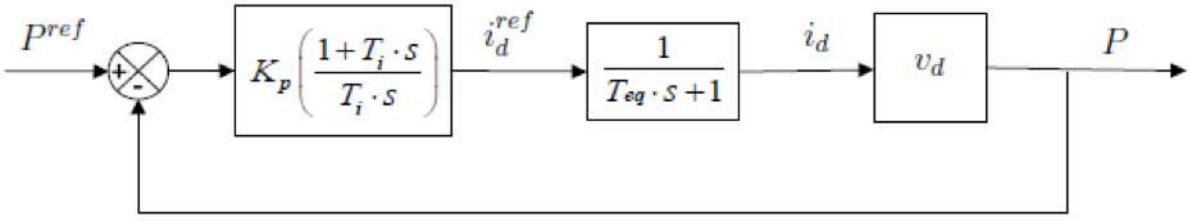

Figure A.4 – Active power regulator

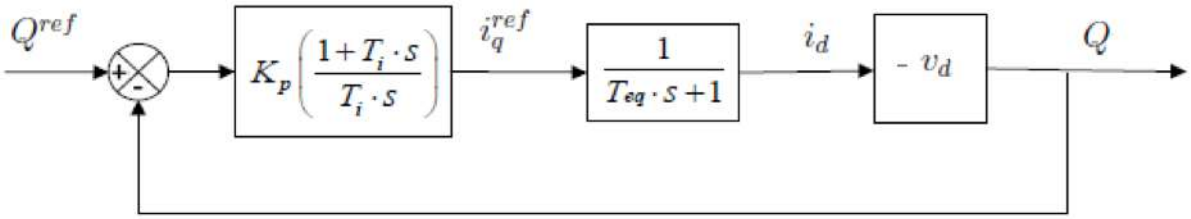

Figure A.5 – Reactive power regulator

of controlling active and reactive power would be open loop control, i.e.,

$$\begin{aligned} i_d^{ref} &= \frac{2}{3}\frac{P^{ref}}{v_d} \\ i_q^{ref} &= -\frac{2}{3}\frac{Q^{ref}}{v_d} \end{aligned} \tag{A.3.1}$$

However, more precise control is achieved by using a closed-loop, using a PI command (as in Figures A.4 and A.5).

A.4 Control of DC voltage

In any case, the control of the DC voltage is necessary in order to ensure the power balance.

A DC voltage regulator is essential to maintain the exchange of active power between the converters. By ignoring the losses in the converters and in the phase reactors, and by equalizing the powers on the AC and DC side (using equations (A.1.6) and (A.1.5)), it has

$$i_{dc} = \frac{v_d}{u_{dc}} i_d \tag{A.4.1}$$

Any imbalance between the AC and DC powers will cause a variation in the DC voltage. From

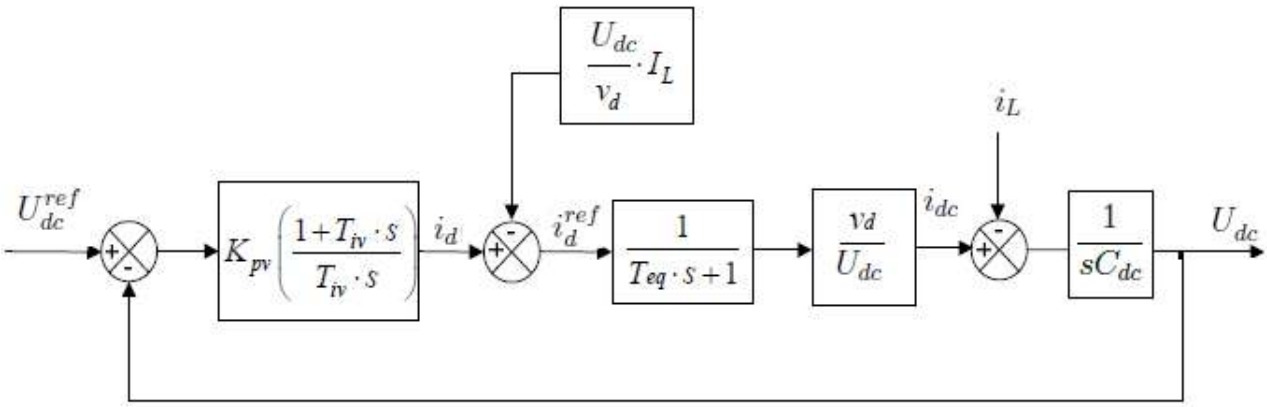

Figure A.6 – DC voltage control

equations (A.1.6) and (A.4.1), it draws,

$$C_{dc}\frac{du_{dc}}{dt} = \frac{v_d}{u_{dc}}i_d - i_L \tag{A.4.2}$$

It can be seen that the equation (A.4.2) is nonlinear in u_{dc}. By linearizing it around an equilibrium point U_{dc0} and by considering i_L as a disturbance signal, the transfer between Δu_{dc} and Δi_d is then written

$$\Delta u_{dc} = \frac{v_{d_0}}{u_{dc0}}\frac{1}{sC_{dc}}\Delta i_d \tag{A.4.3}$$

The transfer function is then written

$$G(s) = \frac{v_{d_0}}{u_{dc0}}\frac{1}{sC_{dc}} \tag{A.4.4}$$

By setting $C = \frac{u_{dc0}}{v_{d_0}}C_{dc}$, it has:

$$G(s) = \frac{1}{sC} \tag{A.4.5}$$

Under equilibrium conditions, $C_{dc}\frac{du_{dc}}{dt} = 0$, therefore the current reference i_d^{ref} must be $\frac{u_{dc}}{v_d}i_L$ which is the term which ensures the exact compensation of the load variation. The complete block diagram of the DC voltage control is given in Fig. A.6.

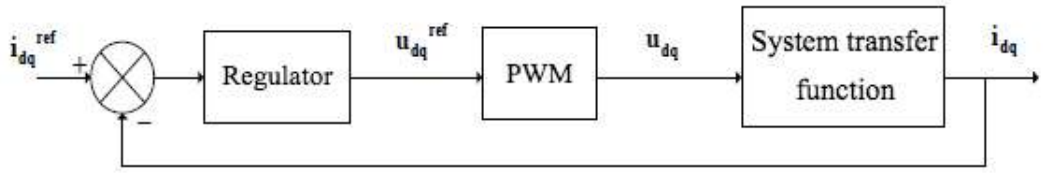

Figure A.7 – Current control

A.5 Control of current

The internal current control loop can be implemented in the d_q referential, based on the model of the system described above. The control loop consists of two regulators, compensation terms and decoupling factors. Inside the control block there are two regulators, respectively, for the currents on the d axis and the q axis.

The regulator illustrated in Fig. A.7 becomes

$$H(s) = K_p + \frac{K_i}{s} = K_p \left(\frac{1 + T_i s}{T_i s} \right) \tag{A.5.1}$$

where K_p is the proportional gain and T_i is the integral time constant.

The internal current loop generates a reference voltage u_{dq}^{ref}, which is written, in the reference $\alpha\beta$,

$$u_{\alpha\beta}^{ref} = e^{j\theta_1} u_{dq}^{ref}$$

where θ_1 is the angle of the reference frame dq used by the control system and which is given by the PLL (phase-locked loop). The reference vector $u_{\alpha\beta}^{ref}$ is used as the input signal for the PWM converter of the VSC. The latter is considered to be very fast and precise as long as the modulus of the reference vector does not exceed the maximum value above from which the behavior of the PWM (Pulse Width Modulation) is no longer considered linear, i.e.,

$$\left| u_{dq}^{ref} \right| = \left| u_{\alpha\beta}^{ref} \right| \leq u_{\max}$$

where $u_{\max}$ is proportional to the voltage DC. Moreover, the fact is considered that the reference tracking is done according to a time constant T_a usually equal to half of the switching period T_{switch}. It then has

$$u_{dq} = \frac{1}{1 + T_a s} u_{dq}^{ref}$$

where $T_a = T_{\text{switch}}/2$ The PWM converter adds a harmonics term due to switching. However, the phase reactors as well as the filters installed make it possible to eliminate the effect of harmonics due to switching seen from the AC side.

Appendix B

Model simulation and linearization

Introduction

The nonlinear system is simulated in the software EUROSTAG.

The operation of electricity networks is becoming increasingly complex. Decisions depend on more factors, due to higher exchanges between zones (interconnection), the complexity of equipment and also the number of constraints in relation with economics, environment and system security.

In order to optimize the effectiveness of investments and to keep operating costs to a minimum, both planners and operators must have the appropriate simulation package permitting to rapidly and reliably produce adequate models and studies.

As previous packages only partly satisfied these requirements, ELECTRICITE DE FRANCE and TRACTEBEL jointly developed EUROSTAG. The last versions are now developed by TRACTEBEL and RTE (the french transmission system operator). With this powerful and user-friendly software, the expert gets out of the tedious tasks of traditional system modeling and focus his/her attention on the essential, thanks to the extended dynamic modeling concept, central piece of the Eurostag approach.

In the Dynamic Simulation, evolutions in the system must be described in a form using a system of algebraic-differental equations. The system initial state in the Dynamic Simulation must be a steady state. A Load Flow Computation interfaced with the Dynamic Simulation enables initialization of the dynamic system under realistic conditions, specifying conventionally the constant voltage buses, generation and consumption.

B.1 Simulation

In this thesis, the main excitation simulation on the nonlinear system is based on a short circuit at a the terminal bus. In EUROSTAG, two representations of short-circuits exist : one, simplified, for three-phases balanced short circuits, usable on a non Fortescue area ; the other, with a phase by phase description, for unbalanced short-circuits, usable on a Fortescue area.

For this research, the first type is used. Such a short-circuit may be :

— Transitory or permanent. A transitory short-circuit is definitely eliminated by removal of the voltage (tripping of the circuit-breakers either side of it). A permanent short-circuit will

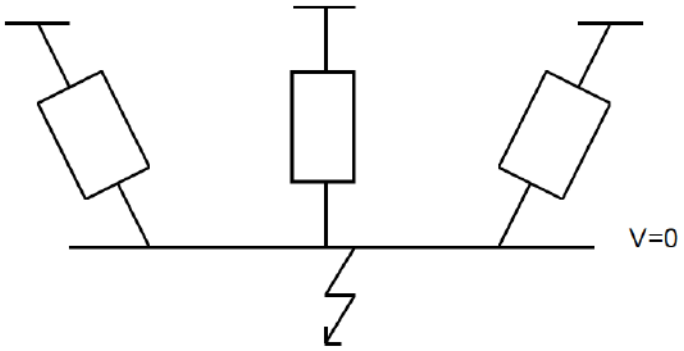

Figure B.1 – Short-circuit at a the terminal bus without impedance.

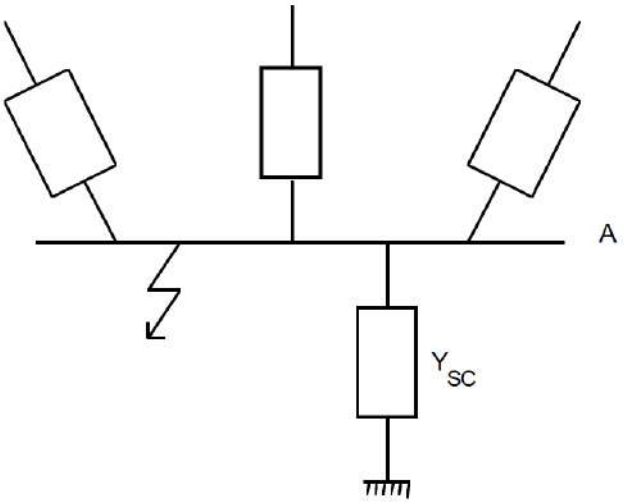

Figure B.2 – Short-circuit at a the terminal bus with impedance.

reappear when the voltage is applied once more.

— With or without impedance.

— Situated on a bus or along a line.

If without impedance, like in Fig. B.1, the advent of the short-circuit corresponds to the elimination of the the terminal bus obtained by doing away with line and column corresponding to it in the admittance matrix, without correcting the individual admittances of the neighbouring buses. If with impedance, like in Fig. B.2, the short-circuit admittance is termed Y_{SC}.

B.2 Power system linearization

The power system is described by the compact vector–matrix representation of (B.2.1).

$$\begin{aligned} \dot{\boldsymbol{x}} &= \boldsymbol{f}(\boldsymbol{x}, \boldsymbol{u}) \\ \boldsymbol{y} &= \boldsymbol{g}(\boldsymbol{x}, \boldsymbol{u}) \end{aligned} \tag{B.2.1}$$

In (B.2.1), x is a vector of n state variables, u is a vector of m system inputs, y is a vector of p system outputs, and f and g are vectors of non-linear equations.

An equilibrium point can be defined at which $x = x_0$ and $u = u_0$ such that (B.2.1) is equal to zero. By making a small perturbation (Δ) from this point, (B.2.2) can be established.

$$\dot{x}_0 + \Delta\dot{x} = f\left(x_0 + \Delta x, u_0 + \Delta u\right) \tag{B.2.2}$$

As only small perturbations are considered, a first order Taylor's series expansion of (B.2.2) can be used as a suitable approximation. This can be similarly completed for (B.2.1) with respect to system outputs, and simplified, to provide the linearized state space power system model consisting of (B.2.3).

$$\begin{aligned} \Delta\dot{x} &= A\Delta x + B\Delta u \\ \Delta y &= C\Delta x + D\Delta u \end{aligned} \tag{B.2.3}$$

In (B.2.3) the following definitions are used:

$$\boldsymbol{A} = \begin{bmatrix} \frac{\partial f_1}{\partial x_1} & \cdots & \frac{\partial f_1}{\partial x_n} \\ \vdots & \ddots & \vdots \\ \frac{\partial f_n}{\partial x_1} & \cdots & \frac{\partial f_n}{\partial x_n} \end{bmatrix}, \boldsymbol{B} = \begin{bmatrix} \frac{\partial f_1}{\partial u_1} & \cdots & \frac{\partial f_1}{\partial u_m} \\ \vdots & \ddots & \vdots \\ \frac{\partial f_n}{\partial u_1} & \cdots & \frac{\partial f_n}{\partial u_m} \end{bmatrix}$$

$$\boldsymbol{C} = \begin{bmatrix} \frac{\partial g_1}{\partial x_1} & \cdots & \frac{\partial g_1}{\partial x_n} \\ \vdots & \ddots & \vdots \\ \frac{\partial g_p}{\partial x_1} & \cdots & \frac{\partial g_p}{\partial x_n} \end{bmatrix}, \boldsymbol{D} = \begin{bmatrix} \frac{\partial g_1}{\partial u_1} & \cdots & \frac{\partial g_1}{\partial u_m} \\ \vdots & \ddots & \vdots \\ \frac{\partial g_p}{\partial u_1} & \cdots & \frac{\partial g_p}{\partial u_m} \end{bmatrix}$$

After simulation, it is possible for a user to obtain the result of the linearization in the vicinity of $(X0, Y0)$ of the algebraic-differential equations system solved by EUROSTAG. This also allows to apply particular treatment to specific blocks like limits, delays, dead bands and hysteresis cycles. Some limited block outputs are also processed specifically. Such as blocks with saturated outputs are replaced by a unit gain. This is equivalent to ignore the bounds of the block. And for a dead band block, The equations are replaced by:

$$\mathrm{y} = \mathrm{x} - \frac{\mathrm{x}_{\max} - \mathrm{x}_{\min}}{2}, \forall \mathrm{x} \tag{B.2.4}$$

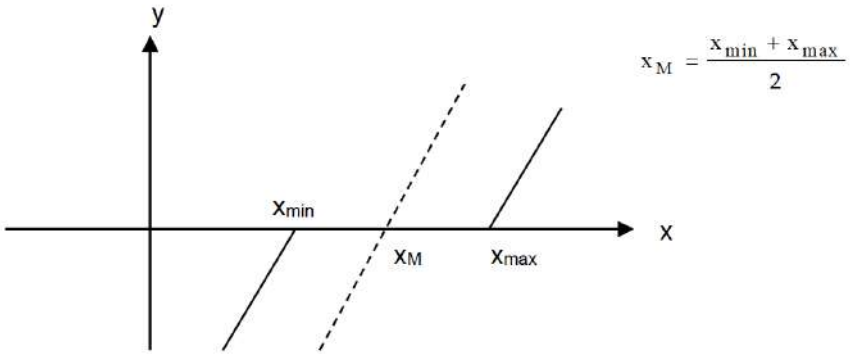

Figure B.3 – Dead band

which is equivalent to replace the full lines by the dashed one in the Fig. B.2.

Appendix C

MODAL ANALYSIS

C.1 Introduction

SMAS3 software is used to calculate the modes and eigenvalues, etc. of system. SMAS3 (Selective Modal Analysis of Small Signal Stability) is a state of the art computer program package for the study of small signal stability in electric power systems.

As mentioned in Introduction, Selective Modal Analysis is a relevant computational method for the analysis of small signal stability implemented in SMAS3. Other methods have also been implemented (Complete Eigenanalysis, Modified Arnoldi Method, Dominant Pole Spectrum Eigensolver, Linear Time Response and Frequency Response) making SMAS3 a highly comprehensive tool. In addition, it contains tools for location and coordinated design of power system stabilizers. SMAS3 program package has been developed by Instituto de Investigación Tecnológica (IIT) of Universidad Pontifica Comillas (Madrid, Spain) with the support of Iberdrola, and Red Eléctrica de España. Eurostag - SMAS3 connection has been developed by IIT with the support of RTE France.

SMAS3 is used to computed eigenvalues (modes), transfer function residues, Participation factors.

C.2 Eigenvalues

Eurostag provides the state matrix J of a implicit linear model of the power system:

$$\begin{bmatrix} \Delta\dot{\mathbf{x}} \\ \mathbf{0} \end{bmatrix} = \mathbf{J} \begin{bmatrix} \Delta\mathbf{x} \\ \Delta\mathbf{r} \end{bmatrix} \tag{C.2.1}$$

where:

Δx is the vector of state variables and Δr is the vector of algebraic variables. The vector of algebraic variables contains the vector the dynamic device algebraic variables Δz, the vector of dynamic device input variables Δu and the vector of bus voltage components Δv. Therefore, the vector of algebraic variables can be written as:

$$\Delta\mathbf{r}^T = \left[\Delta\mathbf{z}^T \Delta\mathbf{u}^T \Delta\mathbf{v}^T\right] \tag{C.2.2}$$

and equation (C.2.1) can be rewritten as:

$$\begin{bmatrix} \Delta\dot{\mathbf{x}} \\ \mathbf{0} \\ \mathbf{0} \\ \mathbf{0} \end{bmatrix} = \begin{bmatrix} \mathbf{J}_{11}\mathbf{J}_{12}\mathbf{J}_{13}\mathbf{J}_{14} \\ \mathbf{J}_{21}\mathbf{J}_{22}\mathbf{J}_{23}\mathbf{J}_{24} \\ \mathbf{J}_{31}\mathbf{J}_{32}\mathbf{J}_{33}\mathbf{J}_{34} \\ \mathbf{J}_{41}\mathbf{J}_{42}\mathbf{J}_{43}\mathbf{J}_{44} \end{bmatrix} \begin{bmatrix} \Delta\mathbf{x} \\ \Delta\mathbf{z} \\ \Delta\mathbf{u} \\ \Delta\mathbf{v} \end{bmatrix} \tag{C.2.3}$$

SMAS3 uses a implicit linear model of the power system which only algebraic variables are the bus voltage components:

$$\begin{aligned} \begin{bmatrix} \Delta\mathbf{x} \\ \mathbf{0} \end{bmatrix} &= \begin{bmatrix} \mathcal{A}_{11} & \mathcal{A}_{12} \\ \mathcal{A}_{21} & \mathcal{A}_{22} \end{bmatrix} \begin{bmatrix} \Delta\mathbf{x} \\ \Delta\mathbf{v} \end{bmatrix} + \begin{bmatrix} \mathcal{B}_1 \\ \mathcal{B}_2 \end{bmatrix} \Delta\mathbf{u} \\ \Delta\mathbf{y} &= \begin{bmatrix} \mathcal{C}_1\mathcal{C}_2 \end{bmatrix} \begin{bmatrix} \Delta\mathbf{x} \\ \Delta\mathbf{v} \end{bmatrix} + \mathcal{D}\Delta\mathbf{u} \end{aligned} \tag{C.2.4}$$

The conversion of the Eurostag model form to the SMAS3 model form comprises two steps. First, the input and the output variables are singled out. Second, the device algebraic variables are eliminated.

Consider now a dynamic system described by a set of nonlinear differential equations written in explicit form (the derivatives of the state variables depend only on the state variables x):

$$\begin{aligned} \dot{\mathbf{x}} &= \mathbf{f}(\mathbf{x}) \\ \mathbf{x} &\in \Re^{N\times 1} \end{aligned} \tag{C.2.5}$$

If the set of non linear differential equations (C.2.5) is linearized around an operating point $x = x_0$, it results in:

$$\begin{aligned} \Delta\mathbf{x} = \left.\frac{\partial\mathbf{f}(\mathbf{x})}{\partial\mathbf{x}}\right|_{\mathbf{x}=\mathbf{x}_0} \Delta\mathbf{x} &= \mathbf{A}\Delta\mathbf{x} \\ \mathbf{A} &\in \mathbb{R}^{N\times N} \\ \Delta\mathbf{x} &= \mathbf{x} - \mathbf{x}_0 \end{aligned} \tag{C.2.6}$$

The solution of the set of linear differential equations (C.2.6) provides the response of the linearized dynamic system to initial conditions different form zero. Such solution depends on the exponential of the state matrix A according to:

$$\Delta\mathbf{x} = e^{\mathbf{A}t}\Delta\mathbf{x}(0)$$

The exponential of the state matrix A may be computed using the Taylor expansion:

$$e^{\mathbf{A}t} = \mathbf{I} + \frac{\mathbf{A}}{1!}t + \frac{\mathbf{A}^2}{2!}t^2 + \cdots$$

However, this method is not always numerically robust. A physically meaningful alternative is based on the eigenvalues and eigenvectors of the state matrix A. An eigenvalue Λ_i of the state matrix A

and the associated right V_i and left W_i eigenvectors are defined as:

$$\begin{aligned} \mathbf{A}\mathbf{v}_i &= \mathbf{v}_i\lambda_i \\ \mathbf{w}_i^T\mathbf{A} &= \lambda_i\mathbf{w}_i^T \end{aligned} \tag{C.2.7}$$

The study of equation (C.2.7) indicates that the right and left eigenvectors are not uniquely determined (they are computed as the solution of a linear system of N equations and N+1 unknowns). An approach to eliminate that degree of freedom is to introduce a normalization such as:

$$\mathbf{w}_i^T\mathbf{v}_i = 1 \tag{C.2.8}$$

In case of N distinct eigenvalues, equations (C.2.7)-(C.2.8) can be written together for all eigenvalues in matrix form as:

$$\begin{aligned} \mathbf{A}\mathbf{V} &= \mathbf{V}\Lambda \\ \mathbf{W}\mathbf{A} &= \Lambda\mathbf{W} \\ \mathbf{W}\mathbf{V} &= \mathbf{I} \end{aligned} \tag{C.2.9}$$

where $\Lambda, \mathbf{V}\text{y}\mathbf{W}$ are respectively the matrices of eigenvalues and right and left eigenvectors:

$$\begin{aligned} \Lambda &= \begin{bmatrix} \lambda_1 & & \\ & \ddots & \\ & & \lambda_N \end{bmatrix} \\ \mathbf{V} &= \begin{bmatrix} \mathbf{v}_1 \cdots \mathbf{v}_N \end{bmatrix} \\ \mathbf{W} &= \begin{bmatrix} \mathbf{w}_1^T \\ \vdots \\ \mathbf{w}_N^T \end{bmatrix} \end{aligned} \tag{C.2.10}$$

If the exponential of the state matrix e_{At} is expressed in terms of eigenvalues and right and left eigenvectors of the state matrix (C.2.9), it results in:

$$\begin{aligned} e^{\mathbf{A}t} &= \mathbf{V}\mathbf{W} + \frac{\mathbf{V}\Lambda\mathbf{W}}{1!}t + \frac{\mathbf{V}\Lambda^2\mathbf{W}}{2!}t^2 + \cdots \\ &= \mathbf{V}\left(\mathbf{I} + \frac{\Lambda}{1!}t + \frac{\Lambda^2}{2!}t^2 + \cdots\right)\mathbf{W} = \mathbf{V}e^{\Lambda t}\mathbf{W} \end{aligned} \tag{C.2.11}$$

The solution of the set of linear differential equation (C.2.6) can be expressed in terms of the eigenvalues and right and left eigenvectors of the state matrix A as:

$$\Delta\mathbf{x} = \mathbf{V}e^{\Lambda t}\mathbf{W}\Delta\mathbf{x}(0) = \sum_{i=1}^{N}\mathbf{v}_i e^{\lambda_i t}\left[\mathbf{w}_i^T\Delta\mathbf{x}(0)\right] \tag{C.2.12}$$

The study of equation (C.2.12) allows drawing the following conclusions:

— The system response is expressed as the combination of the system response for N modes.
— The eigenvalues of the state matrix determine the system stability. A real negative (positive) eigenvalue indicates an exponentially decreasing (increasing) behaviour. A complex eigenvalue of negative (positive) real part indicates an oscillatory decreasing (increasing) behaviour.
— The components of the right eigenvector v_i indicate the relative activity of each variable in the i-th mode.
— The components of the left eigenvector W_i weight the initial conditions (they are the excitations) in the i-th mode.

C.3 Transfer function residues

Consider that in the linear dynamic system written in explicit form (C.2.6) an input u and an output y have been selected:

$$\begin{aligned} \Delta\dot{\mathbf{x}} &= \mathbf{A}\Delta\mathbf{x} + \mathbf{b}\Delta u \\ \Delta y &= \mathbf{c}^T\Delta\mathbf{x} \end{aligned} \tag{C.3.1}$$

It is applied to the system (C.3.1) a variable transformation defined by the matrix of right eigenvectors $\Delta x = V\Delta\tilde{x}$:

$$\begin{aligned} \Delta\dot{\mathbf{x}} &= \Lambda\Delta\tilde{\mathbf{x}} + \mathbf{W}\mathbf{b}\Delta u \\ \Delta y &= \mathbf{c}^T\mathbf{V}\Delta\tilde{\mathbf{x}} \end{aligned} \tag{C.3.2}$$

$$\left.\begin{aligned} \Delta\dot{\tilde{x}}_i &= \lambda_i\Delta\tilde{x}_i + \mathbf{w}_i^T\mathbf{b}\Delta u \\ \Delta y &= \mathbf{c}^T\mathbf{v}_i\Delta\tilde{x}_i \end{aligned}\right\} i = 1,\ldots,N \tag{C.3.3}$$

Thus, the transfer function between Δu and Δy is obtained applying the Laplace transform to the equations (C.3.2) and eliminating the Laplace transform of the state variables $\Delta x(s)$:

$$\frac{\Delta y(s)}{\Delta u(s)} = \mathbf{c}^T(s\mathbf{I} - \mathbf{A})^{-1}\mathbf{b} \tag{C.3.4}$$

The transfer function (C.3.4) can also be written as a partial fraction expansion in terms of the poles i p and the associated residues $R_{\Delta y/\Delta u,i}$.

$$\frac{\Delta y(s)}{\Delta u(s)} = \sum_{i=1}^{N}\frac{R_{\Delta y/\Delta u,i}}{(s-p_i)} \tag{C.3.5}$$

If equation (C.3.4) is written in terms of the eigenvalues and eigenvectors of the state matrix, it

becomes:

$$\frac{\Delta y(s)}{\Delta u(s)} = \mathbf{c}^T\mathbf{V}(s\mathbf{I} - \Lambda)^{-1}\mathbf{W}\mathbf{b} = \sum_{i=1}^{N} \frac{\mathbf{c}^T\mathbf{v}_i\mathbf{w}_i^T\mathbf{b}}{(s - \lambda_i)} \tag{C.3.6}$$

The comparison of equations (C.3.5) and (C.3.6) confirms that the eigenvalues of the state matrix are the poles of the open loop transfer function and that the transfer function residues can be computed as the product of the modal controllability and observability factors.

$$R_{\Delta y/\Delta u,i} = \mathbf{c}\mathbf{v}_i\mathbf{w}_i^T\mathbf{b} = v_{\Delta y,i}w_{\Delta u,i} \tag{C.3.7}$$

C.4 Participation factors

The participation factor of the j-the variable in the i-th mode is defined as the product of the j-th components of the right v_{ji} and left w_{ji} eigenvector corresponding to the i-th mode:

$$p_{ji} = w_{ji}v_{ji}$$

The participation factor of a variable in a mode is nondimensional magnitude. In other words, it is independent on the units of the state variables.

In addition, as a results of the adopted normalization (C.2.8), the sum of the participation factors of all variables in a mode and the sum of the participation factors of all modes in a variable are equal to unity.

$$\sum_{j=1}^{N} p_{ji} = \sum_{i=1}^{N} p_{ji} = 1$$

The participation factor of the j-th variable in the i-th mode is also the eigenvalue sensitivity of the i-th eigenvalue λ_i with respect to the j-th diagonal element of the state matrix a_{jj} :

$$p_{ij} = \frac{\partial \lambda_i}{\partial a_{jj}}$$

Appendix D

Models and regulators parameters

D.1 Parameters

D.1.1 Control model parameters

Curve fitting parameters: $\omega_\Lambda^- = 1.256$ rad/s and $\omega_\Lambda^+ = 13.8$ rad/s, α_k=1, β_k=1.

The transfer function of control model in Chapter 1:

$$f(s) = \frac{Nco_{n-1}s^{n-1} + ... + Nco_1 s + Nco_0}{Dco_n s^n + ... + Dco_1 s + Dco_0} \tag{D.1.1}$$

$n = 12$. Parameters are shown in Table D.1.

i=	Nco	Dco
12	/	1
11	0.01504	11.14
10	0.08873	240.2
9	0.6758	1804
8	- 0.8807	2.02e04
7	- 88.8	1.071e05
6	- 763.7	7.974e05
5	- 6857	2.945e06
4	- 3.609e04	1.582e07
3	- 1.61e05	3.755e07
2	- 6.049e05	1.492e08
1	- 1.246e06	1.758e08
0	- 3.278e06	5.147e08

Table D.1 – Transfer function of control model

D.1.2 Classic POD controller parameters:

In Chapter 1, for classic POD in formula 3.1: $K = 2.5614$; $T_1 = 0.4746$; $T_2 = 0.0688$; $T_w = 1$; $n = 2$.

D.1.3 LQG POD controller:

The gains obtained from Chapter 3:
L=[-164.1718 47.4770 80.3341 57.6205 96.3393 -19.5135 2.8027 48.0027 35.0776 8.5834 -7.8243 -0.3291 -9.2020]^T;
K_r= [13.7682 -3.3704 -4.0354 6.5771 7.0691 4.3546 2.4524 -1.5362 1.1628 0.7133 -0.4256 -0.6244 -0.5161].
For application, the transfer function from u to Q_{pod} is H_1, the transfer from $\Delta\theta$ to u is H_2:

$$H_1 = \sum_{i=0}^{n-1}\sum_{j=0}^{n}\frac{N1_i(s)}{D1_j(s)} = \frac{N1_{n-1}s_n + ... + N1_1 s + N1_0}{D1_n s_n + ... + D1_1 s + D1_0} \tag{D.1.2}$$

$$H_2 = \frac{N2_{n-1}s^{n-1} + ... + N2_1 s + N2_0}{D2_n s^n + ... + D2_1 s + D2_0} \tag{D.1.3}$$

$n = 13$. Parameters are shown in Table D.2

i,j=	N1	D1	N2	D2
13	/	1	/	1
12	-3.681	43.19	1781	43.19
11	-189.3	785.2	1.814e04	785.2
10	-3051	1.092e04	3.614e05	1.092e04
9	-3.894e04	1.087e05	2.343e06	1.087e05
8	-3.575e05	8.942e05	2.358e07	8.942e05
7	-2.571e06	5.837e06	9.686e07	5.837e06
6	-1.513e07	3.203e07	6.336e08	3.203e07
5	-7.04e07	1.431e08	1.381e09	1.431e08
4	-2.672e08	5.266e08	6.488e09	5.266e08
3	-8.032e08	1.557e09	-3.658e08	1.557e09
2	-1.735e09	3.469e09	5.733e09	3.469e09
1	-2.923e09	5.716e09	-9.87e10	5.716e09
0	-1.42e09	4.454e09	-1.387e11	4.454e09

Table D.2 – Transfer function of LQG POD paramaters

D.1.4 Mixed sensitivity H_∞ controller:

The transfer function of Mixed sensitivity H_∞ controller in Chapter 4 is:

$$K(s) = \frac{N_{n-1}s^{n-1} + ... + N_1 s + N_0}{D_n s^n + ... + D_1 s + D_0} \tag{D.1.4}$$

In (D.1.4), $n = 15$. Parameters of Mixed sensitivity H_∞ controller are shown in Table D.3

i=	N	D
15	/	1
14	9.41e05	4.582e05
13	9.443e07	7.774e06
12	1.125e09	1.466e08
11	1.901e10	1.478e09
10	1.374e11	1.456e10
9	1.247e12	9.822e10
8	5.945e12	6.262e11
7	3.508e13	2.906e12
6	1.077e14	1.27e13
5	4.295e14	3.941e13
4	7.385e14	1.168e14
3	1.804e15	2.146e14
2	1.055e15	3.853e14
1	-3.282e13	2.593e14
0	3.297e14	1.084e13

Table D.3 – Transfer function of Mixed sensitivity H_∞ POD paramaters

D.1.5 ZPETC

The unstable zeros in control model of nominal case:
$29.147300161588191 + 0.000000000000000i$;
$2.856900859630420 + 11.173666499781438i$;
$2.856900859630420 - 11.173666499781438i$;
$0.036372937940382 + 4.910700827352009i$;
$0.036372937940382 - 4.910700827352009i$;
$0.000008954970019 + 0.000000000000000i$;

$$ZPETC(s) = \frac{NC_n s^n + ... + NC_1 s + N_0}{DC_n s^n + ... + DC_1 s + DC_0} \tag{D.1.5}$$

$n = 5$. Parameters are shown in Table D.4

i=	NC	DC
5	-1	1
4	- 34.93	20
3	- 326.2	155
2	- 4739	580
1	- 7506	1044
0	- 9.35e04	1720

Table D.4 – Transfer function of ZPETC paramaters

D.1.6 Reference model:

The transfer function of reference model:

$$f_r(s) = \frac{Nr_{n-1}s^{n-1} + ... + Nr_1 s + Nr_0}{Dr_n s^n + ... + Dr_1 s + Dr_0} \tag{D.1.6}$$

$n = 12$. Parameters are shown in Table D.5.

i=	Nr	Dr
12	/	1
11	0.02143	19.54
10	0.1264	355.5
9	0.9629	3773
8	- 1.255	3.638e04
7	- 126.5	2.492e05
6	- 1088	1.565e06
5	- 9771	7.205e06
4	- 5.143e04	3.094e07
3	- 2.294e05	9.178e07
2	- 8.618e05	2.646e08
1	- 1.776e06	4.098e08
0	- 4.671e06	7.333e08

Table D.5 – Transfer function of reference model

D.1.7 ROSCF controller:

The gains calculated in Chapter 3:
Y_R=1.150696148547366e-12;
X_R=2.009746646814367e-13.
Then, the controller is:

$$K = 5.725578148724988$$

.

D.1.8 DDOFC controller:

For application, the controller in state-space format is

$$\begin{aligned} \dot{x} &= A_c x + B_c u \\ y &= C_c x \end{aligned} \tag{D.1.7}$$

The transfer function of controller DDOFC $K(s)$:

$$K(s) = \frac{Nd_{n-1}s^{n-1} + ... + Nd_1 s + Nd_0}{Dd_n s^n + ... + Dd_1 s + Dd_0} \tag{D.1.8}$$

Since the order of the controller depends on the control model plus reference model, $n = 26$. Parameters are shown in Table D.6

i=	Nd	Dd
26	/	1
25	5.267e05	4.057e04
24	1.713e07	1.465e06
23	4.532e08	4.032e07
22	8.033e09	7.692e08
21	1.225e11	1.234e10
20	1.496e12	1.621e11
19	1.616e13	1.865e12
18	1.481e14	1.856e13
17	1.217e15	1.65e14
16	8.672e15	1.3e15
15	5.573e16	9.242e15
14	3.119e17	5.888e16
13	1.568e18	3.402e17
12	6.764e18	1.768e18
11	2.567e19	8.326e18
10	7.833e19	3.519e19
9	1.879e20	1.341e20
8	1.951e20	4.546e20
7	- 7.141e20	1.372e21
6	- 6.079e21	3.617e21
5	- 2.359e22	8.277e21
4	- 6.919e22	1.593e22
3	-1.507e23	2.516e22
2	- 2.483e23	3.057e22
1	- 2.907e23	2.551e22
0	- 1.568e23	1.08e22

Table D.6 – Transfer function of DDOFC POD paramaters

Sources primaires

ABB, AB (2008), « It's time to connect–Technical description of HVDC Light® technology », *in*: *Informationsmaterial des Herstellers*.

Aboul-Ela, Magdy E, AA Sallam, James D McCalley, and AA Fouad (1996), « Damping controller design for power system oscillations using global signals », *in*: *IEEE Transactions on Power Systems* 11.*2*, pp. 767–773.

« Analysis of inter-area oscillations of 1*st* december 2016. ENTSO-E SG SPD Report » (n.d.), *in*: RTE.

Anderson, Paul M and Aziz A Fouad (2008), *Power system control and stability*, John Wiley & Sons.

Arioua, L and B Marinescu (2016), « Robust grid-oriented control of high voltage DC links embedded in an AC transmission system », *in*: *International Journal of Robust and Nonlinear Control* 26.*9*, pp. 1944–1961.

Arioua, Leyla and Bogdan Marinescu (2015), « Multivariable control with grid objectives of an HVDC link embedded in a large-scale AC grid », *in*: *International journal of electrical Power & Energy Systems* 72, pp. 99–108.

Arrillaga, Jos and Jos Arrillaga (1998), *High voltage direct current transmission*, vol. 29, Iet.

Arrillaga, Jos, Yong He Liu, and Neville R Watson (2007), *Flexible power transmission: the HVDC options*, John Wiley & Sons.

Bakhshi, Mohsen, Mohammad Hosein Holakooie, and Abbas Rabiee (2017), « Fuzzy based damping controller for TCSC using local measurements to enhance transient stability of power systems », *in*: *International Journal of Electrical Power & Energy Systems* 85, pp. 12–21.

Belhocine, M, B Marinescu, and F Xavier (2017), « Input signal and model structure analysis for the hvdc link pod control », *in*: *2017 IEEE Manchester PowerTech*, IEEE, pp. 1–6.

Bensenouci, Ahmed and AM Abdel Ghany (2007), « Mixed H/H 2 with pole-placement design of robust LMI-based output feedback controllers for multi-area load frequency control », *in*: *EUROCON 2007-The International Conference on" Computer as a Tool"*, IEEE, pp. 1561–1566.

Boyd, Stephen, Laurent El Ghaoui, Eric Feron, and Venkataramanan Balakrishnan (1994), *Linear matrix inequalities in system and control theory*, SIAM.

Byerly, RT, RJ Bennon, and DE Sherman (1982), « Eigenvalue analysis of synchronizing power flow oscillations in large electric power systems », *in*: *IEEE Transactions on Power Apparatus and Systems 1*, pp. 235–243.

Chaudhuri, Balarko and Bikash C Pal (2004), « Robust damping of multiple swing modes employing global stabilizing signals with a TCSC », *in*: *IEEE Transactions on Power Systems* 19.*1*, pp. 499–506.

Chen W. H., Yang W. and Lu X. (2014), « Impulsive observer-based stabilisation of uncertain linear systems », *in*: *IET Control Theory and Applications* 8.*3*, pp. 149–159.

Chilali, Mahmoud and Pascal Gahinet (1996), « H-infinity design with pole placement constraints: an LMI approach », *in*: *IEEE Transactions on automatic control* 41.*3*, pp. 358–367.

Do Bomfim, Antonio LB, Glauco N Taranto, and Djalma M Falcao (2000), « Simultaneous tuning of power system damping controllers using genetic algorithms », *in*: *IEEE Transactions on Power Systems* 15.*1*, pp. 163–169.

Du, Zhengchun, Wei Liu, and Wanliang Fang (2006), « Calculation of rightmost eigenvalues in power systems using the Jacobi–Davidson method », *in*: *IEEE Transactions on Power Systems* 21.*1*, pp. 234–239.

Dullerud, Geir E and Fernando Paganini (2013), *A course in robust control theory: a convex approach*, vol. 36, Springer Science & Business Media.

Eriksson, Robert and Lennart Soder (2011), « Wide-area measurement system-based subspace identification for obtaining linear models to centrally coordinate controllable devices », *in*: *IEEE Transactions on Power Delivery* 26.*2*, pp. 988–997.

Hassouneh, Munther A, Hsien-Chiarn Lee, and Eyad H Abed (2004), « Washout filters in feedback control: Benefits, limitations and extensions », *in*: *American Control Conference, 2004. Proceedings of the 2004*, vol. 5, IEEE, pp. 3950–3955.

Heniche, Annissa and Innocent Kamwa (2008), « Assessment of two methods to select wide-area signals for power system damping control », *in*: *IEEE Transactions on Power Systems* 23.*2*, pp. 572–581.

Hoagg, Jesse B and Dennis S Bernstein (2007), « Nonminimum-phase zeros-much to do about nothing-classical control-revisited part II », *in*: *IEEE Control Systems Magazine* 27.*3*, pp. 45–57.

« IEEE recommended practice for excitation system models for power system stability studies (ieee std 421.5-2005) » (2005), *in*: *Energy Development and Power Generating Committee of the Power Engineering Society* 95, p. 96.

Iwasaki, Tetsuya and Robert E Skelton (1994), « All controllers for the general H control problem: LMI existence conditions and state space formulas », *in*: *Automatica* 30.*8*, pp. 1307–1317.

J., Song and He S. (2015), « Robust finite-time H_∞ control for one-sided Lipschitz nonlinear systems via state feedback and output feedback », *in*: *Journal of the Franklin Institute* 352.*8*, pp. 3250–3266.

Kamwa, Innocent, Robert Grondin, and Yves Hébert (2001), « Wide-area measurement based stabilizing control of large power systems-a decentralized/hierarchical approach », *in*: *IEEE Transactions on power systems* 16.*1*, pp. 136–153.

Kanev, Stoyan, Carsten Scherer, Michel Verhaegen, and Bart De Schutter (2004), « Robust output-feedback controller design via local BMI optimization », *in*: *Automatica* 40.*7*, pp. 1115–1127.

Ke, DP and CY Chung (2012), « An inter-area mode oriented pole-shifting method with coordination of control efforts for robust tuning of power oscillation damping controllers », *in*: *IEEE Transactions on Power Systems* 27.*3*, pp. 1422–1432.

Kose, IE and Faryar Jabbari (1999), « Robust control of linear systems with real parametric uncertainty », *in*: *Automatica* 35.*4*, pp. 679–687.

Kotb, Omar, Mehrdad Ghandhari, Javier Renedo, Luis Rouco, and Robert Eriksson (2017), « On the design and placement of a supplementary damping controller in an embedded VSC-MTDC network », *in*: *Innovative Smart Grid Technologies Conference Europe (ISGT-Europe), 2017 IEEE PES*, IEEE, pp. 1–6.

Kundur, P, GJ Rogers, DY Wong, L Wang, and MG Lauby (1990), « A comprehensive computer program package for small signal stability analysis of power systems », *in*: *IEEE Transactions on Power Systems* 5.*4*, pp. 1076–1083.

Kundur, Prabha, Neal J Balu, and Mark G Lauby (1994), *Power system stability and control*, vol. 7, McGraw-hill New York.

Laila, Dina Shona, Mats Larsson, BC Pal, and Petr Korba (2009), « Nonlinear damping computation and envelope detection using Hilbert transform and its application to power systems wide area monitoring », *in*: *2009 IEEE Power & Energy Society General Meeting*, IEEE, pp. 1–7.

Latorre, Hector F, Mehrdad Ghandhari, and Lennart Söder (2008), « Active and reactive power control of a VSC-HVdc », *in*: *Electric Power Systems Research* 78.*10*, pp. 1756–1763.

Lee, B, H Song, S-H Kwon, D Kim, and K Iba (2003), « Calculation of rightmost eigenvalues in power systems using the block Arnoldi Chebyshev method (BACM) », *in*: *IEE Proceedings-Generation, Transmission and Distribution* 150.*1*, pp. 23–27.

Li, Yong, Christian Rehtanz, Sven Ruberg, Longfu Luo, and Yijia Cao (2012), « Wide-area robust coordination approach of HVDC and FACTS controllers for damping multiple interarea oscillations », *in*: *IEEE transactions on power delivery* 27.*3*, pp. 1096–1105.

Liao, Kai, Zhengyou He, Yan Xu, Guo Chen, Zhao Yang Dong, and Kit Po Wong (2016), « A sliding mode based damping control of DFIG for interarea power oscillations », *in*: *IEEE Transactions on Sustainable Energy* 8.*1*, pp. 258–267.

Lu, Chao, Xiaochen Wu, Jingtao Wu, Peng Li, Yingduo Han, and Licheng Li (2012), « Implementations and experiences of wide-area HVDC damping control in China southern power grid », *in*: *2012 IEEE Power and Energy Society General Meeting*, IEEE, pp. 1–7.

Mahmoud, Magdi S and Lihua Xie (2000), « Positive real analysis and synthesis of uncertain discrete time systems », *in*: *IEEE Transactions on Circuits and Systems I: Fundamental Theory and Applications* 47.*3*, pp. 403–406.

Marinescu, Bogdan and David Petesch (2014), « Three-level coordination in power system stabilization », *in*: *Electric Power Systems Research* 111, pp. 40–51.

Martins, Nelson and Paulo EM Quintão (2003), « Computing dominant poles of power system multivariable transfer functions », *in*: *IEEE Transactions on Power Systems* 18.*1*, pp. 152–159.

Meyer, B. and M. Stubbe (1992), « EUROSTAG, a single tool for power system simulation », *in*: *Transmission and Distribution International* 3.*1*, pp. 47–52.

Ming, Yin, Li Gengyin, Li Guangkai, Liang Haifeng, and Zhou Ming (2004), « Modeling of VSC-HVDC and its active power control scheme », *in*: *2004 International Conference on Power System Technology, 2004. PowerCon 2004.* Vol. 2, IEEE, pp. 1351–1355.

Mokhtari, Maghsoud, Farrokh Aminifar, Daryoosh Nazarpour, and Sajjad Golshannavaz (2012), « Wide-area power oscillation damping with a fuzzy controller compensating the continuous communication delays », *in*: *IEEE Transactions on Power Systems* 28.*2*, pp. 1997–2005.

Mondal, D, A Sengupta, and A Chakrabarti (2012), « Robust control of inter-area oscillations in a multimachine network employing LMI based wide area TCSC controller », *in*: *Electrical and Electronic Engineering* 2.*2*, pp. 23–30.

Padhy, Bibhu Prasad, SC Srivastava, and Nishchal K Verma (2011), « Robust wide-area TS fuzzy output feedback controller for enhancement of stability in multimachine power system », *in*: *IEEE Systems Journal* 6.*3*, pp. 426–435.

Padiyar, KR (2012), *Analysis of subsynchronous resonance in power systems*, Springer Science & Business Media.

Papangelis, Lampros, Marie-Sophie Debry, Patrick Panciatici, and Thierry Van Cutsem (2017), « Coordinated supervisory control of multi-terminal HVDC grids: A model predictive control approach », *in*: *IEEE Transactions on Power Systems* 32.*6*, pp. 4673–4683.

Pascal, G, N Arkadi, JL Alan, and C Mahmoud (1995), « LMI control toolbox user's guide », *in*: *IEEE Xplore, The MathWorks, Inc* 1, pp. 1–12.

Peres, Wesley, Ivo Chaves Silva Júnior, and João Alberto Passos Filho (2018), « Gradient based hybrid metaheuristics for robust tuning of power system stabilizers », *in*: *International Journal of Electrical Power & Energy Systems* 95, pp. 47–72.

Pipelzadeh, Yousef, Balarko Chaudhuri, and Tim C Green (2012), « Control coordination within a VSC HVDC link for power oscillation damping: A robust decentralized approach using homotopy », *in*: *IEEE Transactions on Control Systems Technology* 21.*4*, pp. 1270–1279.

Preece, R, AM Almutairi, O Marjanovic, and JV Milanović (2011), « Damping of electromechanical oscillations by VSC-HVDC active power modulation with supplementary wams based modal LQG controller », *in*: *2011 IEEE Power and Energy Society General Meeting*, IEEE, pp. 1–7.

Preece, Robin, Jovica V Milanovic, Abddulaziz M Almutairi, and Ognjen Marjanovic (2013), « Damping of inter-area oscillations in mixed AC/DC networks using WAMS based supplementary controller », *in*: *IEEE Transactions on Power Systems* 28.*2*, pp. 1160–1169.

Qi, Junjian, Jianhui Wang, Hui Liu, and Aleksandar D Dimitrovski (2016), « Nonlinear model reduction in power systems by balancing of empirical controllability and observability covariances », *in*: *IEEE Transactions on Power Systems* 32.*1*, pp. 114–126.

Ray, Swakshar and Ganesh K Venayagamoorthy (2008), « Real-time implementation of a measurement-based adaptive wide-area control system considering communication delays », *in*: *IET generation, transmission & distribution* 2.*1*, pp. 62–70.

Reed, Gregory, Ronald Pape, and Masatoshi Takeda (2003), « Advantages of voltage sourced converter (VSC) based design concepts for FACTS and HVDC-link applications », *in*: *2003 IEEE Power Engineering Society General Meeting (IEEE Cat. No. 03CH37491)*, vol. 3, IEEE, pp. 1816–1821.

Rimorov, Dmitry, Innocent Kamwa, and Geza Joós (2015), « Quasi-steady-state approach for analysis of frequency oscillations and damping controller design », *in*: *IEEE Transactions on Power Systems* 31.*4*, pp. 3212–3220.

Rogers, Graham (2012), *Power system oscillations*, Springer Science & Business Media.

Rouco, L (2001), « Coordinated design of multiple controllers for damping power system oscillations », *in*: *International journal of electrical power & energy systems* 23.*7*, pp. 517–530.

Rouco, L and IJ Perez-Arriaga (1993), « Multi-area analysis of small signal stability in large electric power systems by SMA », *in*: *IEEE transactions on power systems* 8.*3*, pp. 1257–1265.

Sanchez-Gasca, Juan J, Nicholas W Miller, Atsushi Kurita, and Susumu Horiuchi (1989), « Multivariable control for damping inter-area oscillations in power systems », *in*: *IEEE Control Systems Magazine* 9.*1*, pp. 28–32.

Sauer, Peter W, C Rajagopalan, and MA Pai (1991), « An explanation and generalization of the AESOPS and PEALS algorithms (power system models) », *in*: *IEEE transactions on power systems* 6.*1*, pp. 293–299.

Scherer, Carsten, Pascal Gahinet, and Mahmoud Chilali (1997), « Multiobjective output-feedback control via LMI optimization », *in*: *IEEE Transactions on automatic control* 42.*7*, pp. 896–911.

Skogestad, Sigurd and Ian Postlethwaite (2007), *Multivariable feedback control: analysis and design*, vol. 2, Wiley New York.

Soliman, Hisham M and Khaled A El Metwally (2017), « Robust pole placement for power systems using two-dimensional membership fuzzy constrained controllers », *in*: *IET Generation, Transmission & Distribution* 11.*16*, pp. 3966–3973.

Suplin, Vladimir and Uri Shaked (2005), « Robust H output-feedback control of linear discrete-time systems », *in*: *Systems & control letters* 54.*8*, pp. 799–808.

Tayal, 5V K and JS Lather (2015), « Reduced order H TCSC controller & PSO optimized fuzzy PSS design in mitigating small signal oscillations in a wide range », *in*: *International Journal of Electrical Power & Energy Systems* 68, pp. 123–131.

Tomizuka, Masayoshi (1987), « Zero phase error tracking algorithm for digital control », *in*: *Journal of Dynamic Systems, Measurement, and Control* 109.*1*, pp. 65–68.

Tripathy, M and S Mishra (2015), « Coordinated tuning of PSS and TCSC to improve Hopf Bifurcation margin in multimachine power system by a modified Bacteria Foraging Algorithm », *in*: *International journal of electrical power & energy systems* 66, pp. 97–109.

Uchida, Naoyuki and Taiji Nagao (1988), « A new eigen-analysis method of steady-state stability studies for large power systems: S matrix method », *in*: *IEEE Transactions on Power Systems* 3.*2*, pp. 706–714.

Ustinov, SM, JV Milanović, and VA Maslennikov (2002), « Inherent dynamic properties of interconnected power systems », *in*: *International journal of electrical power & energy systems* 24.*5*, pp. 371–378.

VanAntwerp, Jeremy G and Richard D Braatz (2000), « A tutorial on linear and bilinear matrix inequalities », *in*: *Journal of process control* 10.*4*, pp. 363–385.

Vance, Katelynn, Anamitra Pal, and James S Thorp (2012), « A robust control technique for damping inter-area oscillations », *in*: *Power and Energy Conference at Illinois (PECI), 2012 IEEE*, IEEE, pp. 1–8.

Wang, Lei and Adam Semlyen (1990), « Application of sparse eigenvalue techniques to the small signal stability analysis of large power systems », *in*: *IEEE Transactions on Power Systems* 5.*2*, pp. 635–642.

Xie, Lihua, Minyue Fu, Carlos E de Souza, et al. (1992), « H_∞ control and quadratic stabilization of systems with parameter uncertainty via output feedback », *in*: *IEEE Transactions on Automatic Control* 37.*8*, pp. 1253–1256.

Zhang, Lidong, Lennart Harnefors, and Hans-Peter Nee (2011), « Interconnection of two very weak AC systems by VSC-HVDC links using power-synchronization control », *in*: *IEEE transactions on power systems* 26.*1*, pp. 344–355.

Zhou, Kemin and John Comstock Doyle (1998), *Essentials of robust control*, vol. 104, Prentice hall Upper Saddle River, NJ.

Zhou, Kemin, John Comstock Doyle, Keith Glover, et al. (1996), *Robust and optimal control*, vol. 40, Prentice hall New Jersey.

Zolotas, Argyrios C, Petr Korba, Balarko Chaudhuri, and Imad M Jaimoukha (2007), « H_2 LMI-based robust control for damping oscillations in power systems », *in*: *System of Systems Engineering, 2007. SoSE'07. IEEE International Conference on*, IEEE, pp. 1–8.

Titre : Commande des liaisons à courant continu (HVDC) pour l'amortissement des oscillations inter-zones

Mot clés : Oscillations de puissance, modes inter-zones, HVDC, PSS, POD, électronique de puissance, robustesse.

Résumé : Cette thèse aborde le problème d'amortissement des oscillations de puissance (modes inter-zones) d'un réseau de transport maillé – comme c'est le cas du réseau européen - par l'intermédiaire d'une liaison à courant continu à haute tension (High-Voltage Direct Current-HVDC). Dans ce contexte particulier, les modes inter-zones sont à des fréquences plus élevées que d'habitude – autour de 1Hz. Ceci est un défi important pour la commande car, d'autres dynamiques du réseau existent dans cette plage de fréquence. En effet, les régulateurs standard (PSS et POD type IEEE) ne donnent pas des réponses satisfaisantes et d'autres lois de commande ont été proposées. Elles prennent en compte plus d'information du système électrique avoisinant la HVDC en utilisant un modèle de commande plus riche. De plus, la robustesse est améliorée afin de fournir des bonnes réponses en cas de variations du réseau (évolution de la charge, déclenchements des lignes et des générateurs, . . .) et des paramètres de la ligne HVDC. Enfin, des zéros instables (réponses à déphasage non minimal) ont été mis en évidence et étudiés dans ces situations d'insertion des HVDC dans des réseaux AC maillés. Les régulateurs proposés atténuent aussi l'effet négatif de ces zéros sur les performances de la boucle fermée. Les résultats sont facilement implantables en pratique car il s'agit de régulateur à retour de sortie. Aussi, bien que développées pour les HVDC, les méthodologies d'analyse et commande proposées peuvent être étendues à d'autres éléments utilisant de l'électronique de puissance comme, par exemple, des générateurs d'énergies renouvelables connectés au réseau par des convertisseurs de puissance.

Title: Control of direct current connections (HVDC) for the damping of inter-area oscillations

Keywords: Power oscillations, inter-area modes, HVDC, PSS, POD, power electronics, robustness.

Abstract: This thesis addresses the problem of damping power oscillations (inter-area modes) of a meshed transport network - as it is the case of the European network - through a High Voltage Direct Current-(HVDC) link. In this particular context, inter-area modes are at higher frequencies than usual - around 1Hz. This is an important challenge for the control system, as other network dynamics exist in this frequency range. Standard controllers (PSS and POD type IEEE) give un-satisfactory results and other control approaches have been proposed. They take into account more information from the electrical system surrounding the HVDC using a richer control model. Besides, the robustness is improved in order to provide good responses in case of network variations (load evolution, line, and generator trips,..., etc.) and HVDC line parameters changes. Finally, unstable zeros (non-minimum phase behavior) have been highlighted and studied in these situations of HVDC inserted in meshed AC networks. The proposed controllers also mitigate the negative effect of these zeros on the performances of the closed-loop. The results are easily implemented in practice because they are feedback controllers. Also, although developed for HVDC, the proposed analysis and control methodologies can be extended to other elements using power electronics such as, for example, renewable energy generators connected to the grid by power converters.